Politecnico di Milano

School of civil, environmental and land management engineering

Master thesis

Experimental Tests on a Reinforced Concrete Frame with Polystyrene Infills

Author:

Marko ĐURANOVIĆ

Supervisor:

Prof. Ing. Liberato FERRARA

December 2016

ABSTRACT

The aim of this thesis will be to investigate the behaviour of a reinforced concrete frame infilled with polystyrene blocks instead of masonry. This was done by performing a test on a full scale mock-up in a laboratory. After the test, analytical and FEA solutions were presented and compared. Since this is fairly new way of using polystyrene, there are no analytical solutions derived for it, so solutions for masonry infill adjusted for polystyrene material were implemented. Forces coming from the experimental test were larger than the predicted ones. This was due to a thick mortar layer which was applied on both sides of the mock-up and was not taken into account in analytical and FEA solutions. Also all of the material properties used for predicting the behaviour were characteristic values found in literature and not obtained by testing material samples. Even so, behaviour of this frame was very similar to the behaviour of a bare frame as it was expected from the beginning, and makes it easier to use when modelling behaviour of a whole structure.

ACKNOWLEDGEMENTS

vi

Contents

x

LIST OF FIGURES

LIST OF TABLES

Chapter 1

Introduction

In current structural engineering practice, one of the most used types of structural systems is frame system with infill walls. Traditionally, masonry was present as an infill material and was regarded as the best choice for it. Nowadays, since optimization of costs and quality is a major concern, new materials are being invented and new ways of using them are being patented constantly.

Trying to overcome some of the drawbacks of masonry (large weight when used in big amounts, and influence on the stiffness of the whole structure) which are giving problems to engineers when designing structures, especially for earthquake resistance, this research will assess the use of polystyrene panels covered with a thin mortar layer interconnected with glass fibers as the infill material. Polystyrene was selected knowing that it has low weight, would not alter the stiffness in great amount and can act as an insulation by itself.

1.1 OBJECTIVE AND SCOPE

In this thesis an investigation will be performed on how reinforced concrete (RC) frames behave when polystyrene panels are used as the infill. In order to achieve this, an experimental test on a full scale mock-up was performed along with finite element modelling of several different models.

This project intends to demonstrate what are the effects of polystyrene panels on post elastic behaviour of an RC frame.

1.2 IMPORTANCE AND SIGNIFICANCE OF THIS STUDY

As mentioned before, masonry used as infill material has some drawbacks that affect the whole structure. Polystyrene panels can avoid some of these inconveniences, but with this new way of using polystyrene, a lot of uncertainties arise. These unknowns will be explained in order to have a clear understanding of the response of a structure when using polystyrene as infill in everyday constructions. Several possible failure modes may occur and each one of them must be properly investigated, in order to determine what they are dependent on.

1.3 POSSIBLE CONNECTION BETWEEN MASONRY AND POLYSTYRENE INFILL

Since not many (if any) studies like this have been performed, a familiar starting point has to be determined. In this case, a logical starting point is to study masonry infills, for which a lot of experiments have been done and countless papers have been written.

This analogy between polystyrene and masonry can be justified by the fact that both of the materials can be considered to have brittle behaviour compared to a RC frame's one. For the masonry infill, several "common" failure modes have been determined, and those modes will be adopted for polystyrene also. Although, it cannot be said that these modes are the same for both cases, it is a reasonable starting point. Also, some analytical methods exist which were used when more refined methods are unavailable. These solutions will have to be calibrated to suit the case of using polystyrene instead of masonry.

Chapter 2

Review of literature

In the following chapter some of the key aspects and results from previous studies on masonry-infilled RC frames are presented. Particular attention is given to single story – single bay frames. Different cases are considered regarding infill reinforcement, which influences the behaviour, modelling and expected failure modes.

2.1 INTRODUCTION

Masonry infilled frames represent a common construction technique employed in buildings all over the world. However, it is a common mistake to regard these infills as "non-structural components", and consider just the bare frame for the analysis of the structural response. Although the masonry is not detailed accordingly to act as a shear wall, if it's in contact with the frame it will tend to prevent the RC frame to deform as it would normally do if there was no infill present. For this reason, the infill will have a non-negligible stiffness (and energy dissipation contribution) under the dynamic response of the structure, especially under low intensity excitations. Maximum displacements and energy dissipation demands for the frame elements are also expected to reduce. (Decanni, Mollaioli, Mura, & Saragoni, 2004)

If the structure is modelled as a bare frame, with "added mass" due to the "non-structural infills", the fundamental period of the structure will be overestimated (the structure will be more flexible in the model), and thus, the seismic forces will be, in some cases, underestimated, resulting in different seismic response than the one anticipated by the designer. Needless to say, neglecting the infill rigidity is, in many cases, not a conservative approach and should be avoided. In general, according to (Decanni, Mollaioli, Mura, & Saragoni, 2004), the overall response of the structure can be significantly improved by the

3

presence of the infills, even after accounting for the added mass for the inertial loads. Different types of models have been developed to study the behaviour of these structures, and the most typical failure modes have been outlined in several research papers.

Masonry is a much stiffer and stronger material than polystyrene, and therefore, it is expected for the two systems to behave differently. However, in the absence of any previous studies done specifically on polystyrene infilled frames, studying the behaviour of masonry infilled frames gives a good starting point as to what to expect.

2.2   BARE FRAME BEHAVIOUR

Reinforced concrete frame structures are a well-known type of lateral load resisting system, which has been studied thoroughly in the past. These types of structures are known to have a very ductile behaviour, with large hysteresis loops under cyclic loading (Figure 2-1), which means they are able to dissipate a great amount of energy. Another big advantage of frame structures is their great flexibility under seismic actions. Due to this feature, they usually have longer fundamental periods, and hence, reduced inertial loads. Figure 2-1 shows the expected plastic hinges that form on the structure (at top and bottom of columns and at the faces of the beam) under cyclic loading. The experimental results are usually in very good agreement with the numerical predictions for this type of structure, which can be estimated, e.g., by means of a non-linear cyclic analysis.
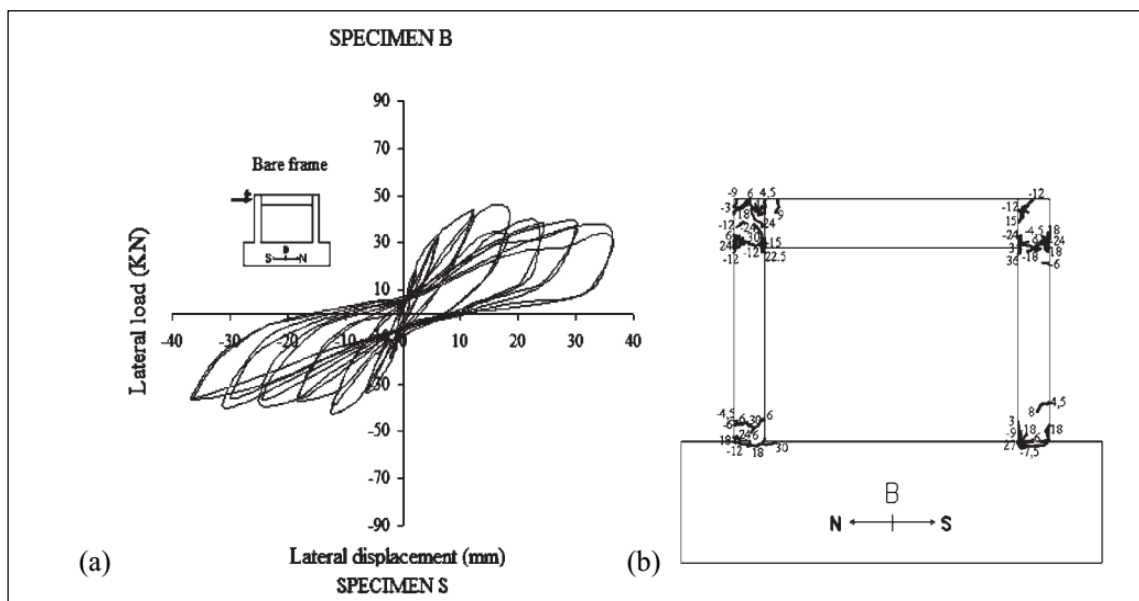
Figure 2-1. Bare frame behaviour under cyclic loading **(Kakaletsis & Karayannis, 2008)**

2.2.1 Modelling

The bare frame model is fairly simple. Classical structural mechanics is sufficient to model a frame structure, considering Euler-Bernoulli frame elements for both beams and columns (neglecting shear deformation in the kinematic model).

Boundary conditions at the base of the columns should be suitably accounted for. This is one of the modelling approximations, namely, since in a real structure, only in a very few cases, an edge which is completely restrained (no rotation at all) can be achieved. The use of fully fixed restraints at element ends in structural models is always questionable. It is well known that for different rigidities of a connection, different distribution of internal forces in the structure will be obtained. This issue can be overcome by careful examination of the structure and proper calibration of the model.

Both steel and concrete material properties should be adequately accounted for. Steel distribution in the RC elements needs to be defined, in order to plot a moment-curvature diagram, due to the non-linear nature of the problem.

2.2.2 Failure modes

The single frame depicted in Figure 2-1 is a 3 times statically indeterminate structure. Therefore, a total of 4 plastic hinges are needed in order to obtain the collapse mechanism. Since frame structures are usually slender, their failure is governed by a flexural behaviour. These plastic hinges are expected to form in the regions of the members where the highest moment concentrations are located (top and bottom of columns and at beam ends), as seen from the figure.

2.3 RC FRAME WITH UNREINFORCED MASONRY INFILL

Some masonry infill panels have absolutely no reinforcement, since they are conceived as "non-structural elements" by the designer. The behaviour of panels that have no reinforcement differs greatly from the one of slightly reinforced panels, as it will be discussed later.

2.3.1 Modelling

Two types of models can be differentiated for simulating the in-plane behaviour of infilled RC frames subjected to a lateral force:

- Micro-models: Sophisticated analysis such as Finite Element Method are used to model in detail the behaviour of masonry infilled RC frames. Several types of elements need to be used (continuum elements, for the frame and infill, interphase elements between frame and infill, and sometimes even additional elements for the mortar joints). Usually, non-linear finite elements are needed to model the behaviour appropriately. The data input, and also the computational time, are much more complex than those required when a macro model is employed.

- Macro-models: The simplest case is the so called "simplified model", which uses a single strut to model the masonry infill. This approach is suitable for global effects of the structural behaviour (stiffness, period, drifts) but is not able to capture the failure modes of the individual frames or the infills. Variations to this approach are the so called "multi strut models", which are a more refined version of the latter one. Different layouts are illustrated in Figure 2-2. These models are used to describe the local behaviour, and are able to predict the typical failure modes of the infilled RC frame. Multi strut models are a popular way to proceed, and give acceptable results.
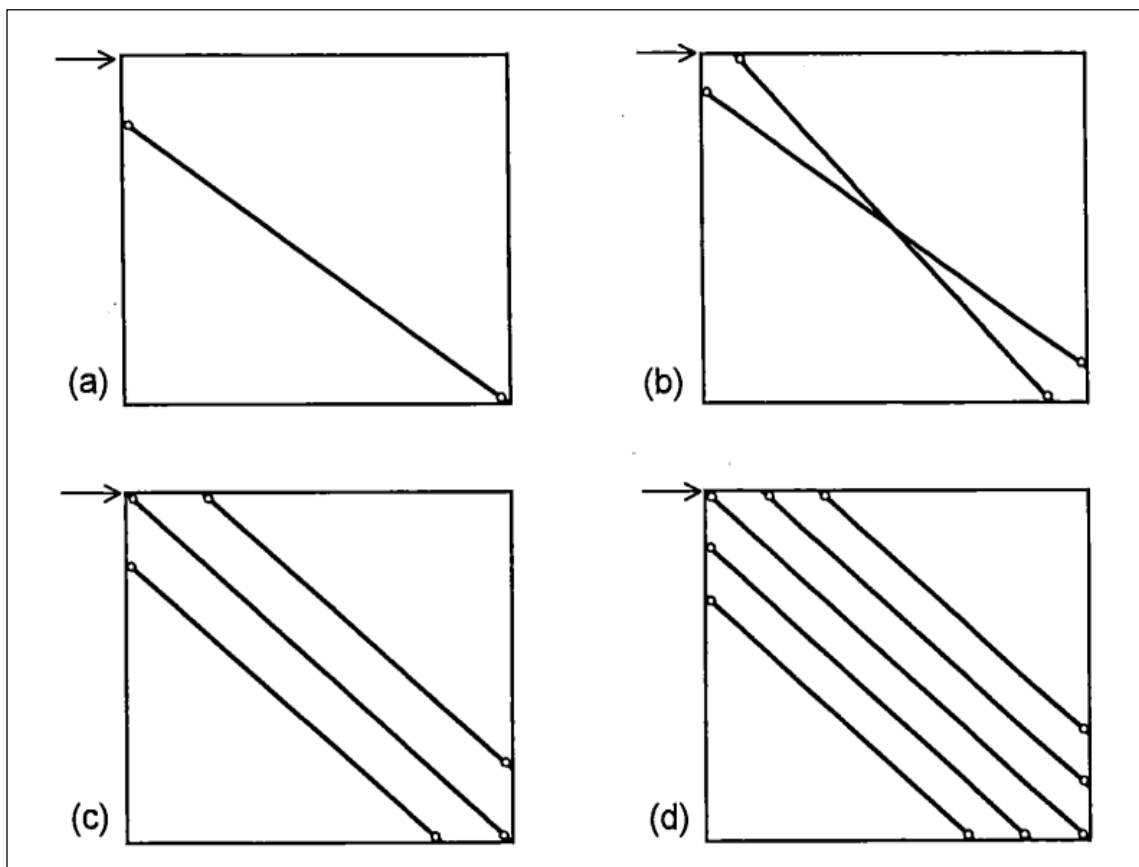
Figure 2-2. Macro models: Single strut (a) and multi strut (b), (c), (d) **(Crisafulli, 1997)**

Masonry is a material that works mainly under compression, and has a negligible tensile strength. For this reason, the panel separates from the frame at the tension areas. Figure 2-3 shows a mechanism that occurs after the separation. So, many authors agree that a suitable model to approximate the effect of having a masonry infill is achieved by adding a compression strut to the bare frame structure, having the same thickness as the wall. A topic of interest is the width "w" of such strut which is the basic parameter for defining its axial stiffness. Several values and formulas can be found in the literature, typically depending on the compressive strength of masonry, and the relative stiffness between frame and infill. Usual values for "w" are shown below.

$$\frac{L}{4} \leq w \leq \frac{L}{3}$$

(**2-1**)

Where:

- L = length of compression strut
- w = width of compression strut

Figure 2-4 shows the variation of "w/L" ratio as a function of the relative stiffness between the frame and infill (λ_h), according to several researchers. Other characteristic properties for strut are considered equivalent to the masonry infill. The stress distribution along the masonry, before and after separation of the frame-infill has occurred, can be seen in Figure 2-5, from a Finite Element Analysis.
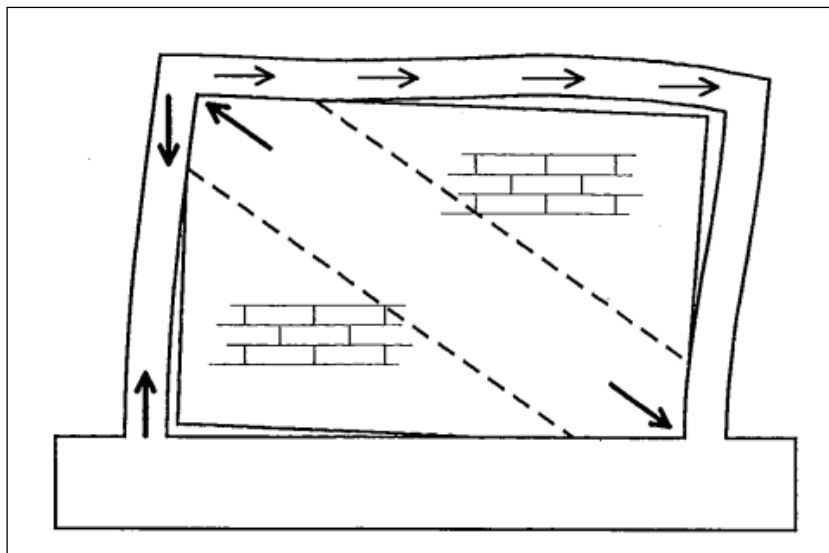
Figure 2-3. Equivalent truss mechanism for infilled frame structure (**Crisafulli, 1997**)
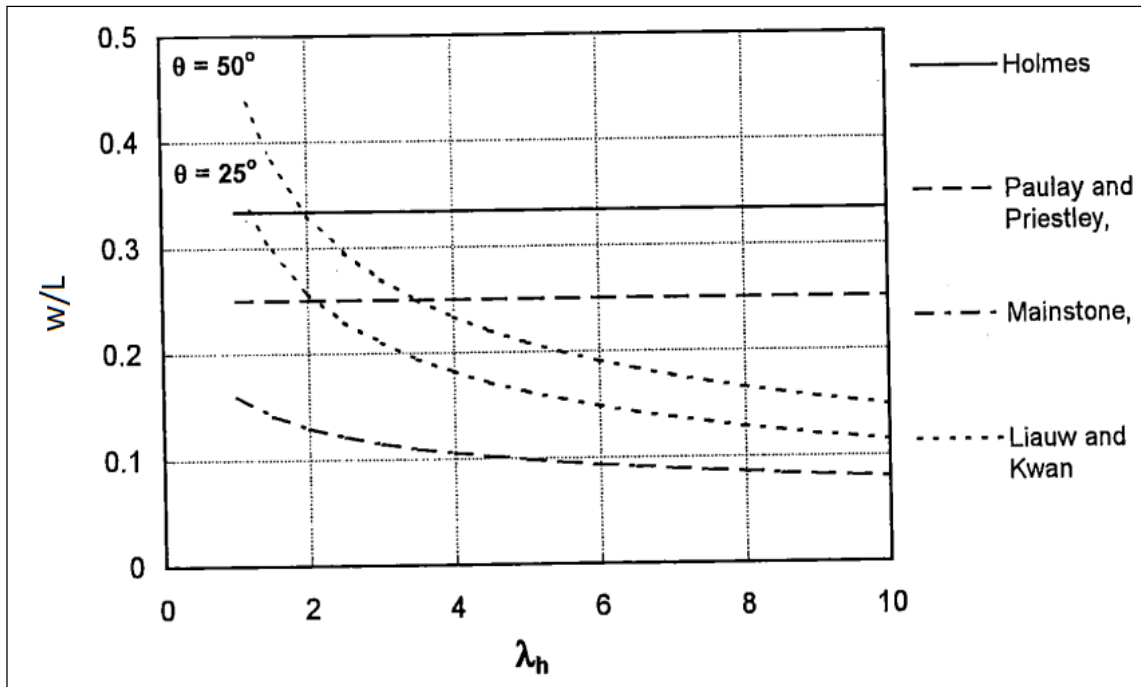
Figure 2-4. Variation of the w/L ratio as a function of λ_h (**Crisafulli, 1997**)
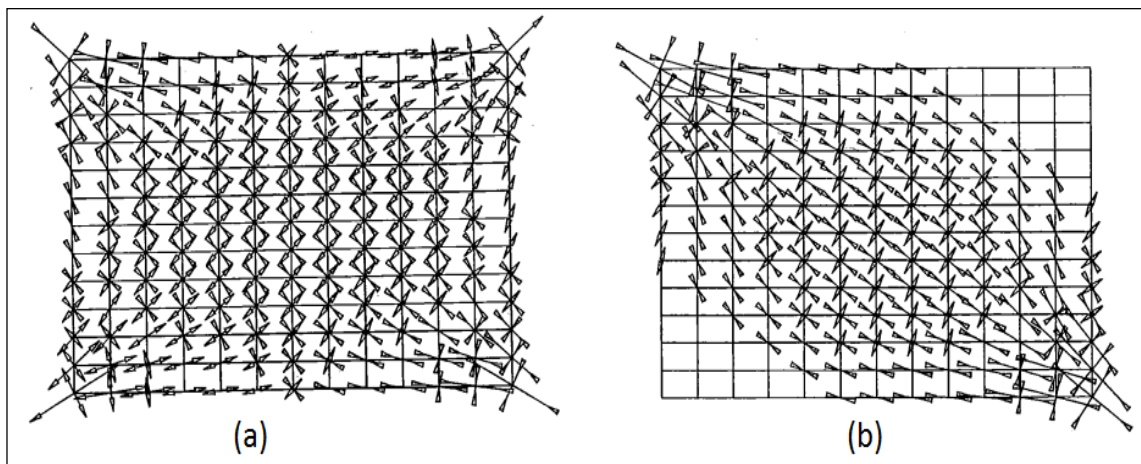
Figure 2-5. Stress distribution in masonry before separation (a) and after separation occurs (b) (**Crisafulli, 1997**)

2.3.2 Behaviour of infilled RC frames under monotonic loading

Initially, under low stresses, the frame and masonry act together as a monolithic element, and behave elastically, similar to a cantilever wall. From Figure 2-5 (a) it can be observed that the stress concentrations occur at the corners, while the panel exhibits mainly shear stresses.

As the load increases, due to increase of stress in masonry panel, and incompatibility between the panel and the frame because of their different deformability properties, cracking occurs at the frame/panel interface, and the panel separates from the frame, except at the diagonally compressed corners. This results in a decrease of the structure stiffness (strength

8

is not significantly affected), and an overload of compression stresses at the compressed corners, which experience a biaxial compression state, as depicted in Figure 2-6. Since only a limited portion of the frame is compressed at the corners, the idea of the equivalent compression strut was proposed by Polyakov in 1958, and later improved by several authors.

Internal action diagrams (bending moment, shear and axial force) can be obtained for the frame through a finite element analysis, or through a multi-strut model. Several multi-strut models have been proposed in the literature, depending on the expected type of failure. A simplified single strut model does not give realistic results for local analysis of the infilled frame, as mentioned before.

Results show that for normal infilled frames, after separation occurs, the maximum bending moments in the columns can be up to six times lower than in the case of the bare frame (Crisafulli, 1997). However, the internal actions highly depend on the relative rigidity between the frame and the infill, as depicted in Figure 2-7 (b). It is interesting to note how for the case of a very rigid frame (compared to the infill), the behaviour tends to the one of the bare frame. In any case, the final behaviour at large drifts (internal actions and global stiffness) always tends towards the one of the bare frame, as the infill panel will be completely cracked and its load carrying capacity will be quite low.
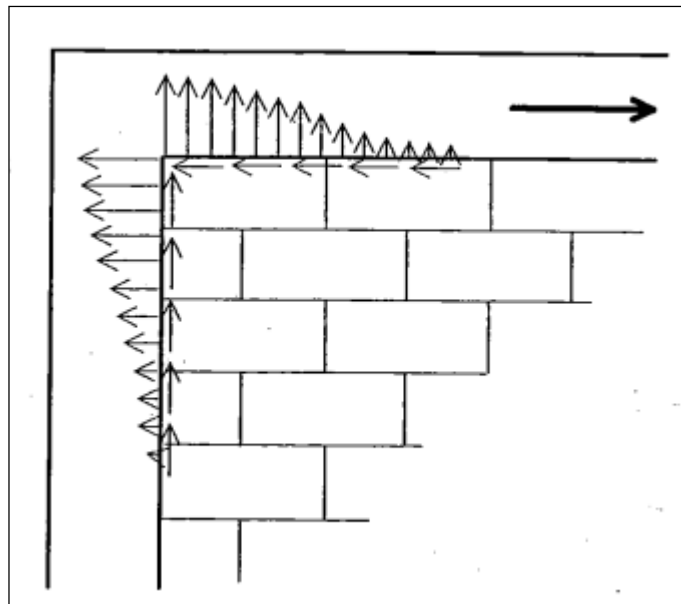
Figure 2-6. Normal and shear stresses acting on a loaded corner of the frame (**Crisafulli, 1997**)
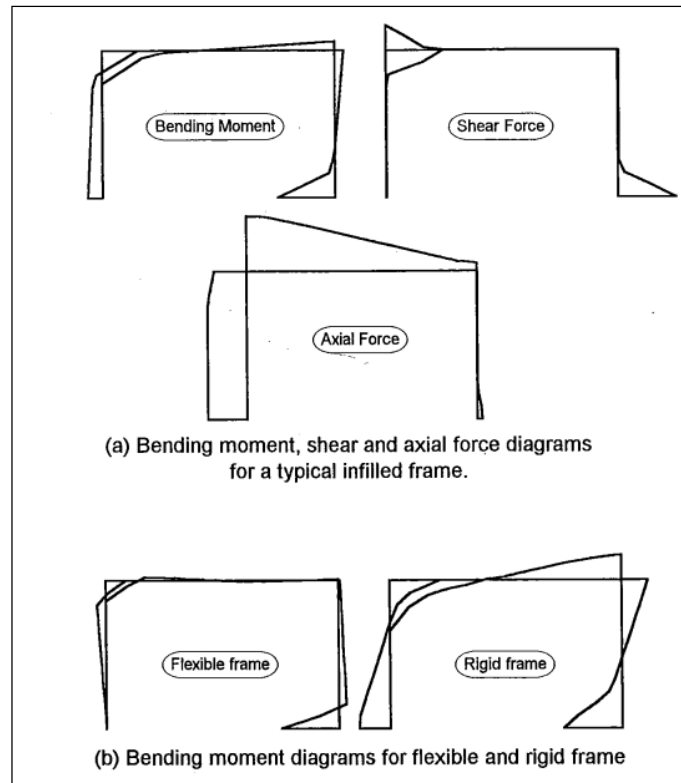
Figure 2-7. Typical bending moment, shear and axial forces diagrams obtained from and infilled RC frame, after separation occurs (**Crisafulli, 1997**)

For the case of non-integral infilled frames (when the infill is placed after casting the frame) the behaviour is similar to the one described previously. However, some differences could arise due to unwanted gaps between frame and masonry (if no expansive mortar is used to prevent them). This results in a low initial stiffness, until the frame deforms enough to close the gaps between itself and the masonry panel. Then there is a significant increase of stiffness, as both members start to work together.

In general, four different stages can be distinguished during monotonic loading of masonry infilled RC frame structures, according to Crisafulli (1997):

1. During the initial stage the structure behaves as a monolithic cantilever wall until separation occurs.
2. Then the behaviour is characterized by the composite interaction between the panel and the frame, although the materials remain mainly uncracked.
3. The induced state of stress into the panel produces different cracking patterns, with significant damage until the maximum lateral resistance is achieved.
4. Finally, the lateral strength decreases and the response is mainly controlled by the frame.

10

2.3.3 Failure modes

The failure type of infilled RC frames depends on several factors (relative rigidity between frame and infill, dimensions of the structure, mechanical properties of components, mortar joint thickness, frame reinforcing steel, vertical loads, amongst others). Several types of failure are defined conventionally, however, the real failure will generally be a combination of the failure modes described in this section. Failure can occur either in the masonry panel, or in the RC frame, and for each of these two different modes have been defined.

2.3.3.1 Failure in masonry panel

"*The failure of the masonry panel can develop by debonding of the mortar joints, cracking or crushing of the masonry units or a combination of these. The occurrence of the different types of failure depends on the material properties and the stress state induced in the panel*"[1]. Figure 2-8 shows a diagram summarizing the different types of failure modes observed for the masonry infills.
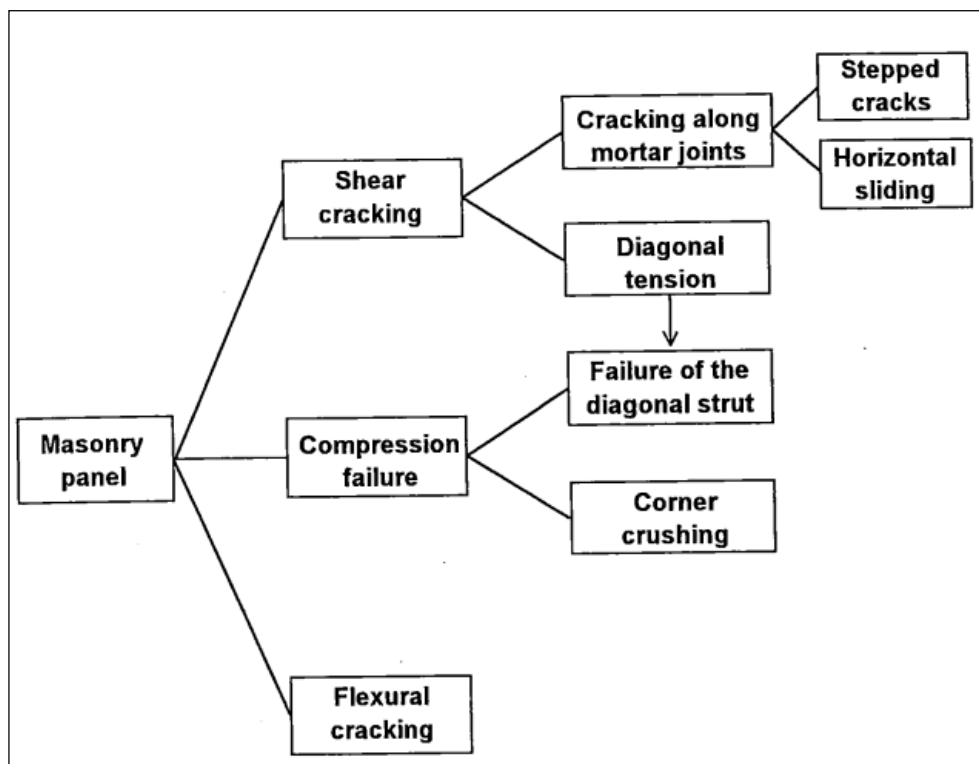
Figure 2-8. Modes of failure observed in masonry infills **(Crisafulli, 1997)**

---

[1] (Crisafulli, 1997)

➢ **Shear Cracking**

This is the most common type of failure according to experimental observations and affected panels in existing buildings. It mainly depends on the bond strength and friction coefficient of the mortar joints, tensile strength of masonry, and the relative values between normal and shear stresses. Depending on the stress ratio, the failure can be along the mortar joints, or cracks that cross the masonry units. The stress ratio can be directly related with the aspect ratio (height/length) of the infill. Cracks along the mortar joints can occur along a horizontal plane, or follow a stepped pattern, as observed in Figure 2-9. According to (Mehrabi & Shing, Seismic Analysis of Masonry-Infilled Reinforced Concrete Frames, 2003), this is the most common type of failure for a relatively weak panel with respect to the surrounding frame. Also, cracking due to diagonal tension (Figure 2-10) has been defined in the literature, which occurs along the diagonal of the infill panel, due to a biaxial tension-compression state, as seen in Figure 2-11. Generally, for high shear stresses (low aspect ratios), cracking along mortar joints is more common. However, when mortar joints are very strong, or the wall has medium to high aspect ratios, diagonal tension could be expected. Diagonal tension is regarded as a very dangerous type of failure, since after the formation of cracks along both diagonals, expulsion of the masonry units becomes imminent.
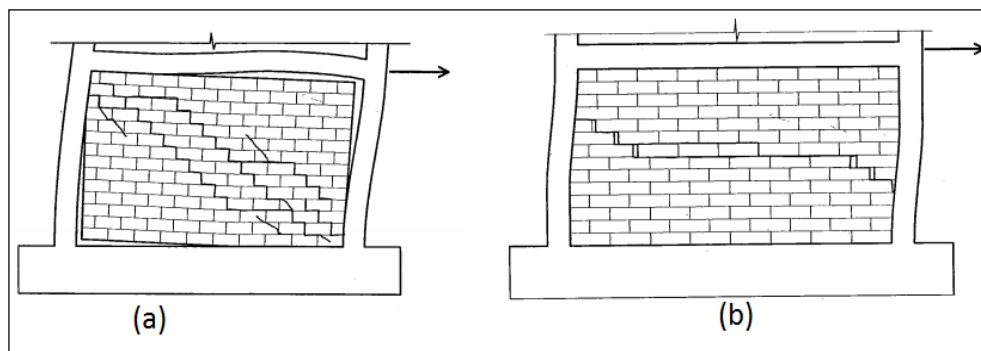
Figure 2-9. Typical failure modes for shear cracking. Stepped cracking pattern (a) or horizontal sliding (b) **(Crisafulli, 1997)**
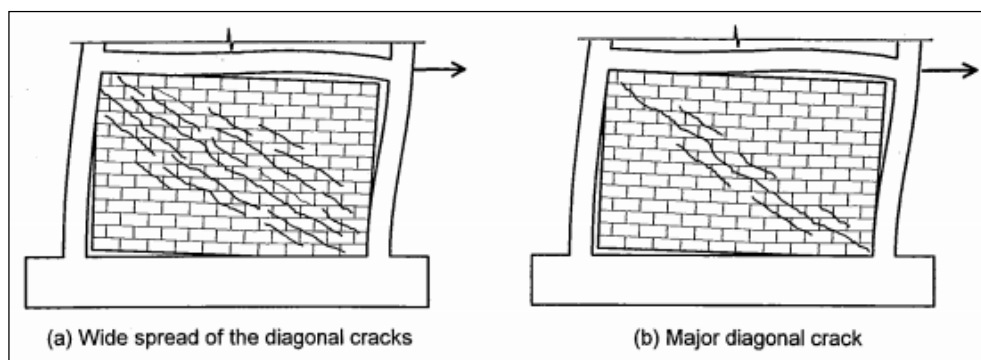
Figure 2-10. Cracking induced by diagonal tension. **(Crisafulli, 1997)**
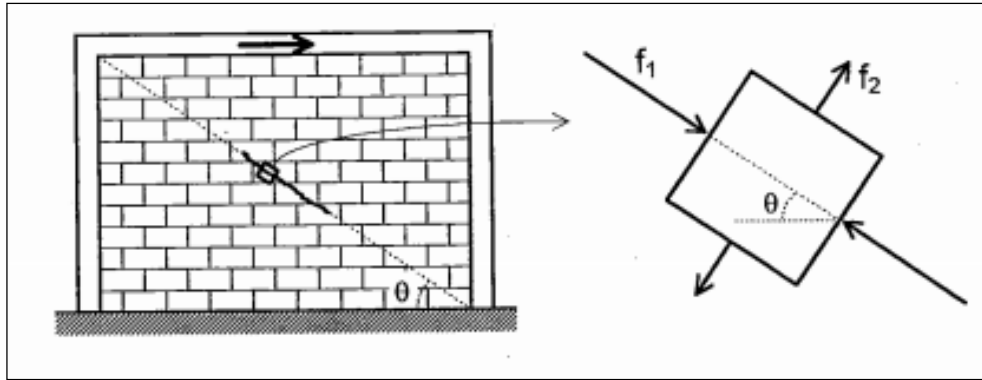
Figure 2-11. Biaxial tension – compression stress state in the infill panel. **(Crisafulli, 1997)**

> **Compression Failure**

Two types of compression failure have been observed in the masonry panels. The first one is the crushing of the loaded corners, where there is a biaxial compressive stress state (Figure 2-12). This type of failure could be expected to occur when the frame is very flexible, hence the contact length between frame and infill decreases, and stresses increase. The second mechanism is due to the compressive failure of the diagonal strut. After separation, as the lateral deformations increase, instability of the compressed strut is eventually reached.
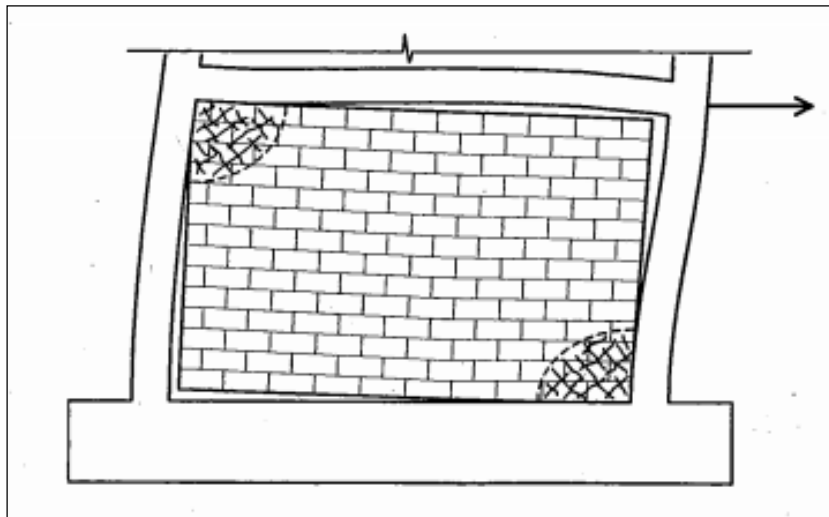
Figure 2-12. Crushing of the loaded corners. **(Crisafulli, 1997)**

> **Flexural Cracking**

This type of failure can be observed where flexure effects are predominant (as in multistorey, slender infilled frames). Cracks develop on the tension side of the infilled frame, in the masonry infill. However, this type of failure is rarely seen, since separation of the

13

frame-infill usually occurs before flexural cracking, and the horizontal actions are resisted through truss mechanism.

2.3.3.2   Failure in the RC frame

Different failure mechanisms have also been observed on the surrounding RC frame during horizontal actions. "*Damage in the frame members usually occurs from flexural plastic hinges, shear failure, yielding under axial forces, compression failure or a combination of these*"[2]. Similar to the previous section, Figure 2-13 shows the different failure modes for the RC frame, which are explained below.
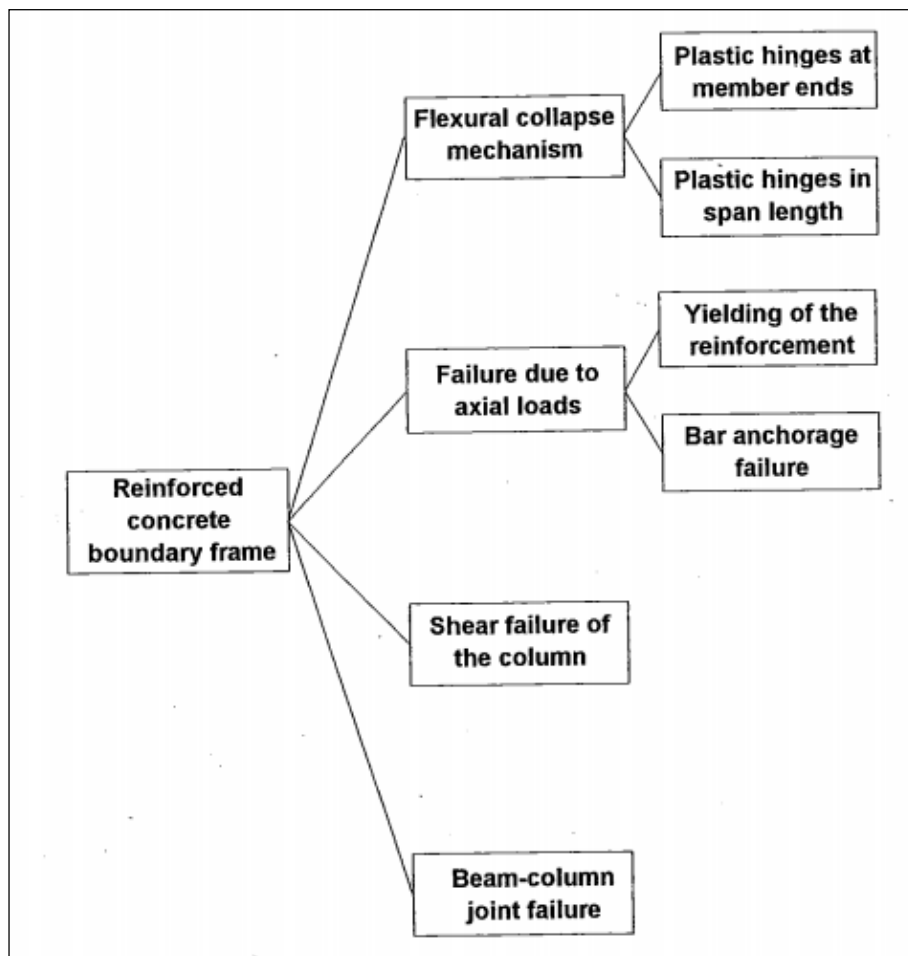
Figure 2-13. Modes of failure observed in RC boundary frames. (**Crisafulli, 1997**)

---

[2] (Crisafulli, 1997)

➢ **Flexural Collapse Mechanism**

This mechanism usually develops after the masonry panel has failed. It is characterized by the formation of plastic hinges at the column ends, where expected maximum bending moments occur. However, when sliding shear in the panel occurs, plastic hinges could form within the span of the column (Figure 2-14b), inducing an undesirable increase of shear forces.

➢ **Failure Due to Axial Loads**

Under lateral loading, columns work as a truss mechanism, under axial forces (tension and compression). After concrete cracks, because of its intrinsic low tensile strength, if the load is further increased, yielding in tension members can be reached. Two types of mechanisms of this nature have been observed. The first one is known as the "flexural failure", and can be observed in slender frames (high aspect ratios), generally multi story frames. Horizontal flexural cracks develop along the tension element because of the high plastic deformations of the longitudinal reinforcement (Figure 2-15). Beams also tend to undergo some plastic elongation, and hence, the interaction between the frame and infill can be significantly degraded or completely lost during this process. The other mechanism is the bar anchorage failure (Figure 2-15b), which can be avoided by providing proper development length for the longitudinal bars.
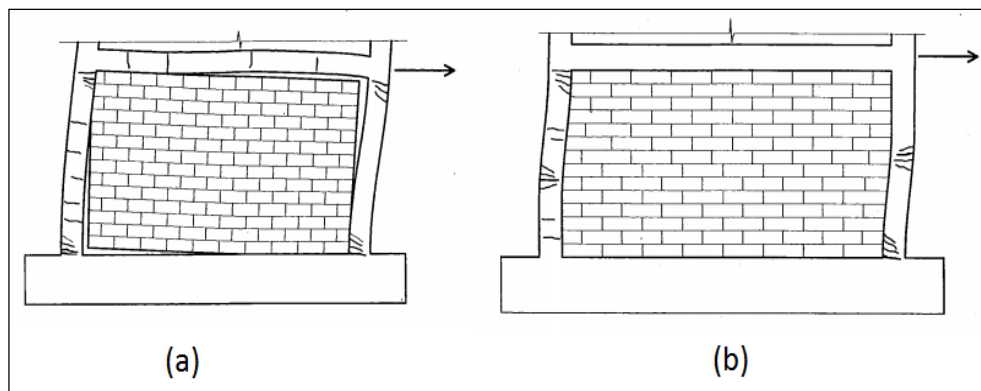
Figure 2-14. Flexural collapse mechanism with formation of plastic hinges at column ends (a) or along the column length (b) **(Crisafulli, 1997)**
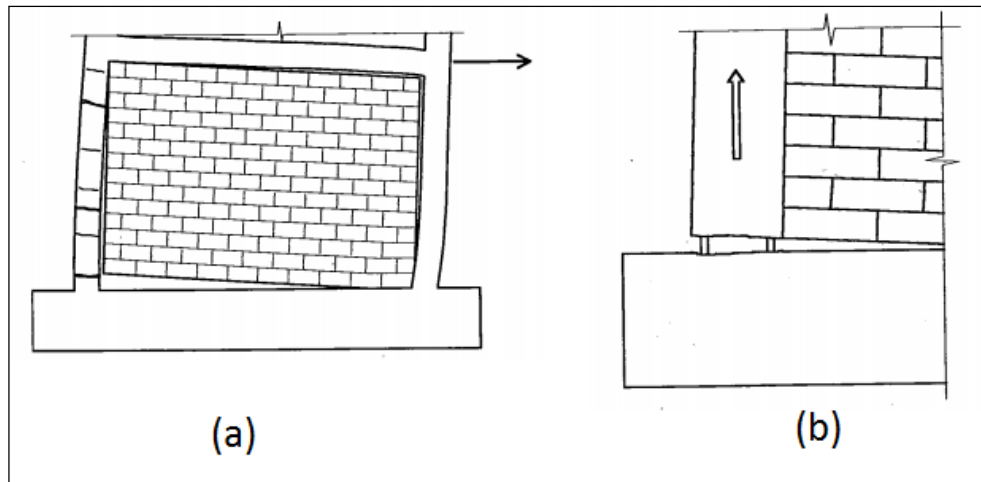
Figure 2-15. Tension failure of the column (a) and bar anchorage failure (b). (**Crisafulli, 1997**)

➢ **Shear Failure of the Columns**

As seen in Figure 2-6, there is a concentration of shear stresses at the loaded corners of the columns, along the contact length, due to the interaction with the infill at these regions. Shear resistance in the columns basically depends on transversal reinforcement, concrete strength and axial load. Although the compression column will have a higher shear resistance, it will also usually have the highest shear action. Figure 2-16a shows a typical shear failure taking place in column members.

➢ **Beam-Column Joint Failure**

Concentration of normal and shear stresses develop close to the loaded corners (Figure 2-6), hence inducing large shear and bending moments. Failure of the joint is a highly unfavourable situation, since it decreases the contact length, and therefore decreases the effective strut width, which results in an increase of the stresses on the masonry. It also decreases the effectiveness of load transfer between the floor beam and the columns and infill. During this failure, a diagonal crack appears at the beam column joint (Figure 2-16b).
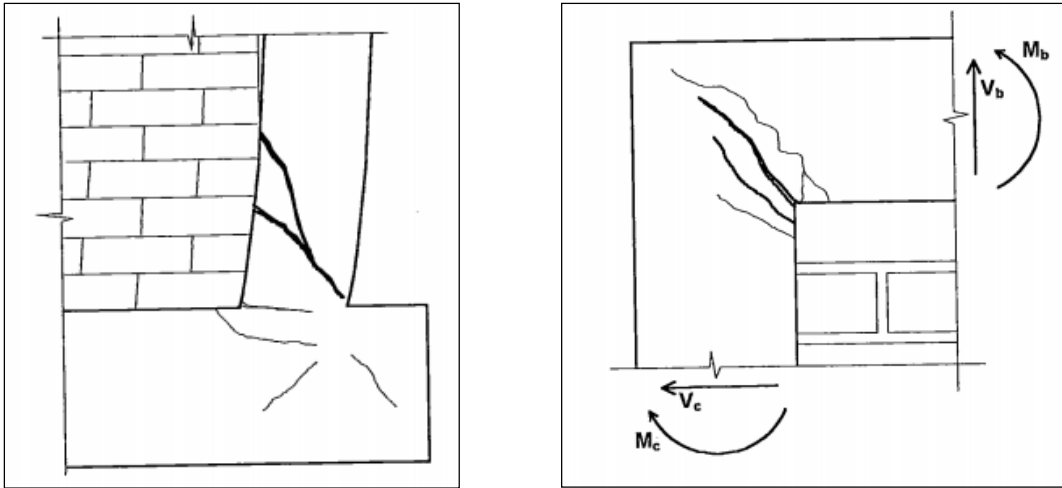
Figure 2-16. (a) Shear failure of the column. **(Crisafulli, 1997)**; **(b)**Beam-Column joint failure. **(Crisafulli, 1997)**

2.3.4 Analytical prediction of lateral resistance and stiffness

A simple analytical approach to quantify the lateral resistance of infilled frames without openings, in the absence of more refined experimental data, was proposed by (Mehrabi & Shing, Seismic Analysis of Masonry-Infilled Reinforced Concrete Frames, 2003). From all the failure mechanisms previously described, this method chooses 5 of them as the most probable ones, as shown in Figure 2-17. For each failure mode, the lateral resistance is obtained by analytical equations developed by (Mehrabi A. B., Shing, Schuller, & Noland, 1994). Finally, the mechanism that results in the lowest lateral resistance value is considered to be the predominant failure mechanism, and hence is considered the lateral load resistance value. This method is briefly described below. It is interesting to point out that, from the research carried out for several masonry infilled RC frames, the most common type of failure mechanism observed in experimental tests for weak infills corresponds to mechanism 5, where large slips along the bed joints and plastic hinges in the columns govern. On the other hand, for strong infills, mechanism 2 is the most common one, which is governed by the diagonal/sliding shear failure of the infill and the shear failure of the windward column.
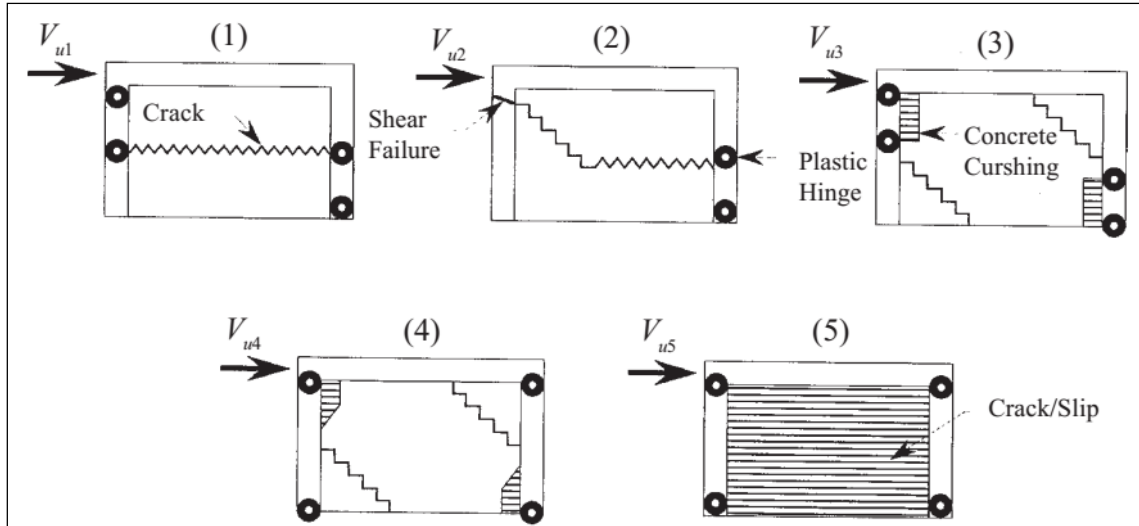
Figure 2-17. Selected failure mechanisms (**Mehrabi & Shing, Seismic Analysis of Masonry-Infilled Reinforced Concrete Frames, 2003**)
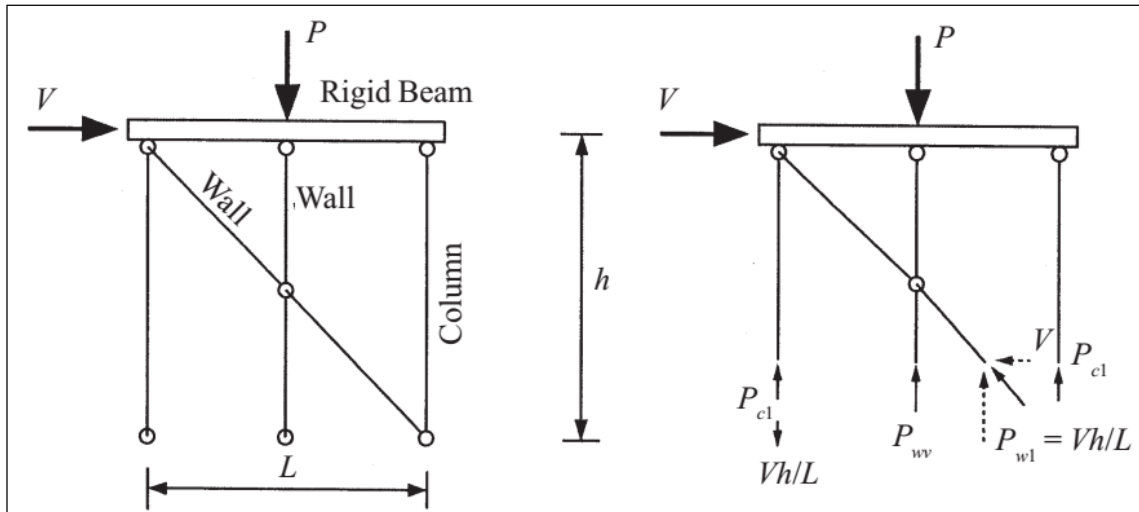
Figure 2-18. Vertical load distribution model (**Mehrabi & Shing, Seismic Analysis of Masonry-Infilled Reinforced Concrete Frames, 2003**)

2.3.4.1   Residual shear strength of cracked wall

The cracking load is evaluated through the model proposed by (Fiorato, Sozen, & Gamble, 1970) shown in Figure 2-18. The beam is rigid and the wall is represented by a diagonal and a vertical strut, which are connected by a hinge. P is the total vertical load, and V the total lateral load. As observed in Figure 2-18, P_{cl} corresponds to the axial force in the columns, due to P, P_{wv} is the axial load in the vertical strut due to P, and P_{wl} is the vertical component of the axial force in the diagonal strut due to P. Hence, for equilibrium, it must be:

$$P = 2P_{cl} + P_{wv} + P_{wl}$$

(**2-2**)

The cracking load is estimated by means of the Mohr-Coulomb criterion:

18

$$V_{wcr} = CA_w + \mu_0 P_w \qquad \text{(2-3)}$$

Where C is a cohesion factor, A_w the cross sectional area of the wall, μ_0 is the initial friction coefficient of masonry mortar joints, and P_w is the total axial load due to P on the wall.

$$P_w = P_{wv} + P_{wl} \qquad \text{(2-4)}$$

It is assumed that the two columns and the infill panel act as two springs in parallel, hence the total axial load is distributed according to their own axial stiffness.

$$P_{wv} = \frac{PA_w}{A_w + 2A_{ceq}} \qquad \text{(2-5)}$$

$$P_{wl} = V_{wcr}\frac{h}{l} \qquad \text{(2-6)}$$

Where:

- h = story height
- L = frame span length
- A_{ceq} = equivalent area of RC columns, in masonry = $A_c \frac{E_c}{E_w}$
- A_c = cross sectional area of RC column = $h_c b_c + A_s \left(\frac{E_s}{E_c} - 1\right)$
- E_c, E_w, and E_s = Elastic moduli of concrete, masonry and steel, respectively
- h_c, b_c = Plan dimensions of RC columns
- A_s = longitudinal rebar area in a column

By combining equations (2-3) - (2-6) the following expression can be derived for the residual shear strength of a cracked wall, V_{wr}:

$$V_{wr} = A_w \frac{\dfrac{\mu_r P}{A_w + 2A_{ceq}}}{1 - \mu_r \dfrac{h}{L}} \qquad \text{(2-7)}$$

The residual shear strength (V_{wr}) is obtained from the cracking load (V_{wcr}), by means of eliminating the cohesion factor (C), and replacing the initial friction coefficient (μ_0) for the residual friction coefficient (μ_r).

2.3.4.2 Crushing load

The crushing lateral load, which corresponds to the crushing of the diagonal compression masonry strut, can be obtained by means of the concept proposed by (Stafford, 1962).

$$V_{crush} = wtf'_m cos\theta$$

(**2-8**)

Where:

- f'_m = the compressive strength of masonry
- t = the wall thickness
- w = the effective strut width, determined by means of Figure 2-4
- θ = the angle between the diagonal strut and a horizontal line

2.3.4.3 Failure Mechanism 1 (shear failure)

The lateral resistance considered in mechanism 1 is the sum of the shear forces in the columns and the shear resistance of the wall, as seen in Figure 2-19. By force equilibrium in the horizontal direction, the lateral load resistance for mechanism 1 is computed as follows:

$$V_{u1} = V_{wr} + F_{cc} + F_{ct}$$

(**2-9**)

Where:

- V_{u1} = lateral load resistance for mechanism 1
- V_{wr} = residual shear strength of wall, obtained by equation (2-7)
- F_{cc} = shear force in leeward column
- F_{ct} = shear force in windward column

The expression for F_{cc} and F_{ct} are derived by moment equilibrium of the free body diagram in Figure 2-19, for each individual column segment, as follows:

$$F_{ct} = \frac{4M_{pct}}{h}$$

(**2-10**)

$$F_{cc} = \frac{4M_{pc}}{h}$$

(**2-11**)

Where:

- M_{pct} = the plastic moment developed in the windward column, considering the effect of the axial force
- M_{pc} = the plastic moment developed in the leeward column, not considering the effect of the axial force
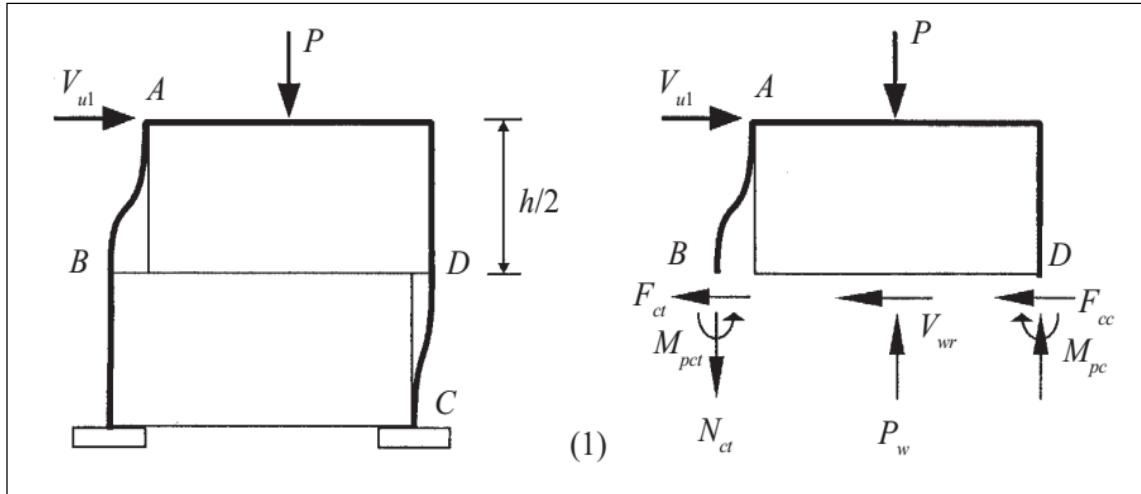
Figure 2-19. Failure mechanism 1 (**Mehrabi & Shing, Seismic Analysis of Masonry-Infilled Reinforced Concrete Frames, 2003**)

2.3.4.4 Failure Mechanism 2 (shear failure with inclined crack)

This mechanism is similar to the first one. However, the crack in the panel is conceived as a diagonal (Figure 2-20), and therefore, the residual stress is slightly modified. Also, the ultimate shear resistance is considered for the windward column (V_{ct}) instead of F_{ct}. It follows:

$$V_{u2} = V'_{wr} + F_{cc} + V_{ct}$$ (**2-12**)

Where:

- V_{u2} = lateral load resistance for mechanism 2
- V'_{wr} = residual shear resistance provided by the horizontal crack, as expressed in equation (2-13)
- F_{cc} = shear force in leeward column, as expressed in equation (2-11)
- V_{ct} = ultimate shear resistance of windward column, as expressed in equation (2-14)

$$V'_{wr} = A_w \frac{\dfrac{\mu_r P}{A_w + 2A_{ceq}}}{1 - 0.5\mu_r \dfrac{h}{L}}$$ (**2-13**)

$$V_{ct} = 0.8V_{cs} + V_{cc}$$ (**2-14**)

Where:

- V_{cs} = shear resistance provided by stirrups
- V_{cc} = shear resistance provided by concrete
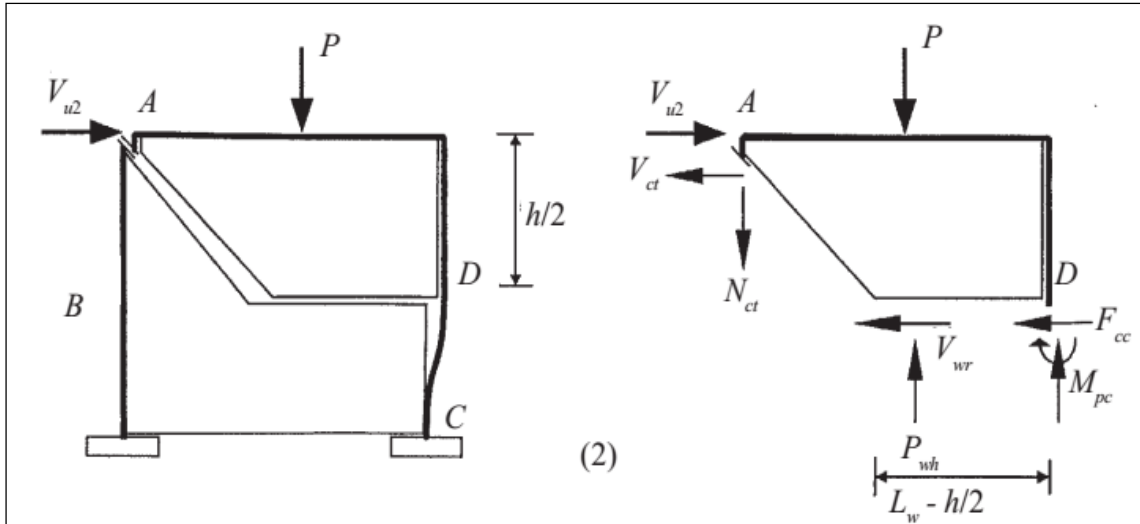
Figure 2-20. Failure mechanism 2 (**Mehrabi & Shing, Seismic Analysis of Masonry-Infilled Reinforced Concrete Frames, 2003**)

2.3.4.5   Failure Mechanism 3 (masonry crushing and plastic hinge formation)

In this mechanism, masonry is assumed to reach the crushing strength along the contact length "y" with the frame, and plastic hinges are assumed to form in the columns (near the beam-column joint, and in point b), as depicted in Figure 2-21. The stress is uniform along "y", so the whole segment AB is under plastic state of stress. Point "B" is the point of maximum moment, and hence, zero shear force. This approach was proposed by (Liuaw & Kwan, 1985).
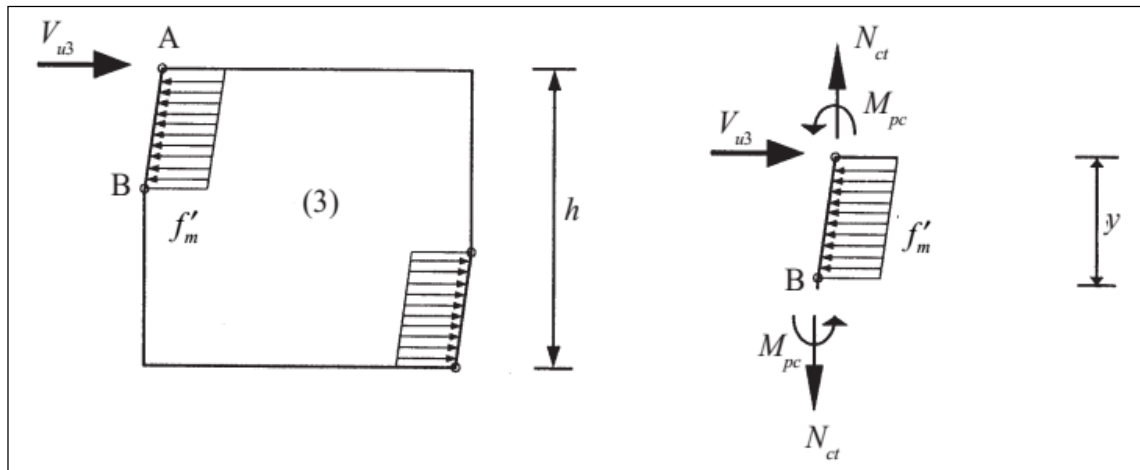
Figure 2-21. Failure mechanism 3 (**Mehrabi & Shing, Seismic Analysis of Masonry-Infilled Reinforced Concrete Frames, 2003**)

From moment equilibrium in segment AB:

$$\frac{f'_m t y^2}{2} = 2M_{pc} \tag{2-15}$$

Where:

- f'$_m$ = compressive strength of masonry
- M$_{pc}$ = plastic moment of the columns (neglecting axial force)
- t = wall thickness

Therefore, from equation (2-15), the contact length can be derived as:

$$y = \sqrt{\frac{4M_{pc}}{f'_m t}}$$ (**2-16**)

Finally, considering force equilibrium in the horizontal direction for the free body diagram of segment AB:

$$V_{u3} = y f'_m t$$ (**2-17**)

2.3.4.6 Failure Mechanism 4 (masonry crushing and plastic hinge formation)

Mechanism 4 is also based on plastic theory, and is proposed, similarly to the previous mechanism, by (Liuaw & Kwan, 1985). The difference in this method is that the plastic hinges are assumed to form at the ends of the columns (Figure 2-22), and the stress on the compressed masonry corners is assumed parabolic along the contact length (αh) because of the linear variation of strains, due to the rotation of the columns. Masonry is assumed to crush at the corners, where the parabolic stress reaches its maximum value.
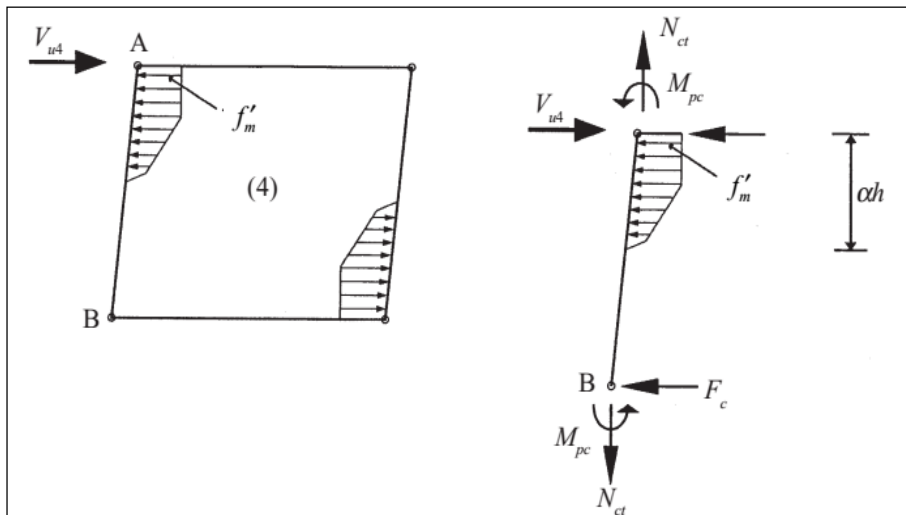
Figure 2-22. Failure mechanism 4 (**Mehrabi & Shing, Seismic Analysis of Masonry-Infilled Reinforced Concrete Frames, 2003**)

Computing moment equilibrium about point A in column AB:

$$F_c h + 0.25 f'_m t(\alpha h)^2 = 2M_{pc}$$ (**2-18**)

Where:

- F_c = shear force in each column

- M_{pc} = plastic moment of column AB, neglecting influence of axial force

Computing force equilibrium for column AB:

$$V_{u4} = 0.67 f'_m t\alpha h + 2F_c = (m_c^2 + 0.67\alpha - 0.5\alpha^2) f'_m th \qquad \text{(2-19)}$$

$$m_c = \sqrt{\frac{4M_p}{f'_m th_c^2}} \qquad \text{(2-20)}$$

The contact length (αh) was proposed by *Stafford Smith* in 1966 as follows:

$$\alpha h = \pi \sqrt[4]{\frac{E_c I_c h}{4 E_w t sin(2\theta)}} \qquad \text{(2-21)}$$

2.3.4.7   Failure Mechanism 5 (residual shear + flexure)

The last mechanism considers the frame and infill to act as two independent resistant members (Figure 2-23), working in parallel, with a displacement compatibility at the compressed corners. Therefore, the total lateral resistance is given by the sum of the residual shear resistance of the fractured wall, and the flexural resistance of the frame.

$$V_{u5} = V_{wr} + F_f \qquad \text{(2-22)}$$

Where:

- V_{u5} = lateral resistance of mechanism 5

- V_{wr} = residual shear resistance of fractured wall, obtained by equation (2-7)

- F_f = flexural resistance of the bare frame, with plastic hinges at column end sections, obtained by means of equation (2-23)

$$F_f = \frac{4M_{pc}}{h} \qquad \text{(2-23)}$$
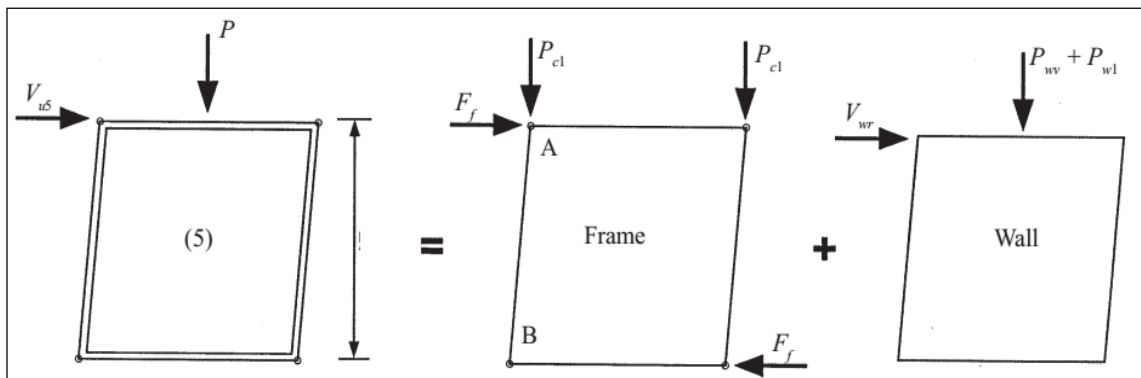
Figure 2-23. Failure mechanism 5 (**Mehrabi & Shing, Seismic Analysis of Masonry-Infilled Reinforced Concrete Frames, 2003)**

2.3.5 Behaviour of infilled RC frames under cyclic loading

According to (Kakaletsis & Karayannis, 2008) it has been shown that the total energy dissipation capacity of a masonry infilled RC frame is around 1.5 times larger than that of a bare frame subjected to the same cyclic loading. This is depicted in Figure 2-24. Another interesting fact is that the loss of strength is smaller than the corresponding loss of energy dissipation. This is due to the noticeable pinching effect.

With reference to the initial stiffness, the one of the infilled frame is approximately 2.5 times larger than the initial stiffness of the bare frame. This can be seen by comparing initial slopes in the diagrams depicted in Figure 2-24(a) and (c).

Various methods have been used to calculate the energy dissipation capacity based on results acquired from cyclic tests. For this purpose, (Valiasis & Stylianidis, 1989) introduced a parameter which is defined as "energy dissipated by cycle divided by corresponding total displacement of the cycle". Tests were conducted on bare frames and masonry infilled ones. Results are shown in Figure 2-25. It can be seen that the energy per unit of total displacement dissipated by the bare frame grows during the whole experiment, while for the infilled frame, a sudden drop can be observed in the range of large displacements (due to masonry degradation). In other words, in the range of large lateral displacements, behaviour of an infilled frame tends to be similar to the behaviour of a bare frame. Regardless of this, energy dissipation of an infilled frame is still considerably larger than that of a bare frame.
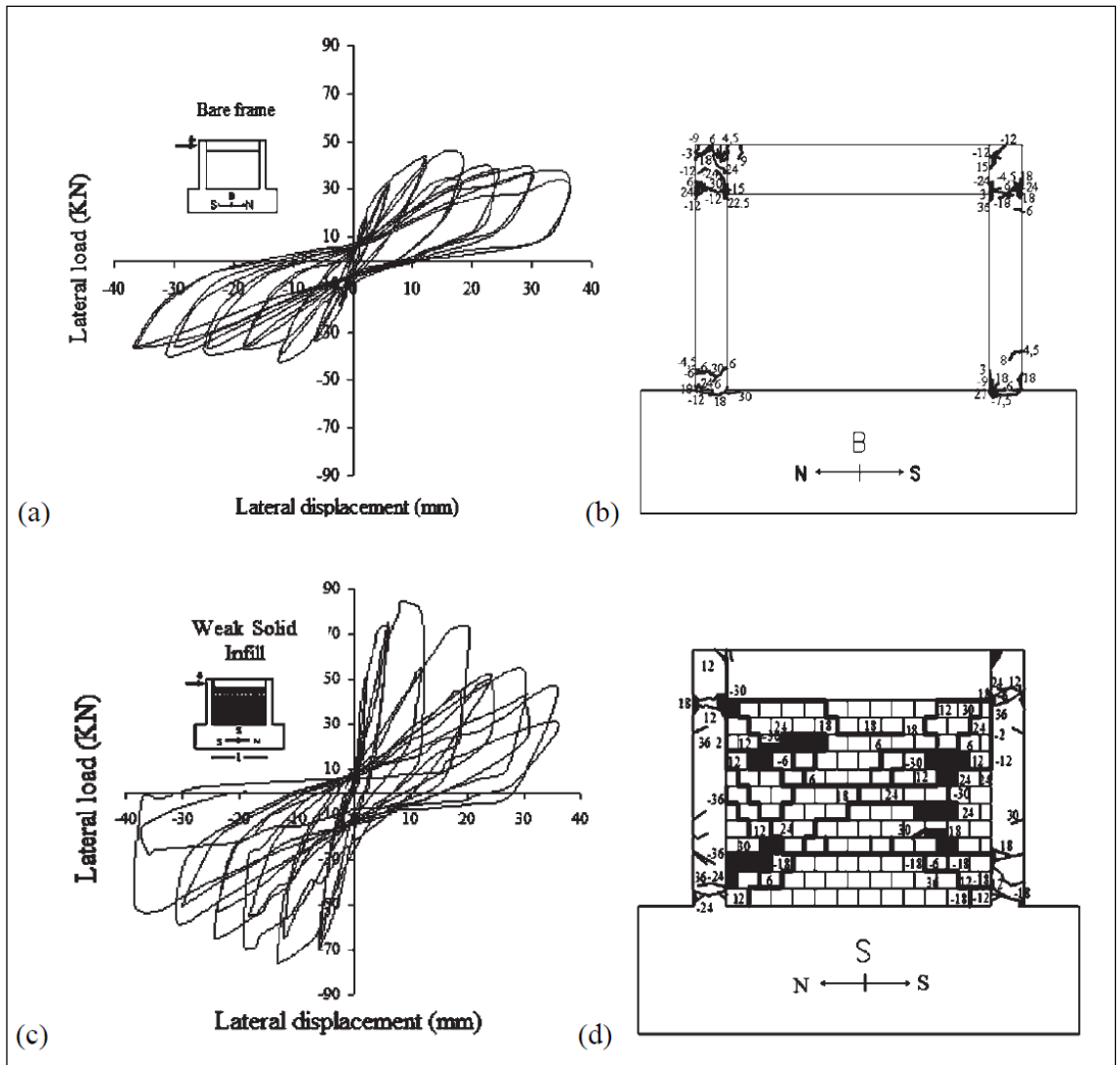
Figure 2-24. Lateral load-displacement hysteresis curves and failure modes of a bare frame (a) (b) and a masonry infilled RC frame (c) (d) (**Kakaletsis & Karayannis, 2008**)
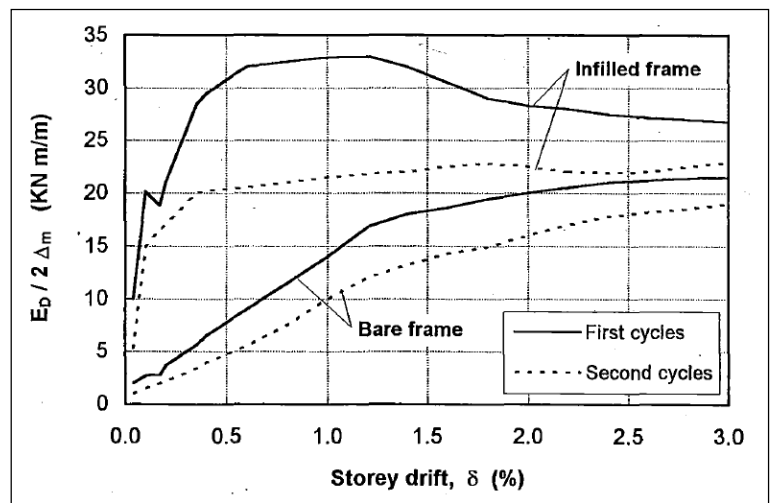
Figure 2-25. Energy dissipated per cycle (**Valiasis & Stylianidis, 1989**)

2.4   RC FRAME WITH SLIGHTLY REINFORCED MASONRY INFILL

2.4.1 Introduction

As mentioned above, since masonry infills are often conceived as non-structural elements, they are most of the times unreinforced. However, it has been shown that adding light reinforcing to the panels can dramatically improve the performance of the infilled frame (Calvi, Bolognini, & Penna, 2004).

Steel reinforcing could be placed either in the bed joints, or as a wire mesh between the infill and the plaster, with no continuity between the steel in the infill and the surrounding RC frame (Figure 2-26). The external mesh option uses roughly twice the amount of steel than the bed joint reinforcing, but gives, according to research tests, the best results in terms of ductility and post-peak behaviour.

Out of plane expulsion is a topic of interest for masonry infilled RC frames. Although the wall can continue to carry load after expulsion, this is considered a dangerous situation for human safety, and should therefore be considered as an Ultimate Limit State situation. Slight reinforcing of the infill greatly improves the out-of-plane resistance, and therefore, expulsion occurs at much higher values of loading.

Reinforcing of infill panels affects mostly the post-peak behaviour of infilled frames. For this reason, there is not much difference in the behaviour for low damage situations in comparison to the unreinforced infills. However, for significant damage limit states (at significant drift values), the slight reinforcement gives a remarkably superior behaviour.
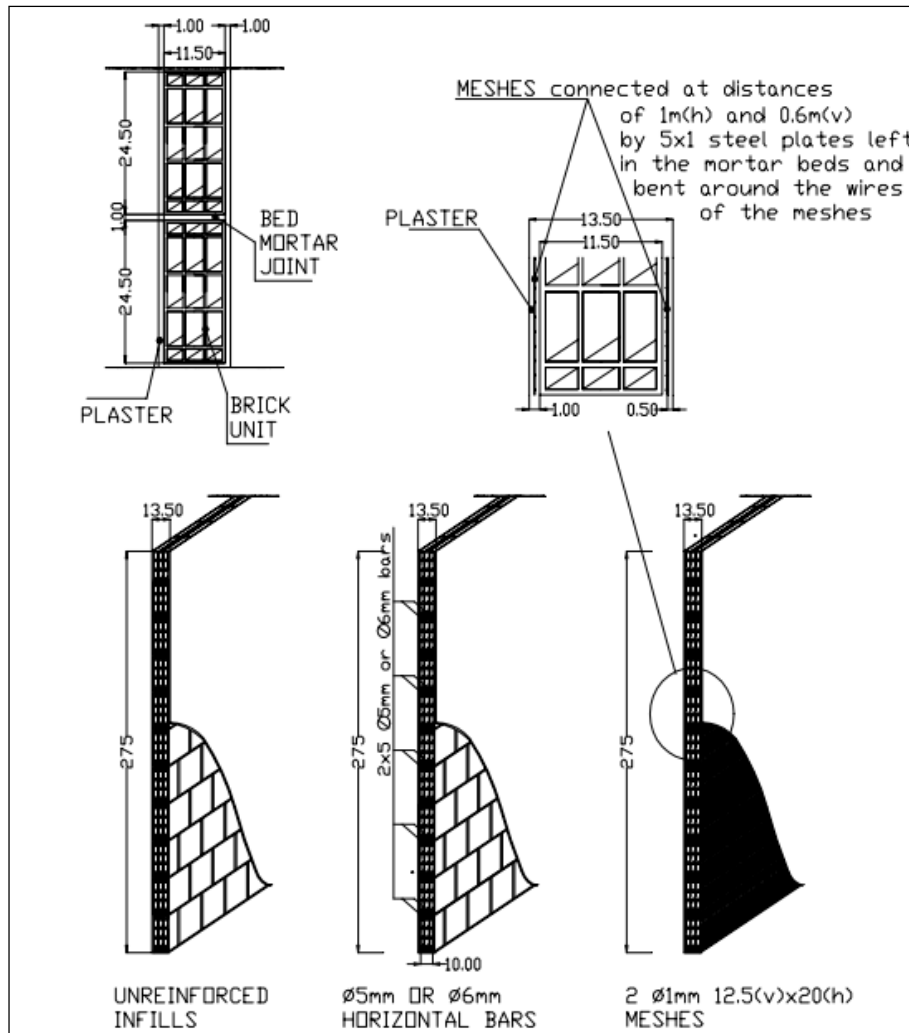
Figure 2-26. Details of reinforcing of the masonry panel **(Calvi, Bolognini, & Penna, 2004)**

2.4.2 Modelling and analysis

Modelling of slightly reinforced infilled frames has been carried out, according to (Calvi, Bolognini, & Penna, 2004), with Takeda-type non-linear elements for beams and columns (which account for concrete cracking and yielding of steel rebars), and using an equivalent diagonal compression strut for the infill panel, with an effective width of 25% of the length of the strut, and force-displacement curves which have been derived from experimental data.

Non-linear analysis was carried out by means of a pushover analysis. Numerical results are in good agreement with the experimental ones, and show how adding a slight amount of reinforcement can have a positive impact on the overall structural response. Also, different ways of reinforcing give different responses and are characterized by different ductility level as represented in Figure 2-27.
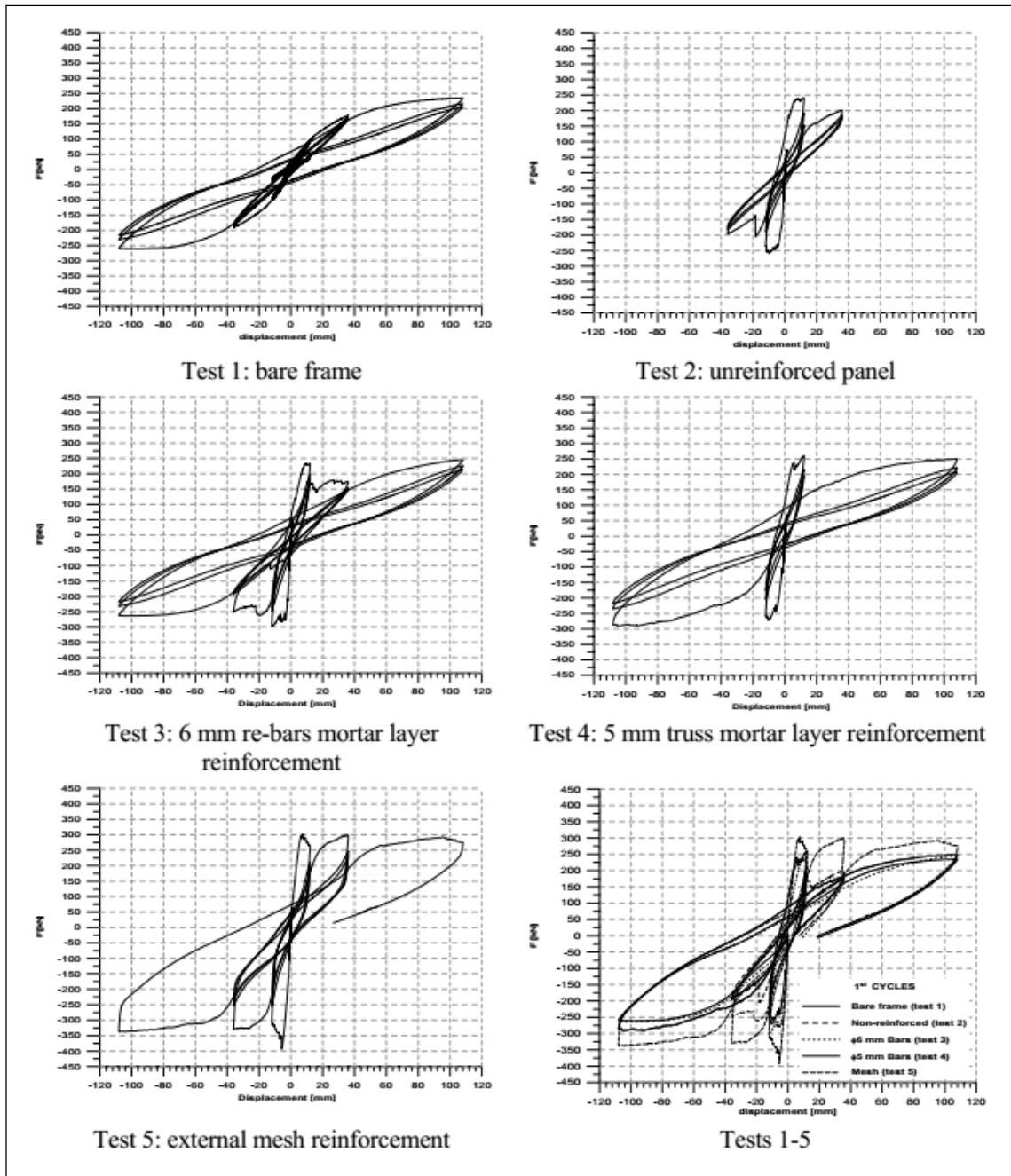
Figure 2-27. Hysteretic loops for different types of reinforcing (**Calvi, Bolognini, & Penna, 2004**)

2.5 COMPARISON OF THE BARE FRAME VS. MASONRY INFILLED FRAME BEHAVIOUR UNDER MONOTONIC LOADING

As from the surveyed literature studies, some common general conclusions can be highlighted.

- The masonry infill has a non-negligible influence on the overall structural response of the frame under lateral loading.
- Its influence is more relevant under low horizontal loading, when the masonry is not fully cracked.
- It can be observed from experimental cyclic tests, that the initial stiffness is always much greater for an infilled frame vs. the bare frame.
- Eventually, at large drifts, the response always tends to the one of the bare frame.
- Serious "pinching" of the hysteresis loops can occur in an infilled frame when it is not reinforced
- Adding a slight amount of steel reinforcement improves the post-peak behaviour and out of plane resistance.
- If adequately designed, the masonry infill is always beneficial in terms of stiffness and energy dissipation vs. the bare frame.

Chapter 3

Prediction of ultimate load via analytical method

A simplified analytical approach that quantifies the lateral resistance of masonry infilled frames, proposed by (Mehrabi & Shing, Seismic Analysis of Masonry-Infilled Reinforced Concrete Frames, 2003) was described in section 2.3.4. The method has been used in this research for the initial estimation of the lateral resistance of polystyrene infilled frames. It is recalled that the method foresees five different possible failure modes in which the infilled frame may fail, out of which the lowest value is the one governing the ultimate resistance (Figure 3-1).

Figure 3-1. Possible failure mechanisms considered (**Mehrabi & Shing, Seismic Analysis of Masonry-Infilled Reinforced Concrete Frames, 2003)**

3.1 DESCRIPTION OF THE EXPERIMENTAL SPECIMEN

The frame under study has the geometrical characteristics depicted in Figure 3-2 and Figure 3-3. For the purpose of estimating the lateral load capacity, also some mechanical properties are required (Table 3.1 and Table 3.2). These vales have been acquired from

Eurocode 2 (for concrete) and through some internet research (for polystyrene). Value of elastic modulus of concrete was calculated using equation (3-1) provided by EC2 with the value of f_{cm} = 28 MPa for concrete C20/25.

$$E_c = 22 \cdot [f_{cm}/10]^{0.3} = 29.96 \text{ GPa}$$

(3-1)

It should be noted that this particular frame has no additional vertical axial load acting on it, and therefore the axial load on columns (P_{cl}) is only due to the frame self-weight. Similarly, the axial load acting on the infill is only due to its own self-weight (P_{wv}). An iterative process was performed in order to determine the lateral load resistance, since some of the failure modes require the total axial load on the columns, which depends on the horizontal load (V), due to frame action.
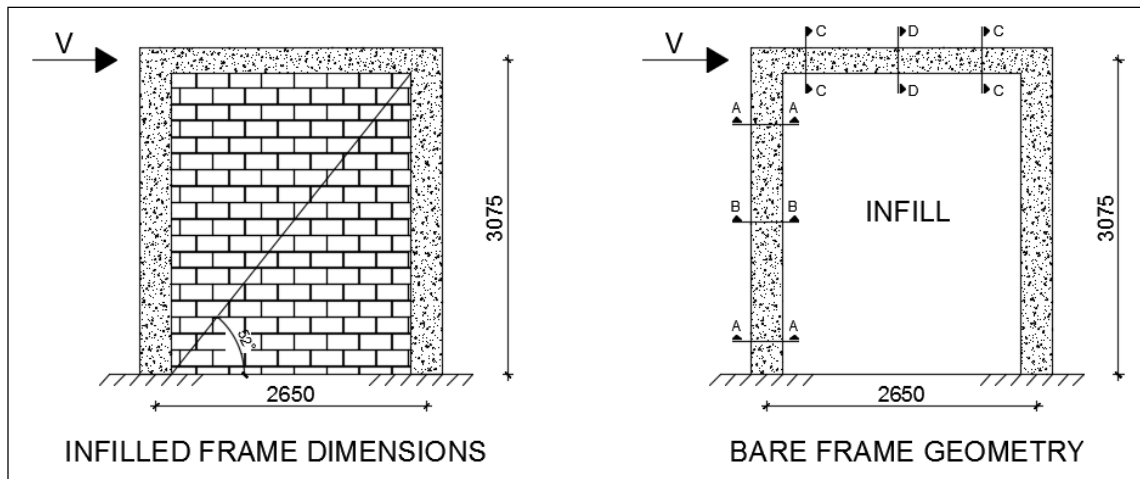
Figure 3-2. Infilled frame geometry
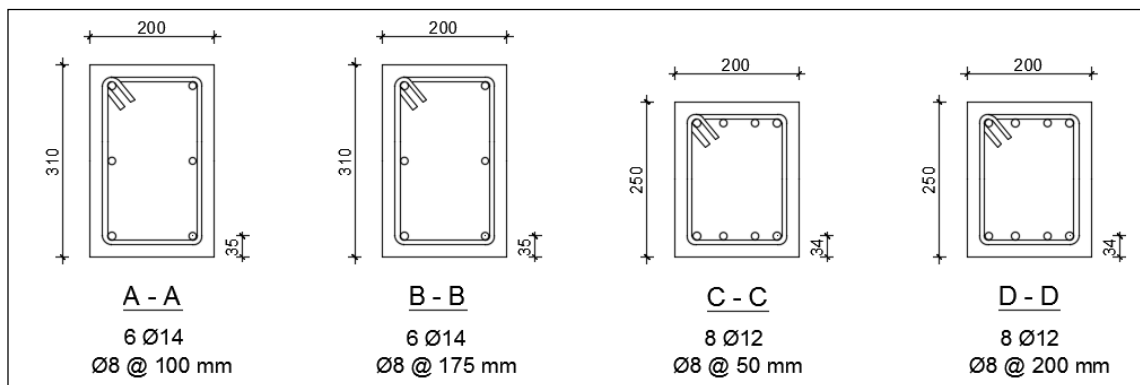
Figure 3-3. Beam and column cross sections

Table 3.1. Material mechanical properties of infilled frame components

	E_c [GPa]	29.96	Concrete Elastic Modulus
	E_p [MPa}	4.35	Polystyrene Elastic Modulus
	E_s [GPa}	210	Steel Elastic Modulus
	f_{pk} [MPa]	0.12	Polystyrene characteristic compressive strength
Material Mechanical Properties	f_{ck} [MPa]	20	Concrete characteristic compressive strength
	f_{yk} [MPa]	450	Steel rebar characteristic tensile strength
	μ_0	0.5	Polystyrene initial friction Coefficient
	μ_r	0.15	Polystyrene residual friction Coefficient
	ρ_c [kN/m3]	25	Reinforced concrete density
	ρ_p [kN/m3]	10.4	Polystyrene density

Table 3.2. Frame geometry and loads

	h [m]	3.075	Height
	L [m]	2.65	Length
	θ [°]	52	Strut angle
	D [m]	4.06	Diagonal length
	w/D	0.25	Assumed compression strut width ratio
	w [m]	1.01	Compression strut width
	V [kN]	70	Total Expected Horizontal Load
	P [kN]	27.20	Total Vertical Load
	h_c [m]	0.31	Column dimensions
	b_c [m]	0.2	Column dimensions
	d [m]	0.276	Concrete column inner lever arm
Geometry and loads	I [m^4]	0.00050	Concrete column moment of inertia
	t_w [m]	0.2	Infill thickness
	A_s [mm^2]	1231.5	Longitudinal steel area in columns
	A_{st} [mm^2]	100.531	Transverse steel area in columns
	s [mm]	175	Stirrup spacing close to mid-height of column
	A_w [m^2]	0.468	Infill Area in horizontal plane
	A_c [m^2]	0.069	Column Area
	A_{ceq} [m^2]	1.04	Equivalent area of RC columns in polystyrene
	P_{wv} [kN]	14.36	Axial load in vertical strut due to P (self-weight)
	P_w [kN]	14.36	Total axial load due to P on the wall
	P_{cl} [kN]	6.42	Total axial load due to P on each column
	V*h/L [kN]	81.23	Total axial load due to V on the columns

Once convergence was reached, the axial load contribution on columns due to the lateral load (V) was taken into account for the computation of the plastic moment capacity of the columns, as well as their shear capacity. For this task an interaction diagram was computed for the columns, which is shown in Figure 3-4, and was used with the respective axial load for each column.
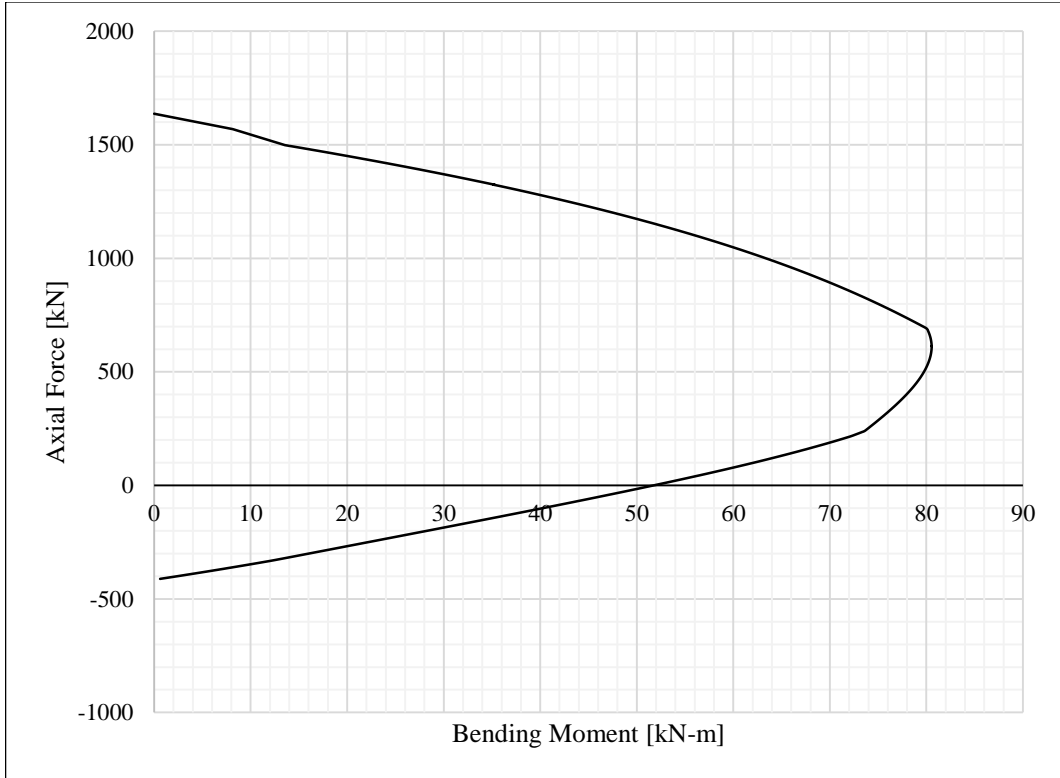
Figure 3-4. Interaction diagram for the columns

3.2 FAILURE MECHANISM 1

Following the procedure explained in section 2.3.4.3, the lateral load resistance due to failure mechanism 1 corresponds to the sum of the shear forces in the columns and the shear resistance of the wall (Figure 3-5), and was computed as follows.

$$V_{u1} = V_{wr} + F_{cc} + F_{ct}$$
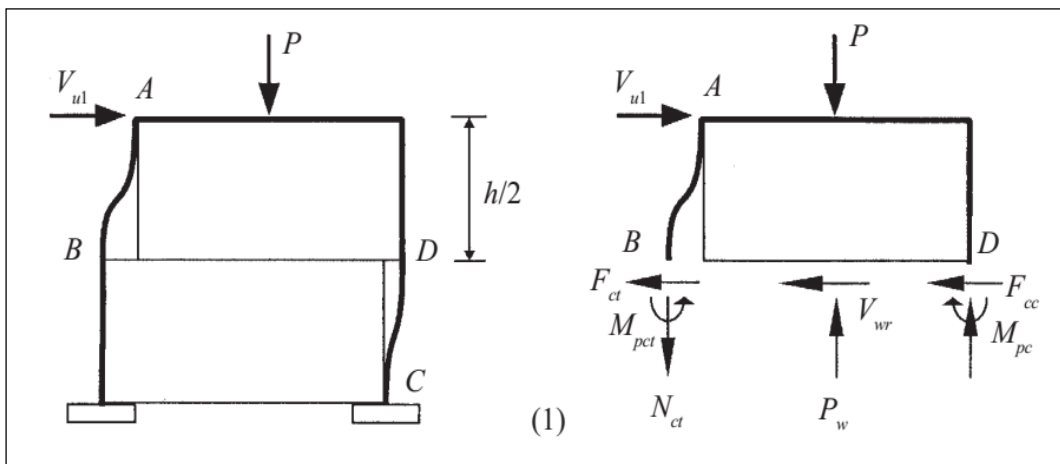
Figure 3-5. Failure mechanism 1 (**Mehrabi & Shing, Seismic Analysis of Masonry-Infilled Reinforced Concrete Frames, 2003**)

$$V_{wcr} = CA_w + \mu_0 P_w$$

$$V_{wr} = \mu_r P_w$$

$$P_w = P_{wv} + P_{wl}$$

$$P_{wv} = 14.36 \ kN$$

$$P_{wl} = V_{wcr} \frac{h}{l}$$

By combining the previous equations, substituting μ_0 for μ_r, and considering C=0, the following expression is obtained for the residual shear strength.

$$V_{wr} = \frac{\mu_r P_{wv}}{1 - \mu_r \dfrac{h}{L}} = \frac{0.15 \cdot 14.36}{1 - 0.15 \cdot \dfrac{3.075}{2.65}} = 2.61 \ kN$$

It now follows to compute the shear force in windward and leeward columns.

$$F_{ct} = \frac{4M_{pct}}{h} \qquad\qquad F_{cc} = \frac{4M_{pc}}{h}$$

The plastic moment on both columns was determined from the interaction diagram in Figure 3-4, with the corresponding axial load on each column (neglecting axial load contribution of "V" in leeward column, and considering the contribution of "V" in windward column).

$$M_{pct} = \ 45.77 \ kN \cdot m \qquad\qquad M_{pc} = 52.34 \ kN \cdot m$$

$$F_{ct} = \frac{4 \cdot 45.77}{3.075} = 59.54 \ kN \qquad\qquad F_{cc} = \frac{4 \cdot 52.34}{3.075} = 68.08 \ kN$$

The lateral load capacity is calculated as follows.

$$\boldsymbol{V_{u1} = V_{wr} + F_{cc} + F_{ct} = 2.61 + 59.54 + 68.08 = 130.23 \ kN}$$

3.3 FAILURE MECHANISM 2

Following the procedure explained in section 2.3.4.4, the lateral load resistance due to failure mechanism 2 was computed. The failure mechanism corresponds to the sum of a slightly modified residual shear stress of the wall (because of the diagonal crack), the ultimate shear resistance in windward column, and the shear force in leeward column (Figure 3-6).

$$V_{u2} = V'_{wr} + F_{cc} + V_{ct}$$
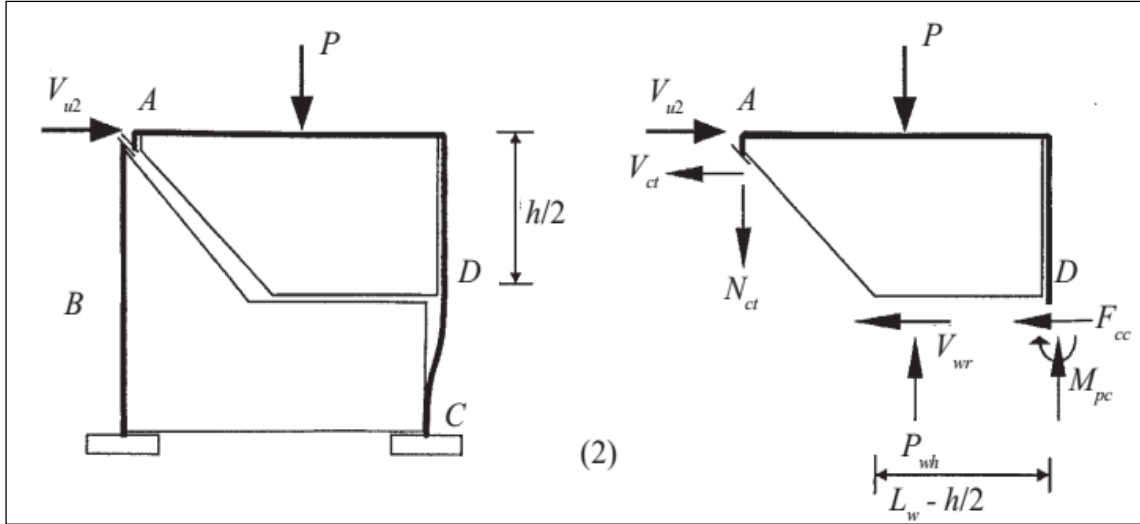
Figure 3-6. Failure mechanism 2 (**Mehrabi & Shing, Seismic Analysis of Masonry-Infilled Reinforced Concrete Frames, 2003**)

$$V'_{wr} = \frac{\mu_r P_{wv}}{1 - 0.5\mu_r \frac{h}{L}} = \frac{0.15 \cdot 14.36}{1 - 0.5 \cdot 0.15 \cdot \frac{3.075}{2.65}} = 2.36 \; kN$$

$$V_{ct} = 0.8V_{cs} + V_{cc}$$

The shear resistance of concrete column was calculated according to EN 1992-1-1:2004, section 6.2.2. Calculations are presented below

$$V_{cc} = \left[C_{Rd,c}k(100\rho_1 f_{ck})^{1/3} + k_1\sigma_{cp}\right]b_w d$$

$$= \frac{\left[0.12 \cdot 1.85 \cdot (100 \cdot 0.002 \cdot 25)^{\frac{1}{3}} - 0.15 \cdot 0.48\right] 200 \cdot 276}{1000}$$

$$= 37.96 \; kN$$

Where:

$C_{Rd,c}$ =	0.12	- concrete shear calculation coefficient	
K =	$1 + \sqrt{\dfrac{200}{d}} = 1.85$	- concrete shear calculation coefficient	
k1 =	0.15	- concrete shear calculation coefficient	
ρ_1 =	0.02	- longitudinal steel area ratio	
σ_{cp} =	-0.48	- axial stress due to design gravity loads (negative in tension)	
v_{min} =	0.39	- concrete shear calculation coefficient	

The minimum value for the shear resistance of concrete is calculated as:

$$V_{cc,min} = (v_{min} + k_1\sigma_{cp})b_w d = \frac{(0.39 - 0.15 \cdot 0.48)200 \cdot 276}{1000} = 17.55 \; kN$$

$$\therefore V_{cc} = 37.96 \; kN$$

36

The shear resistance of stirrups was calculated according to EN 1992-1-1:2004, section 6.2.3. Calculations are presented below. An angle for the compression strut $\theta = 45°$ was assumed for this calculation.

$$V_{cs} = \frac{A_{st}}{s} z f_{yd} \cot\theta = \frac{\frac{100.531}{175} \cdot (276) \cdot 391.3 \cdot 1}{1000} = 62 \; kN$$

The maximum shear force provided by stirrups is limited by the following expression.

$$V_{Rd,max} = \frac{\alpha_{cw} b_w z v_1 f_{cd}}{\cot\theta + \tan\theta} = \frac{1 \cdot 200 \cdot 276 \cdot 0.6 \cdot 11.33}{\cot(45°) + \tan(45°)} \cdot \frac{1}{1000} = 187.63 \; kN$$

V_{cs} is used since it is lesser than $V_{Rd,max}$.

$$\therefore V_{cs} = 62 \; kN$$

It is now possible to compute the ultimate shear resistance of the windward column.

$$V_{ct} = 0.8 V_{cs} + V_{cc} = 0.8 \cdot 62 + 37.96 = 87.60 \; kN$$

It now follows to sum all the contributions together in order to determine the capacity of failure mechanism 2.

$$\boldsymbol{V_{u2} = V'_{wr} + F_{cc} + V_{ct} = 2.36 + 68.08 + 87.60 = 158.04 \; kN}$$

3.4 FAILURE MECHANISM 3

Following the procedure explained in section 2.3.4.5, the lateral load resistance due to failure mechanism 3, which corresponds to crushing of the infill along the contact length, and plastic hinges formation on columns, near to beam-column joint and point B (Figure 3-7), was computed as follows:
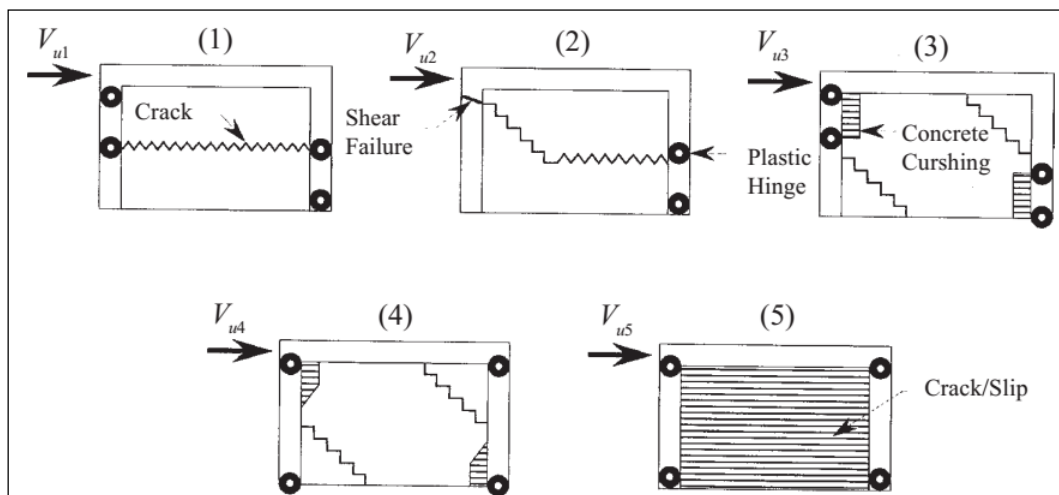
$$V_{u3} = y f_{pk} t$$
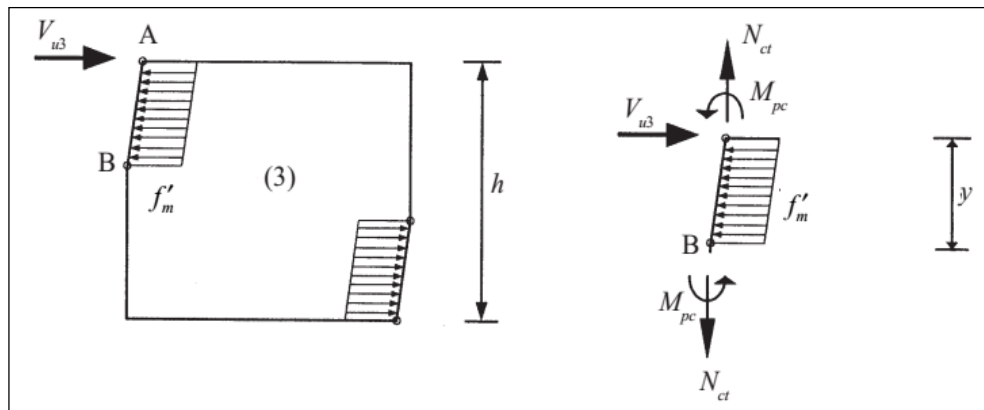
Figure 3-7. Failure mechanism 3 (**Mehrabi & Shing, Seismic Analysis of Masonry-Infilled Reinforced Concrete Frames, 2003**)

The contact length between infill and frame is calculated first.

$$y = \sqrt{\frac{4M_{pc}}{f_{pk} \cdot t}} = \sqrt{\frac{4 \cdot 52.34 \cdot 1000 \cdot 1000}{0.12 \cdot 200}} \cdot \frac{1}{1000} = 2.95 \, m$$

It now follows to compute the lateral load resistance due to failure mechanism 3.

$$V_{u3} = yf_{pk}t = \frac{2950 \cdot 0.12 \cdot 200}{1000} = 70.88 \, kN$$

3.5 FAILURE MECHANISM 4

Following the procedure explained in section 2.3.4.6, the lateral load resistance due to failure mechanism 4 was computed. This failure mode is quite similar to the previous case, but the plastic hinges are assumed to occur at the base of the column (point B in Figure 3-8), and the distribution of stresses along the contact length is assumed to be parabolic.

$$V_{u4} = 0.67f_{pk}t\alpha h + 2F_c$$
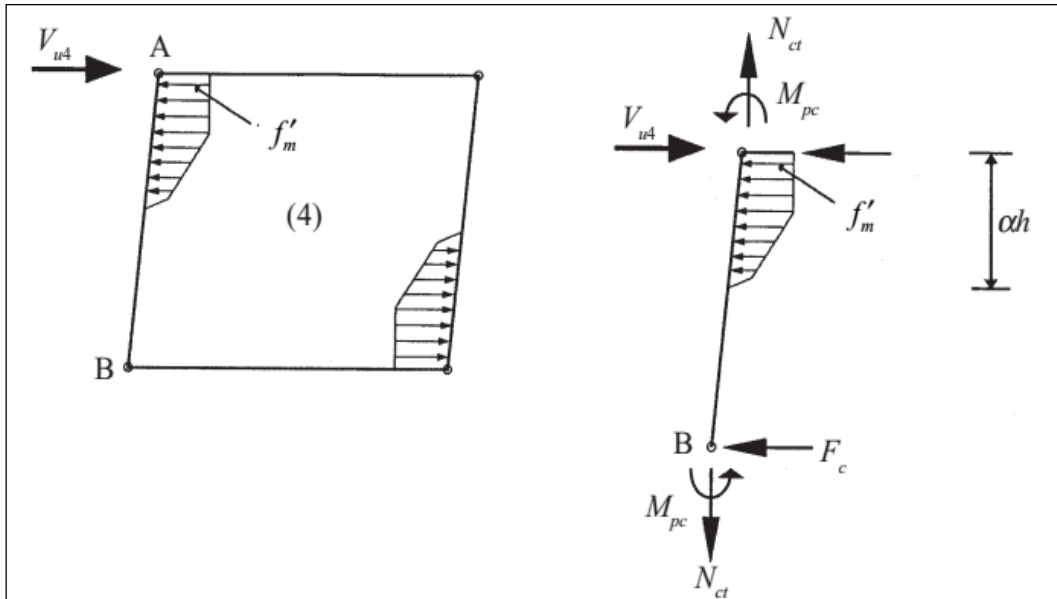
Figure 3-8. Failure mechanism 4 (**Mehrabi & Shing, Seismic Analysis of Masonry-Infilled Reinforced Concrete Frames, 2003**)

The contact length between infill and frame is calculated first.

$$\alpha h = \pi \sqrt[4]{\frac{E_c I_c h}{4E_w t sin(2\theta)}} = \pi \sqrt[4]{\frac{30 \cdot 0.0005 \cdot 3.075}{4 \cdot 4.35 \times 10^{-3} \cdot 0.2 \cdot sin(2 \cdot 52)}} = 6.04 \, m$$

Since the computed contact length is bigger than the structure, the contact length will be limited to the height of the infill $\alpha h = 2.95m$.

Next, the shear force in each column is computed.

$$F_c h + 0.25 f_{pk} t (\alpha h)^2 = 2M_{pc} \quad \rightarrow \quad F_c = \frac{2M_{pc} - 0.25 f_{pk} t (\alpha h)^2}{h}$$

$$F_c = \frac{2 \cdot 52.34 - 0.25 \cdot 0.12 \cdot 1000 \cdot 0.2 \cdot 2.95^2}{3.075} = 17.06 \; kN$$

Now it is possible to determine the lateral resistance of the frame due to failure mechanism 4.

$$\boldsymbol{V_{u4} = 0.67 f_{pk} t \alpha h + 2F_c = 0.67 \cdot 0.12 \cdot 1000 \cdot 0.2 \cdot 2.95 + 2 \cdot 17.06 = 81.56 \; kN}$$

3.6 FAILURE MECHANISM 5

Following the procedure explained in section 2.3.4.7, the lateral load resistance due to failure mechanism 5 was computed. The resistance is composed by the sum of the residual shear resistance of the fractured wall and the flexural resistance of the frame (Figure 3-9). This type of failure mechanism has been observed to occur more often in the case of weak infills. Since polystyrene is much weaker than masonry, it is expected to govern.

$$V_{u5} = V_{wr} + F_f$$
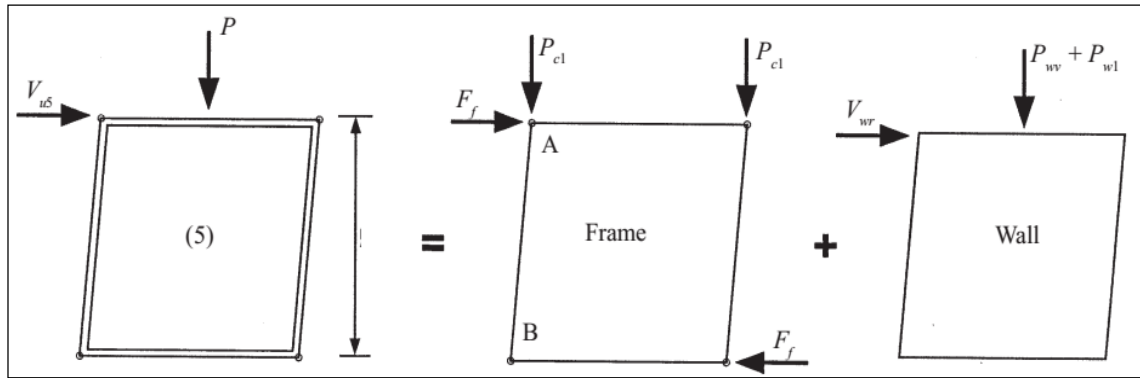
Figure 3-9. Failure mechanism 5 (**Mehrabi & Shing, Seismic Analysis of Masonry-Infilled Reinforced Concrete Frames, 2003**)

The flexural resistance of the bare frame, with plastic hinges at the column end sections, is calculated first.

$$F_f = \frac{4M_{pc}}{h} = \frac{4 \cdot 52.34}{3.075} = 68.08 \; kN$$

The lateral load resistance due to failure mechanism 5 is now computed.

$$\boldsymbol{V_{u5} = V_{wr} + F_f = 2.61 + 68.08 = 70.69 \; kN}$$

3.7 SUMMARY

A summary of results is presented in Table 3.3.

Table 3.3. Summary of lateral resistance for the 5 failure mechanisms

	Vu1 [kN]	130.23	Lateral resistance for mechanism 1
	Vu2 [kN]	158.04	Lateral resistance for mechanism 2
Summary of results	Vu3 [kN]	70.88	Lateral resistance for mechanism 3
	Vu4 [kN]	81.56	Lateral resistance for mechanism 4
	Vu5 [kN]	70.69	Lateral resistance for mechanism 5
	Vu [kN]	70.69	Lateral resistance

It can be seen from Table 3.3 that, as expected, failure mechanism 5 is governing the lateral resistance of the infilled frame.

3.8 SENSITIVITY ANALYSIS

While the geometrical properties of the infilled frame were measured with sufficient accuracy, the mechanical properties could vary to some extent. This is due to the fact that no laboratory tests were carried out in order to determine the mechanical properties of the polystyrene infill, nor of concrete, depicted in Table 3.1. Typical values for concrete class C20/25 were assumed. In the case of polystyrene, typical values found in the literature were adopted in order to use the analytical equations in section 2.3.4.

A sensitivity analysis was carried out, in order to quantify the possible variation in the failure loads due to variation of the mechanical properties, according to the analytical method. From this analysis it is possible to quantify how each of these parameters will influence the final result, by varying only one parameter at a time, and comparing it to the "reference" case, which is the one depicted in Table 3.3. Several parameters, such as compressive strength, elastic modulus, strut width ratio, and residual friction coefficient were investigated.

3.8.1 Residual friction sensitivity analysis

The residual friction coefficient is a parameter which is used for the determination of the residual shear strength of the cracked wall, as shown in section 2.3.4.1. The residual shear strength is used in failure mechanisms 1, 2 and 5, and therefore will be the only ones

affected by the variation of the residual friction coefficient. This parameter cannot be greater than the initial friction coefficient, but must be greater than 0. For this reason, the range of variation for the residual friction coefficient is determined as:

$$0 \leq \mu_r \leq \mu_0 \qquad\qquad \mu_0 = 0.5$$

From Figure 3-10 it can be observed that failure mechanism 3 and 4 are not affected by the variation of the residual friction coefficient, as they don't depend on it. Failure mechanisms 1 and 2 are affected, but don't govern the lateral load resistance, as failure mechanism 5 is still governing. Failure mechanism 5 shows a considerable range of values due to the variation of this parameter, as shown below.

$$68.1\ kN \ \leq V_{u5} \leq 85.2\ kN$$

Due to the fact that failure mechanism 5 does not govern the lateral load resistance when $\mu_r = 0.5$, the global capacity is governed by failure mechanism 3 when the residual friction coefficient adopts very high values. The range of possible values for the lateral load capacity, due to a variation of the residual friction coefficient, is shown below, which is governed by failure mechanism 5 for low values of residual friction coefficient, and by failure mechanism 3 for high values.

$$68.1\ kN \ \leq V_u \leq 70.9\ kN$$

	1	2	3	4	5
REFERENCE	130.2	158.0	70.9	81.6	70.7
$\mu 0 = \mu r$	144.7	165.8	70.9	81.6	85.2
$\mu r = 0$	127.6	155.7	70.9	81.6	68.1
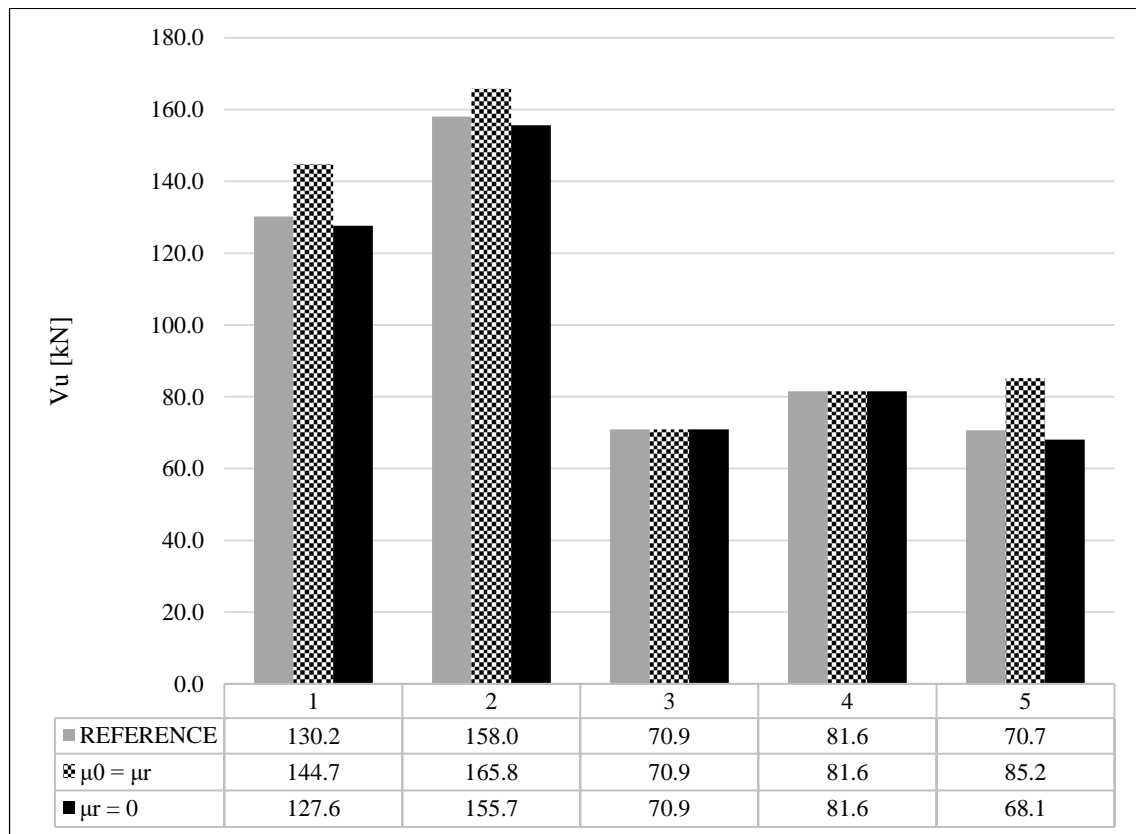
Figure 3-10. Sensitivity analysis for residual friction coefficient

3.8.2 Elastic Modulus sensitivity analysis

A similar analysis as the one performed in section 3.8.1 was carried out for the polystyrene infill elastic modulus (E_p). The range of possible values studied was based on the range of values found in the literature, and is shown below.

$$2.0 \; MPa \; \leq E_p \leq 7.0 \; MPa$$

	1	2	3	4	5
REFERENCE	130.2	158.0	70.9	81.6	70.7
Ep = 2.0 MPa	130.2	158.0	70.9	81.6	70.7
Ep = 7.0 MPa	130.2	158.0	70.9	81.6	70.7
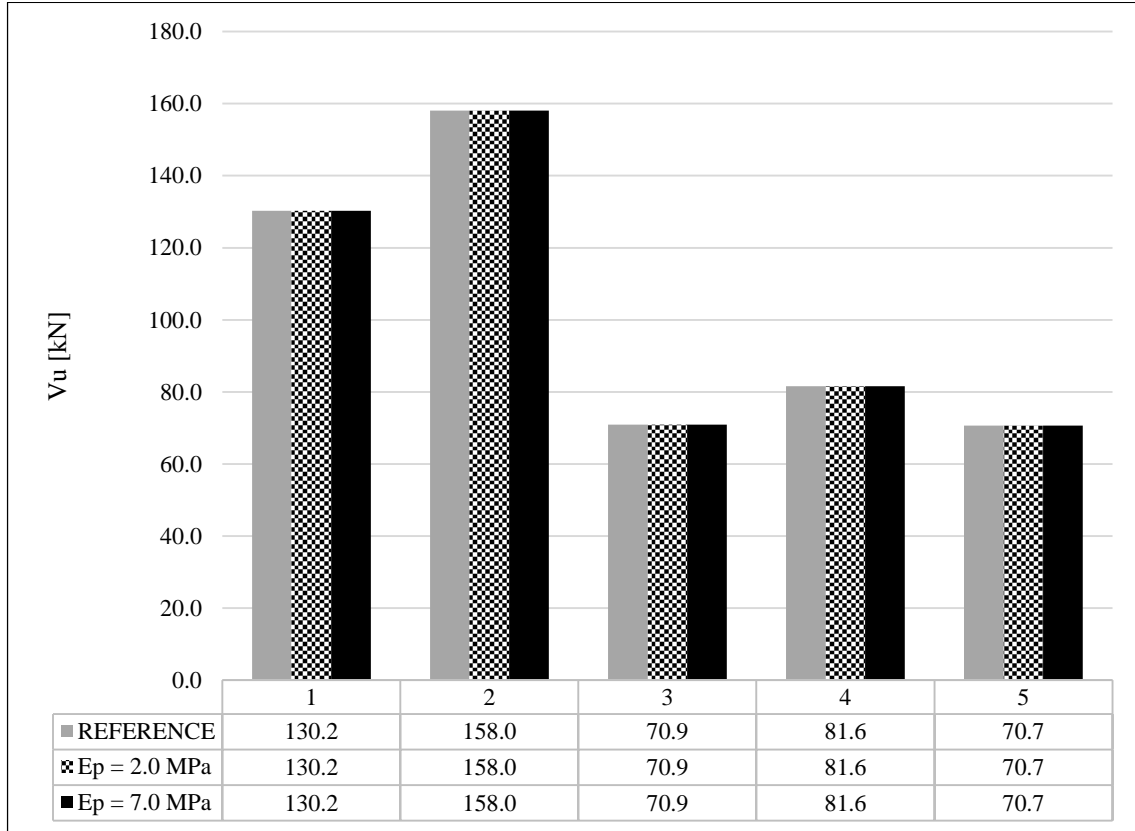
Figure 3-11. Sensitivity analysis for polystyrene elastic modulus

The only failure mechanism affected by this variation is V_{u4}, due to the fact that the contact length between frame and infill depends on the ratio between concrete and polystyrene elastic modulus $\left(\frac{E_c}{E_p}\right)$, as depicted in section 2.3.4.6. However, due to the great flexibility of polystyrene material, the contact length calculated with any of the values in this range exceeds the length of the infill, and therefore the infill length is used instead. For this reason, in the range of interest, polystyrene elastic modulus has no influence in the lateral load resistance of the structure. Having said this, V_{u5} governs the lateral load capacity regardless of the adopted value of E_p, as depicted in Figure 3-11.

3.8.3 Concrete compressive strength sensitivity analysis

Variations in the concrete compressive strength are unavoidable, due to the intrinsic nature of the heterogeneous material. The concrete class specification of the frame is C20/25, and the investigated range of values is shown below.

$$15 \ MPa \leq f_{ck} \leq 40 \ MPa$$

	1	2	3	4	5
■ REFERENCE	130.2	158.0	70.9	81.6	70.7
▨ fck = 15 MPa	130.2	154.2	70.9	81.6	70.7
■ fck = 40 MPa	130.2	168.9	70.9	81.6	70.7
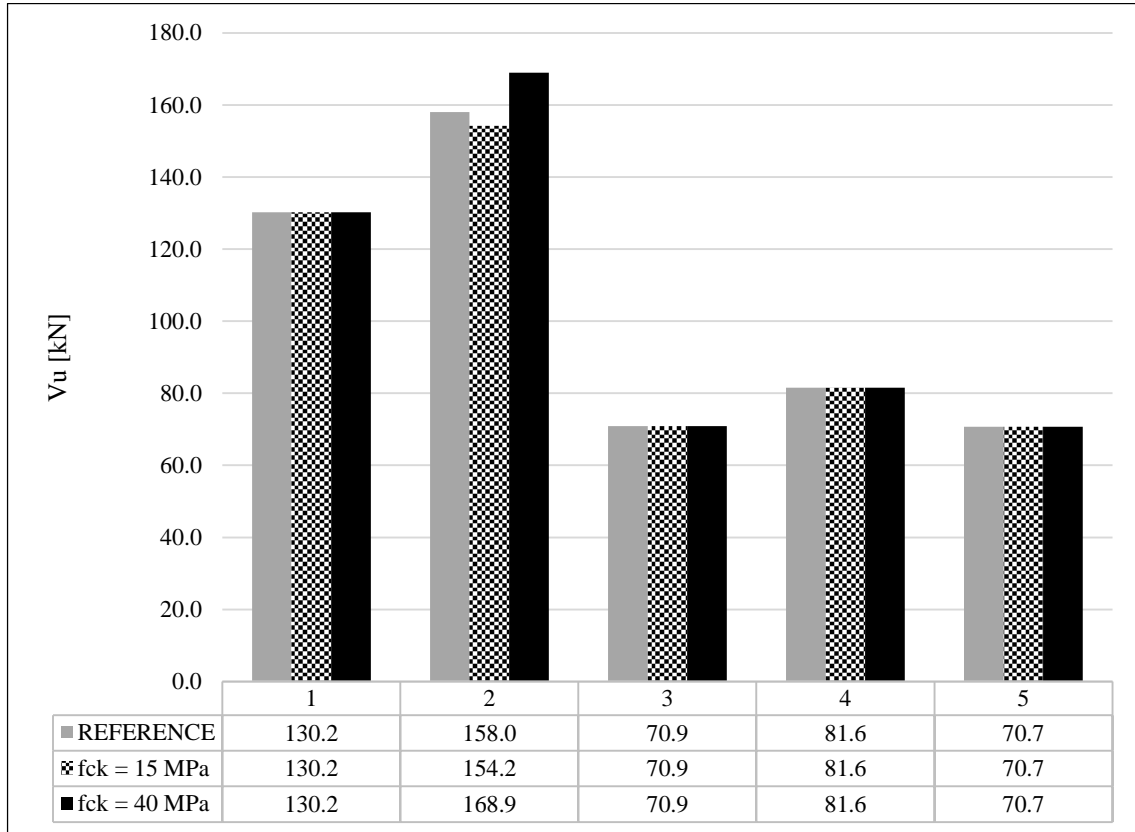
Figure 3-12. Sensitivity analysis for concrete compressive strength

From Figure 3-12 it can be noted that varying the concrete compressive strength only affects V_{u2}, since this mechanism depends on the ultimate shear resistance, which is affected by concrete strength. However, failure mechanism 2 is predominant for very stiff infills (which is the opposite case from polystyrene infills), and as it can be seen from Figure 3-12, the resistance of mechanism 2 is much higher than the rest of the mechanisms, and hence does not govern the global resistance in the range of values here studied. So similarly to the previous case, variation of the concrete compressive strength, although has some influence in V_{u2}, does not have any influence in the final resistance value, since V_{u5} still governs, and does not depend on f_{ck}.

3.8.4 Polystyrene compressive strength sensitivity analysis

Similar to section 3.8.3, the possible variation of polystyrene compressive strength is now studied. The range of values were selected based on the typical values found in the literature, and are presented below.

$$0.1\ MPa \leq f_{pk} \leq 0.2\ MPa$$
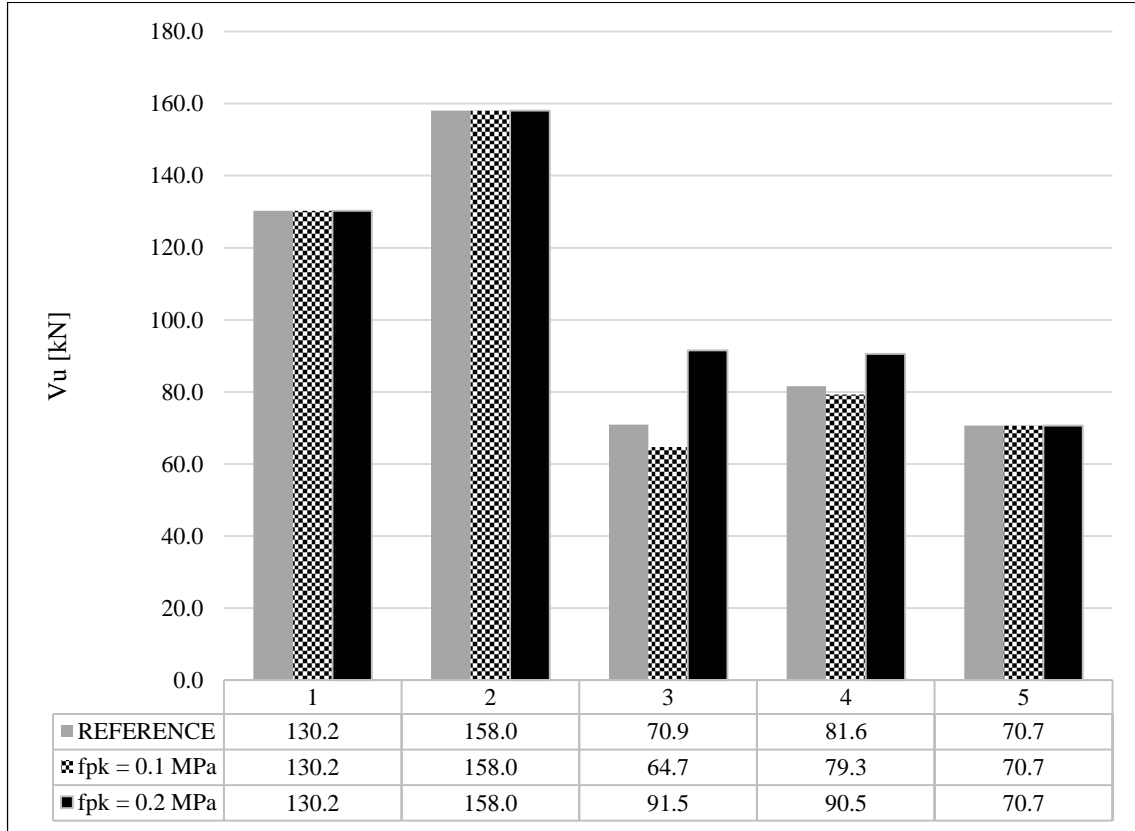
Figure 3-13. Sensitivity analysis for polystyrene compressive strength

	1	2	3	4	5
REFERENCE	130.2	158.0	70.9	81.6	70.7
fpk = 0.1 MPa	130.2	158.0	64.7	79.3	70.7
fpk = 0.2 MPa	130.2	158.0	91.5	90.5	70.7

From Figure 3-13, it's worth pointing out how only failure mechanisms 3 and 4 are influenced by the variation of polystyrene compressive strength. Both these failure mechanisms are very similar, and account for the compressive strength of the infill explicitly, as the infill is assumed to reach the crushing strength along the contact length (Figure 2-21 and Figure 2-22). It is very interesting to see how, for the lower bound values of f_{pk}, failure mechanism V_{u3} starts to govern over V_{u5}. The range of possible values for V_{u3}, V_{u4}, and the global lateral load capacity of the structure (V_u), due to a variation of polystyrene compressive strength, are depicted below.

$$64.7\ kN\ \leq V_{u3} \leq 91.5\ kN$$
$$79.3\ kN\ \leq V_{u4} \leq 90.5\ kN$$
$$64.7\ kN\ \leq V_u \leq 70.7\ kN$$

In the case of the frame considered in this thesis, we expect a combination of these modes.

3.8.5 Compressive strut width ratio sensitivity analysis

A similar analysis was carried out in order to determine the influence of the assumed compressive strut width ratio (w/D). From sections 3.2 - 3.6, it can be observed that the compressive strut width is not an explicit input parameter for any of the failure mechanisms ($V_{u, i}$), and therefore V_u does not depend on w/D. The crushing load, however, depends explicitly on w, as depicted in section 2.3.4.2.

$$V_{crush} = wtf_{pk}cos\theta$$

From the above expression, it can be observed that the crushing load has a linear dependence on w. This can also be observed from Figure 3-14. The possible range of values investigated is based on previous investigations undergone for masonry infilled walls, as shown in Figure 2-4. The extreme values are reported below.

Table 3.4. Extreme values of the crushing load, according to w/D ratio**.**

w/D	V_{crush} [kN]
0.05	3.03
0.45	27.3
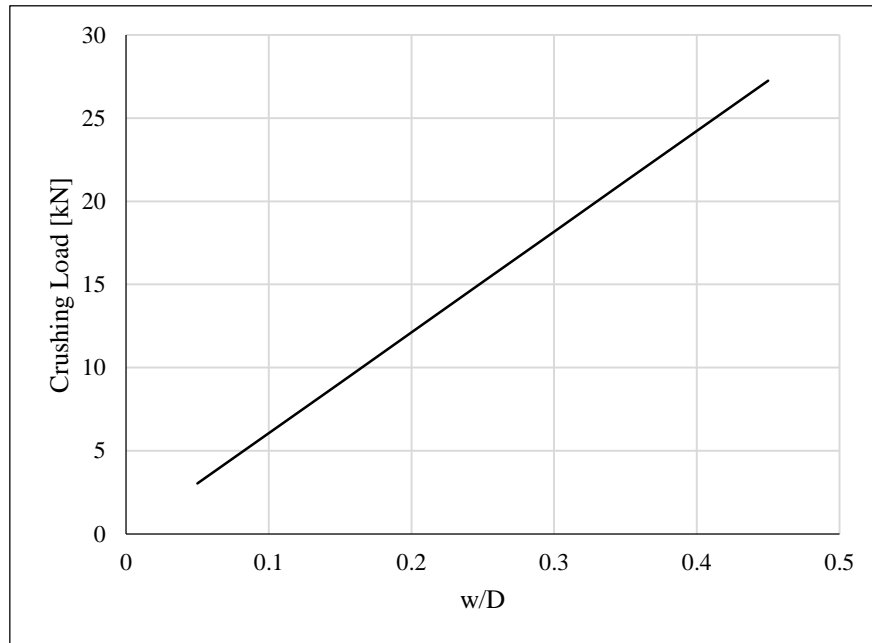
Figure 3-14. Sensitivity analysis for compression strut width ratio on the crushing load

3.8.6 Summary and analysis of results

A summary of the results investigated throughout the current section is proposed below in Table 3.5.

Table 3.5. Sensitivity analysis

Failure mechanism	Reference	Residual friction		Elastic modulus E_p [MPa]		Compressive strength – concrete f_{ck} [MPa]		Compressive strength – polystyrene f_{pk} [MPa]	
		$\mu 0 = \mu_r$	$\mu_r = 0$	1.9	4.35	15	40	0.1	0.2
Vu1 [kN]	130.2	144.7	127.6	130.2	130.2	130.2	130.2	130.2	130.2
Vu2 [kN]	158.0	165.8	155.7	158.0	158.0	154.2	168.9	158.0	158.0
Vu3 [kN]	70.9	70.9	70.9	70.9	70.9	70.9	70.9	64.7	91.5
Vu4 [kN]	81.6	81.6	81.6	81.6	81.6	81.6	81.6	79.3	90.5
Vu5 [kN]	70.7	85.2	68.1	70.7	70.7	70.7	70.7	70.7	70.7
Vu [kN]	70.7	70.9	68.1	70.7	70.7	70.7	70.7	64.7	70.7

From Table 3.5 it can be clearly seen that, except for high values of the residual friction coefficient, or very low values of polystyrene compressive strength, failure mechanism 5 is always governing the global lateral resistance. As a general statement, the only parameter investigated that affects V_{u5} is the residual friction coefficient, and the only parameter that affects V_{u3} is polystyrene compressive strength. For this reason, these two parameters (μ_r and f_{pk}) are the only mechanical properties which could have some influence on the lateral load resistance of the infilled frame, according to the simplified analytical method proposed in this chapter.

Variation of the Elastic modulus of polystyrene affects only V_{u4}. However, in the range of interest, it has no effect on the final value of this failure mechanism. V_{u4} does not govern the global lateral load resistance of the structure under any of the cases here studied, and therefore, a variation of E_p in the range of interest is not expected to influence the lateral load resistance, according to the simplified analytical method studied in this chapter.

Chapter 4

Description of the experiment

This chapter will describe the mock-up and its components, the instruments which are used for this experiment along with their positions and a brief explanation of their mounting process. Last section will explain in which manner the load will be applied and the scheduled testing protocol.

4.1 MOCK-UP AND INSTRUMENTS

The frame subjected to the experiment is built up of two columns 310 x 200 mm and a beam 250 x 200 mm made of reinforced concrete C20/25. Infill blocks are made of polystyrene. All material characteristics are presented in Chapter 3 in Table 3.1. A few tests with a sclerometer were conducted on columns in order to have better picture of concrete strength. An average value of 23.5 MPa was acquired.

Cover layer on one side consists of 40 mm thick mortar layer (with plastic mesh in the middle) and on the other side there is mortar with thermo-insulating foam in total 90 mm thick, which makes the infill 330 mm wide in total. On both sides, there is a GFRP mesh embedded in the cover layer. This mesh is built up of bars with 10 mm in diameter with spacing of 40 cm in both directions. Meshes are connected with transversal connectors.

The wall is resting on a steel plate which is embedded and welded to longitudinal reinforcement of the columns. This plate is used to restrain end sections of the columns to ground. Under each column there are six M24 bolts through which the mock-up is connected to the testing frame. Detail verification of the bolted connection is presented in Annex A.

Figure 4-1. The wall

Lateral force will be applied as a pulling force via steel jack which is connected to a pulling rig. This is depicted in Figure 4-2 and Figure 4-3.

Figure 4-2. Position of the piston

Figure 4-3. Pulling rig

For this test, a total number of 15 measuring transducers will be used. Their locations are shown in Figure 4-4. Twelve of them are Linear Variable Differential Transformers (LVDT) and 3 of them are Wire Drawn Transducers (WDT).
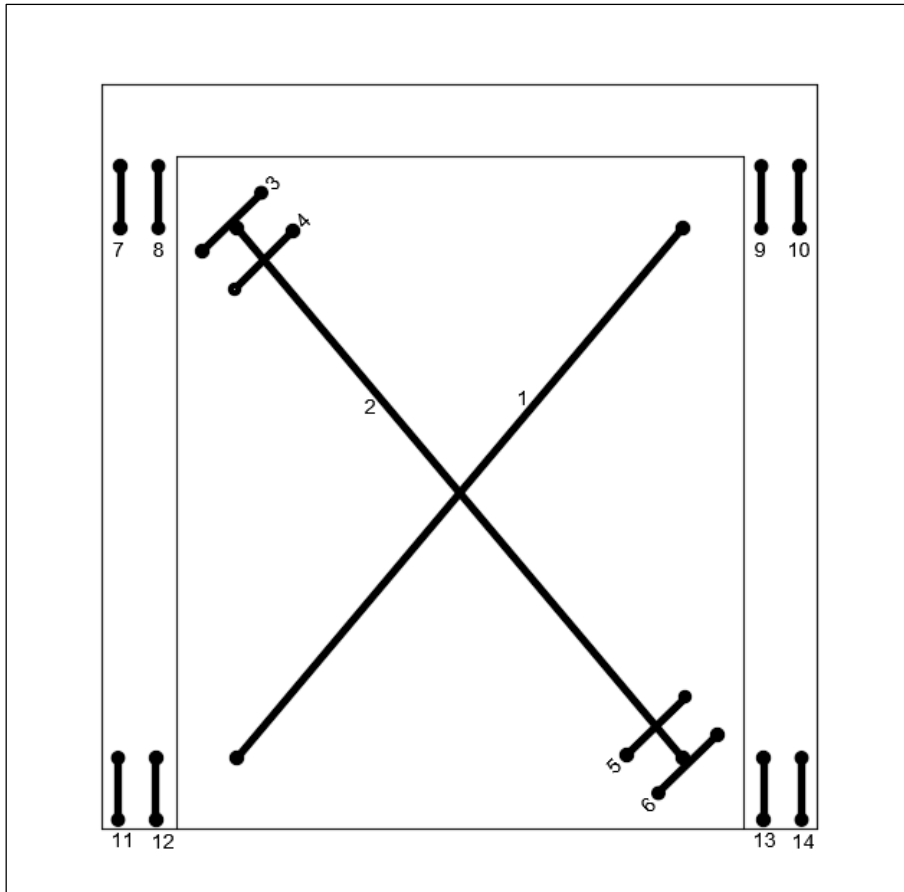
Figure 4-4. Position of the instruments

Instruments numbered 1 and 2 are WDT (Figure 4-6) and they are supposed to measure displacements in diagonal struts. Another WDT will measure horizontal displacement of the beam. All other instruments are LVDTs (Figure 4-5). Results coming from instruments numbered 3 – 6 will be used to obtain strain in diagonal direction which will be later used to define the width of the diagonal strut used for analytical solutions. All other instruments (7 – 14) are measuring displacements of edge segments at the columns in order to obtain rotations and curvatures of cross sections at column ends.

Figure 4-5. One of the LVDT transducers used in the experiment (already installed)

Figure 4-6. Wire Drawn Transducer used in the experiment

In order to obtain correct results for instruments at the columns, mortar layer was removed from these locations so that the readings are coming directly from column surface and not mortar.

After cleaning all of the surfaces where the instruments will be glued, setting up has started. During this process, distance between LVDTs for a given pair was kept constant, and the same was done for distances between mounting blocks and end blocks. At places where this was not possible, variations were kept minimal. Figure 4-7 shows transducers number 13 and 14 after installation.

In some cases, aluminium rods were used as extensions, in order to overcome the distance between mounting block and boundary element. This can be seen in case of instrument number 13 (see Figure 4-7).

Figure 4-7. Transducers number 13 and 14

For WDT instruments, L shaped mounting elements were custom built and used for their installation (Figure 4-8). On the other side of each diagonal an L shaped profile was mounted on the wall to fix the other end of the wire.

Figure 4-8. WDT instruments with their L shaped mounting elements

An additional WDT was placed at the end of the frame to capture horizontal displacement of the beam. That WDT was placed on the ground and using iron wire connected to the piston.

4.2 TEST PROTOCOL

The experiment was displacement controlled, which means that the applied load was the displacement while the force was measured. Different values of the displacements were applied and after each value has been reached, the frame was unloaded and returned to initial zero displacement state. Displacement values were 15 mm, 30 mm, 45 mm, 60 mm, 90 mm and 120 mm. These are equivalent to 0.5%, 1%, 1.5%, 2%, 3% and 4% of drift (see Figure 4-9).

Displacement is applied with a velocity of 0.4 mm/s.
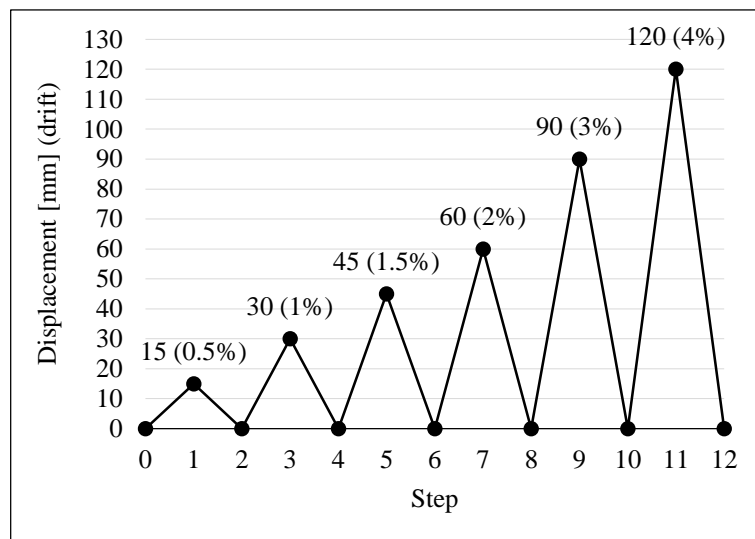
Figure 4-9. Applied displacement

Chapter 5

Experimental results

The following chapter presents the results of the experimental test performed as described in Chapter 4. First section is dedicated to some visual observations made during the experiment and contains some conclusions drawn from those remarks. After that, data acquired from the measuring instruments are presented and commented. First and most important loading-unloading behaviour and the pushover curve after which the behaviour in two diagonals is shown and noted. Then, moment – curvature diagrams of the cross sections of the columns (bottom and top), and at the end, strain in the compressed diagonal.

5.1 VISUAL OBSERVATIONS

As previously said, this experiment was performed in six loading-unloading cycles. Here we will discuss the behaviour of the infilled frame for each one by looking at some of the photos made during the experiment.

5.1.1 First cycle – target displacement 15 mm

Even though the target displacement was not that severe, some cracks occurred in mortar which is very stiff and does not allow any elastic deformation. These cracks occurred on windward (left) side of the frame, which was expected since the load was applied from left to right. Figure 5-1 shows the direction and the extension of these cracks. We can be reminded of a shear behaviour mentioned in Chapter 3.

Only these cracks were observed at this point of the experiment.

Figure 5-1. First cracks in the mortar

5.1.2 Second cycle – target displacement 30 mm

In this cycle, cracks that were already there started to grow and some new ones occurred (Figure 5-2).

Figure 5-2. Growth of the old and creation of the new cracks

We can see that the plastic net which is embedded in the mortar layer keeps pieces of mortar layer from falling down.

5.1.3 Third cycle – target displacement 45 mm

With this cycle, a more severe load is starting to act on the frame and infill. At windward side of the mock-up new cracks occurred close to the bottom corner (Figure 5-3). We can observe a crack which is parallel to the floor which means that the infill started to diverge from the testing frame.

Figure 5-3. New cracks during the third cycle

From Figure 5-2 it can be seen that, at this point, cracks started to occur even on the other side of the mock-up (leeward). Their direction is 45°, which is expected since that diagonal is in tension.
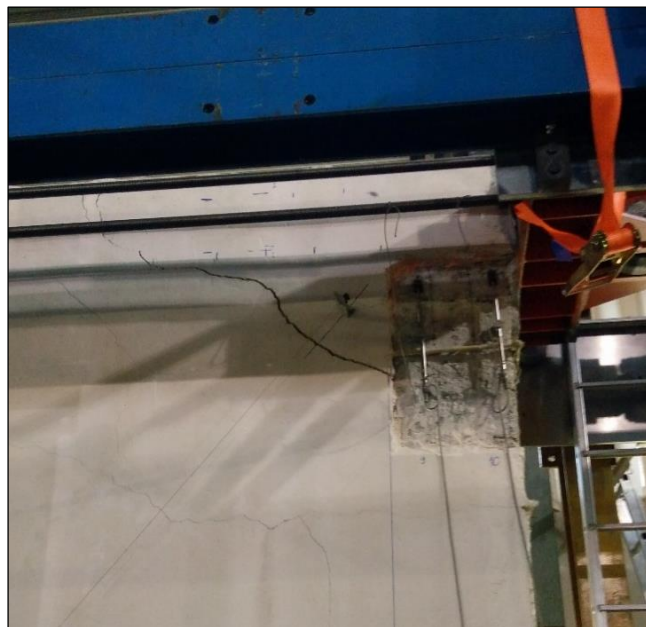
Figure 5-4. Cracks at the leeward side

5.1.4 Fourth cycle – target displacement 60 mm

In this loading-unloading cycle, growth of already occurred cracks and falling off of a few pieces of mortar layer was noticed. This is shown in Figure 5-5. We can see serious detachment of the infill from the bottom.

Figure 5-5. Cracks during the fourth loading cycle

No new cracks occurred on the leeward (right) side of the mock-up.

5.1.5 Fifth cycle – target displacement 90 mm

This cycle was characterized by large damage occurring on mock-up, large enough to detach some of the instruments. Horizontal crack separating infill from the bottom has spread almost through the entire length of the mock-up (Figure 5-6).

We can notice another interesting thing if we look at Figure 5-7 where we see how the mortar layer is kept in place by bars from GFRP mesh, while in between bars the mortar layer tends to fall off.

On the back side of the mock-up (Figure 5-8), we observe that the damage is concentrated at two places and it is not spread like in the front side. This is explained by the fact that, on the back side of the mock-up, mortar is not directly placed on the frame and the infill, but it is delaminated with a layer of thermo-insulating foam which absorbs small deformations occurring in the infill and frame.

Figure 5-6. Fifth cycle damages

Figure 5-7. Out of plane damage during fifth cycle

Figure 5-8. Back side of the mock-up

5.1.6 Final (sixth) cycle – target displacement 120 mm

In the final stage of the experiment, target displacement was 120 mm or 4% drift. We clearly see the uplift of the infill (Figure 5-9) during its whole length. For the first time, we can see cracks occurring in the concrete column. If we look at Figure 5-10 we can see how the infill got separated from the frame. On the leeward side of the frame, we can just note that cracks which were already present just gained in their width and no new cracks occurred (Figure 5-11).

Figure 5-9. Sixth loading cycle – uplift of the infill

Figure 5-10. Infill separation from the frame

Figure 5-11. Sixth load cycle – leeward side

5.2 PUSHOVER CURVE

Data coming from horizontal displacement of the beam and the values of base shear give us loading-unloading curve shown in Figure 5-12. Six different loading-unloading branches can be distinguished, one for each cycle. Values of target displacements at the end of cycles are shown in Figure 4-9.

Figure 5-13 shows how stiffness of the whole structure is changing after each cycle.

It can be seen that during first loading step, until 52 kN of base shear, frame was entirely stiff. That was until first cracks in mortar occurred after which its stiffness started to deteriorate. Peak value of the base shear achieved in the first step was 149 kN at the displacement of 10 mm. The unloading branch has the same slope as the loading one and it can be seen that in order to reach initial state, base shear had to change its sign and reach a minimum value of -45 kN. This was due to plastic deformation occurred in the frame that had to be cancelled.

Second loading branch had a goal to reach target displacement of 30 mm or 1% drift. It can be noted that the new loading branch, looks the same as loading branch for the previous case (until 15 mm displacement) just shifted downwards since there is no rigid part at the beginning due to already formed cracks. Until this point (15 mm) we can say that no major stiffness degradation occurred since the branches have the same slope. After 15 mm mark, structure experiences reduction of the stiffness. This leads to a maximum value of 127 kN

for base shear in the second loading step at the displacement of 25 mm. In order to return the structure to its initial state, base shear had to achieve a value of -51 kN.
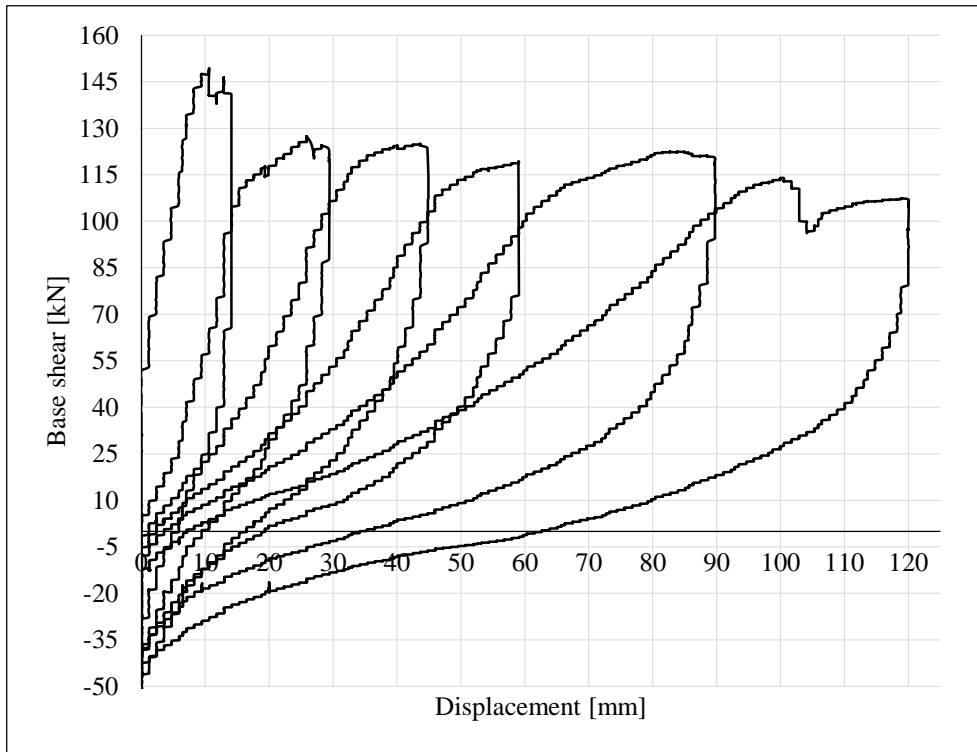
Figure 5-12. Loading-unloading curve

Third, fourth and fifth loading steps have similar behaviour with stiffness being reduced after each cycle. An average peak base shear for these steps was 123 kN and average force required to return the structure to the initial state was -50 kN.

Last loading step, with 120 mm target displacement, started as previous four ones but at 102 mm displacement mark, a sudden drop of resistance occurred where base shear dropped from its peak value for this step (114 kN) to a value of 105 kN. This drop was quite expected in these conditions (almost 4% of drift) and occurred due to formation of cracks in the frame itself, more specifically windward column as shown in Figure 5-9.

Table 5.1 summarises peak base shear forces for each loading cycle and their respective displacements, also shows shear forces required to return the structure in its previous state after loading is completed.

Table 5.1. Max base shear achieved, its respective displacement and min shear for each loading cycle

Loading cycle	Max shear [kN]	Displacement [mm]	Min shear [kN]
I	149.350	10.623	-45.289
II	127.414	25.832	-51.053
III	124.992	43.617	-54.475
IV	119.280	59.068	-48.448
V	122.479	83.774	-44.052
VI	113.979	99.949	-46.937

An interesting observation can be made if we look at areas surrounded by loading-unloading branches for each load cycle. It can be seen that area grows (gets wider) with each step, and if we look at that area as dissipated energy, we can say that after each cycle structure dissipates more energy than in the previous one. This can be regarded as favourable behaviour during an earthquake.
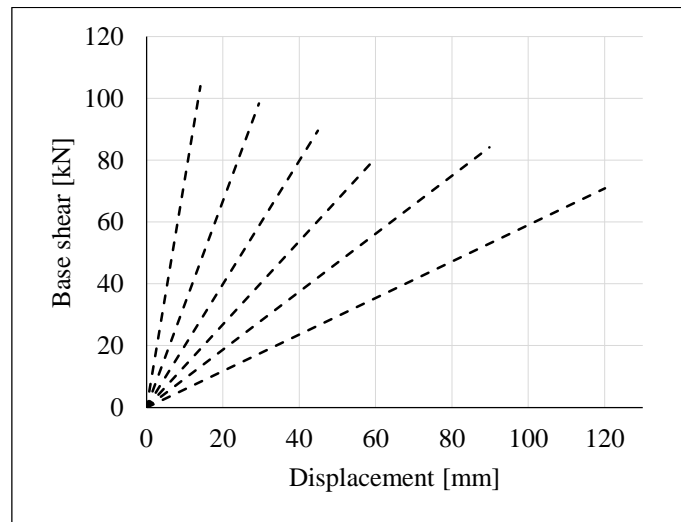
Figure 5-13. Stiffness degradation after each cycle

If we take peak values for each load cycle and their respective displacements, we can obtain a pushover curve (Figure 5-14).

We can see that after initial 150 kN, resistance of the frame gets stabilized around 120 kN mark. This can be justified by the fact that, initially, mortar, frame and infill worked together making the whole structure more stiff and resistant, but after creation of the first cracks in the mortar layer resistance value descends. Also, this stabilization tells us that the structure has quite a ductile behaviour.
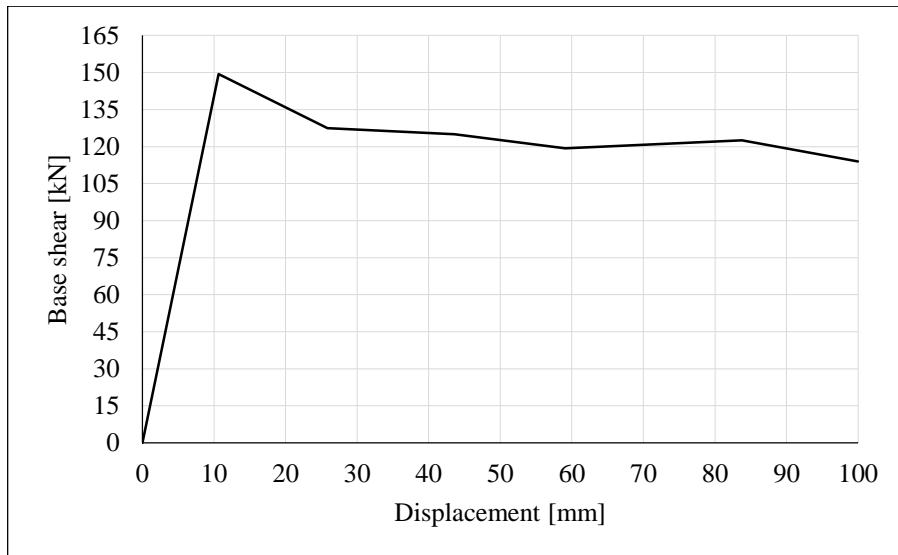
Figure 5-14. Pushover curve from the experiment

If we calculate the resisting bending moment of one of the columns from the frame, as later is presented in detail in section 6.2, we obtain value of 60 kNm which should give us 80 kN as the lateral resistance of the bare frame. Using SAP2000, a pushover for the bare frame was obtained and shown in Figure 5-15 alongside pushover curve obtained from the experiment. It should be noted that the yield limit of the reinforcing steel was set to 550 MPa, which is a more realistic value than the one provided by EC 2.
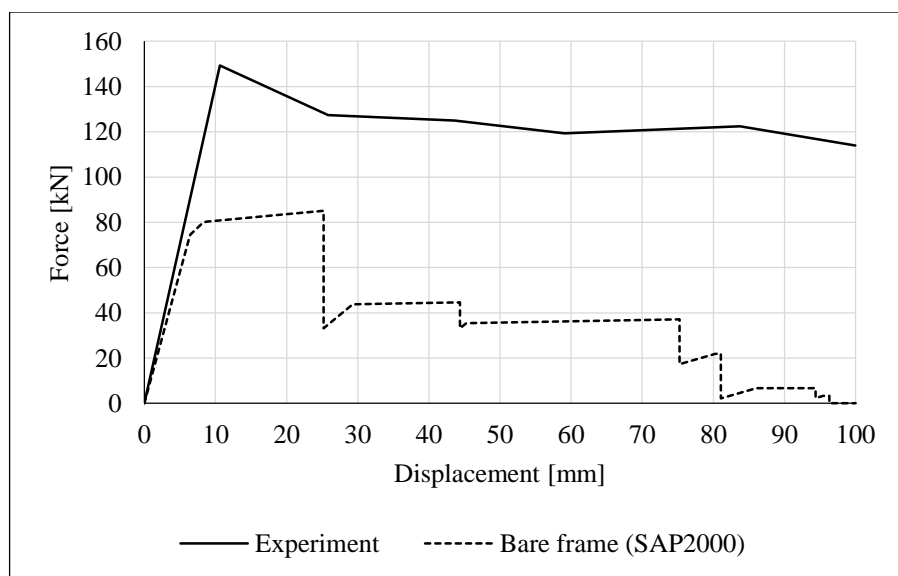
Figure 5-15. Pushover curve of the bare frame (experiment and SAP2000)

If we compare limit base shear coming from the experiment and the one coming from this pushover analysis of the bare frame, we notice an improvement of 25% in resistance of the infilled frame. We can also see that stiffness during elastic phase is almost the same (because of the mortar layer, the experimental one is a bit stiffer).

5.3 DEFORMATIONS IN DIAGONAL DIRECTIONS

. In this section results coming from two WDT instruments placed in compressed diagonal (strut) and the diagonal in tension (tie) are presented and discussed. Even though there is no actual reinforcement placed in tension diagonal, for the sake of simplicity, we will call it a tie.

I should be noted that because of the safety of the instruments, they had to be removed after fourth cycle (60 mm) so results are not showing behaviour for the last two loading-unloading cycles.

Looking at Figure 5-16 we can notice that displacements are not that large, this was expected if we know that no severe damage occurred in this direction. This, we can see in section 5.1 where several photos are showing that major cracks occur in the direction perpendicular to the diagonal in tension (tie). Biggest displacement in the strut occurred during last monitored loading cycle (60 mm) and it was 4.7 mm. Another thing we can notice is that the stiffness does not change dramatically over the cycles which again proves that serious damage in this direction was avoided.
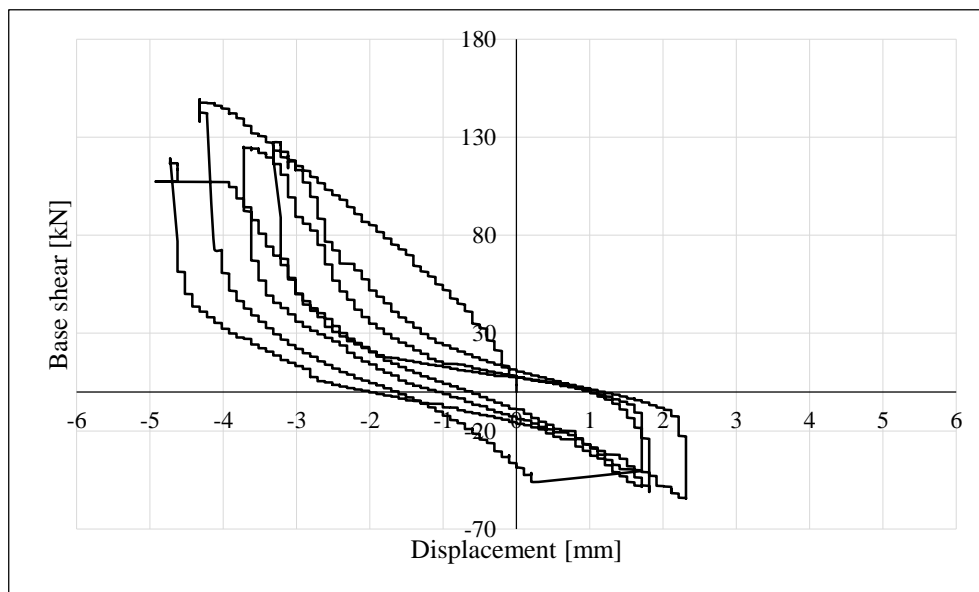
Figure 5-16. Displacements in the strut

Different situation can be seen if we look at the behaviour of the tie (Figure 5-17). Here we notice much larger displacements, going up to 35 mm. This is quite reasonable since we know that the main cracking happened perpendicularly to this diagonal. Also there is no change of sign in displacement. This is because when the base shear changes its sign it is

actually closing the cracks that occurred before. A big drop of stiffness after each cycle was also distinguished, again quite different with respect to the previous case.
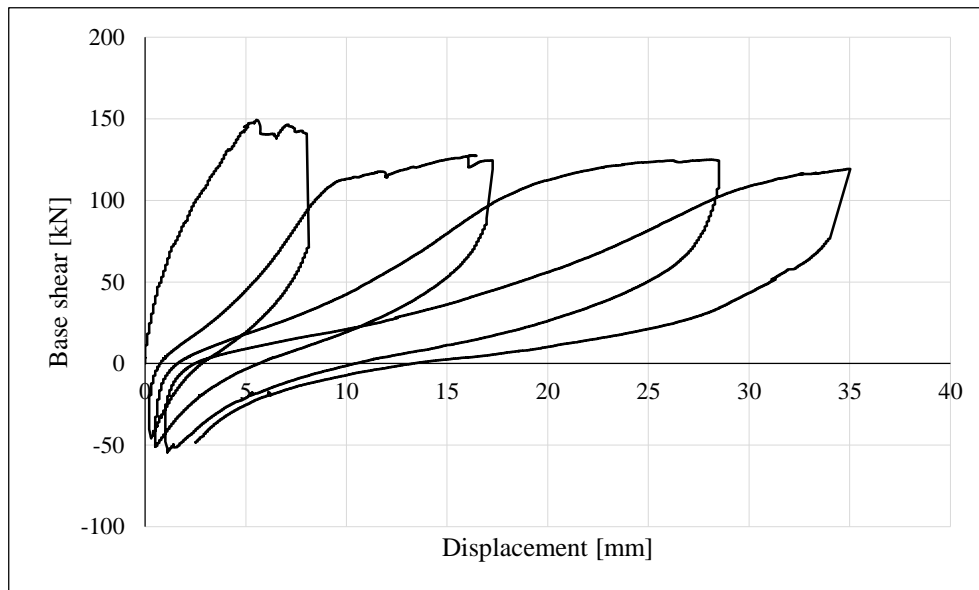
Figure 5-17. Displacements in the tie

5.4 MOMENT – CURVATURE DIAGRAMS

Two different cross sections of columns will be analysed, bottom end and top end of the column. It should be noted that for the purpose of these diagrams, values of bending moments, at said cross sections, were calculated as for a bare frame. Analysis of the bare frame subjected to 1 kN lateral load is presented in Appendix B.

As seen in Figure 5-18 first three loading-unloading cycles were monitored. We can see a great reduction in stiffness after each cycle, also, when the frame reaches initial zero displacement state, curvature changes its sign which tells us that both sides of the column are experiencing tension even though it was a monotonic loading. As expected the biggest curvature is at the end of the third cycle (45 mm) and has a value of 0.021 1/m. During first loading-unloading cycle bigger bending moment than in other two cycles was achieved, similar detail was noted before, in Figure 5-12, where at the beginning of the experiment, the highest force was achieved, while during following cycles it got stabilized at lower level.

66
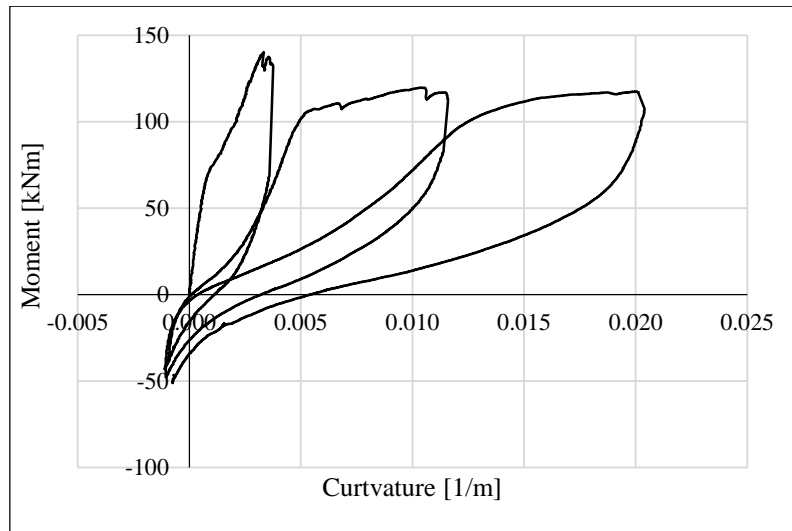
Figure 5-18. Moment – curvature diagram of the bottom cross sections

Before looking at the moment – curvature diagram of the top cross sections (Figure 5-19), it should be mentioned that because of the nature of the testing frame, rotations of the beam cross sections were reduced, so it is alright to expect that the top cross sections of the columns also rotate in smaller amount compared to the bottom ones. Still it is possible to observe a behaviour similar to the one from the previous case, here maximum curvature was 0.011 1/m. One notable difference would be that the curvature has larger negative values than the one of the bottom cross sections.
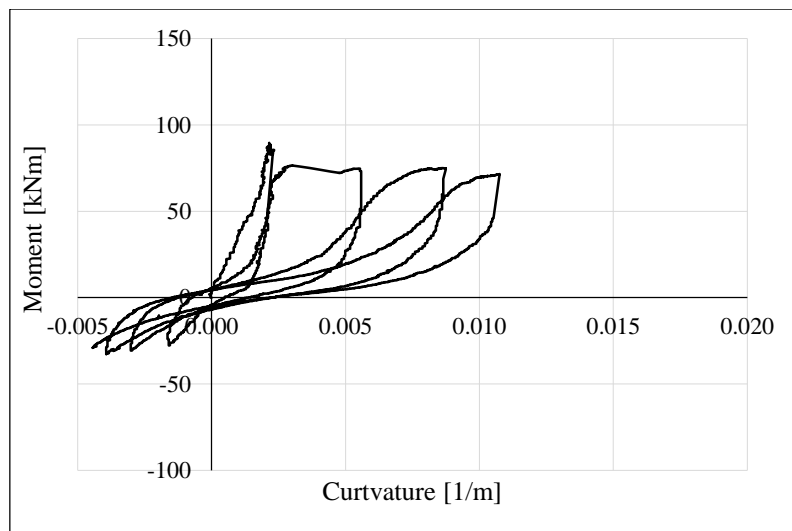
Figure 5-19. Moment – curvature diagram of the top cross sections

We can see that in both diagrams there is some stabilization in post cracking phase. This tells us that the cross sections in columns are having ductile behaviour. Knowing that when the masonry is used as an infill this is not quite a case, we can state that polystyrene infill brought in a more desirable behaviour.

5.5 STRAIN IN THE STRUT

Strain was measured at two ends of the strut, using 4 LVDT transducers (two at each end). Values shown in Figure 5-20 are mean values coming from those instruments. It should be mentioned that these instruments are actually mounted on the mortar layer and not directly on the infill.
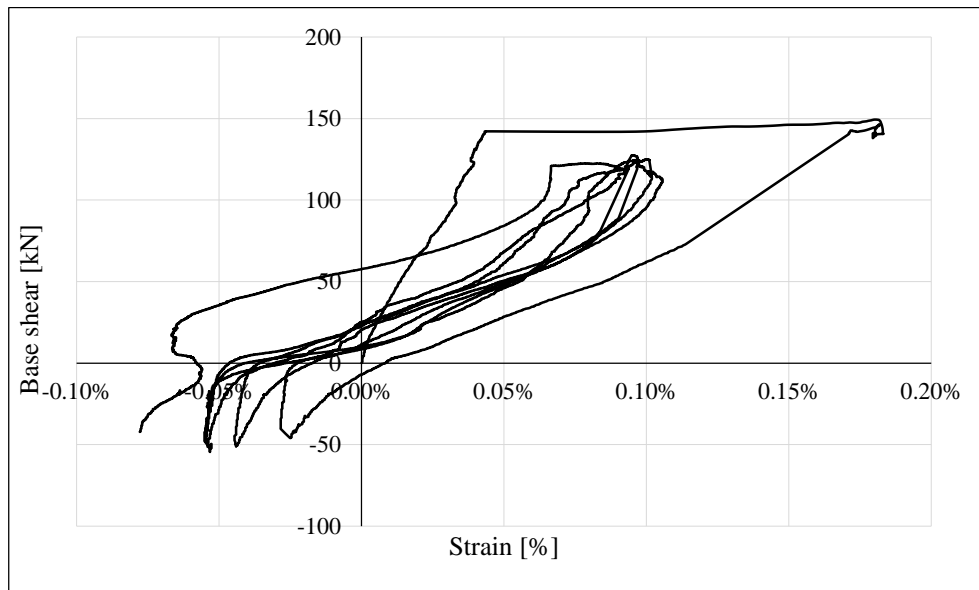
Figure 5-20. Strain in the strut

Looking at Figure 5-20 we see how during the first loading-unloading cycle, at around 142 kN of base shear, strain starts to grow under almost constant load and reaches its maximum value of 0.18%. This happened due to formation of cracks in the diagonal in tension or better said, cracks parallel to the strut. After first cycle, we cannot observe such a phenomenon any longer, but strain always reaches values around 0.10% at the end of each cycle. We can also see that, at the end of each unloading step, strain goes to negative, which would mean that the strut experienced tension at that point (due to poison ratio), and if we look at Figure 5-16 we see that this is indeed true.

Figure 5-21 shows strain in function of top displacement, where we observe an interesting behaviour. Namely, for all loading-unloading cycles (except for the first one), no matter how large the target displacement is, strain has a value around 0.10%. Also, after each cycle negative strain gets bigger.
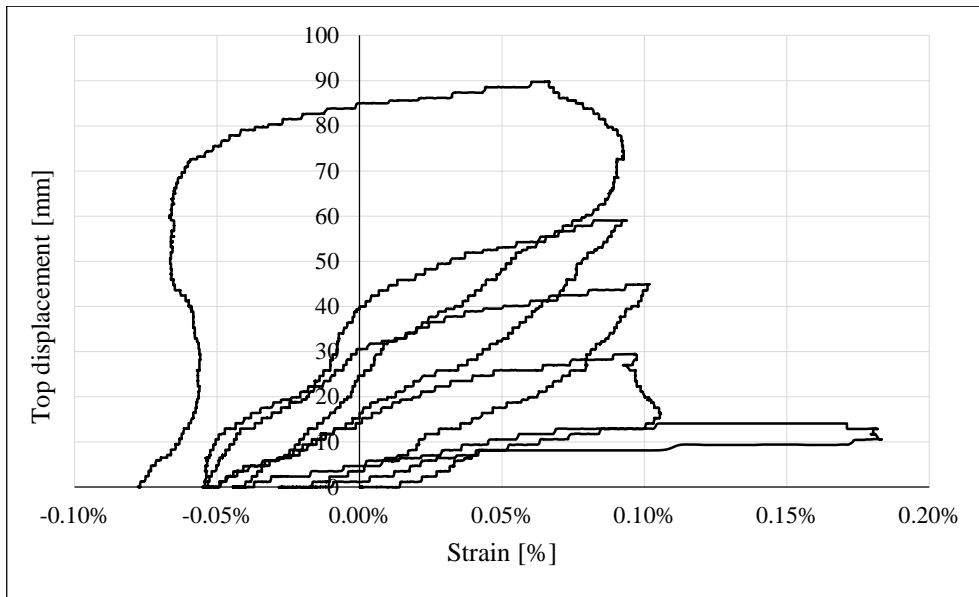
Figure 5-21. Strain in function of top displacement

Chapter 6

Finite element analysis and modelling

Finite element analysis is a very powerful tool for the purpose of structural analysis, broadly used by researchers and designers nowadays, in order to determine stress states, displacements and strains in a very precise way. For this task, MIDAS GEN 2016 (v2.2) was used in order to carry out the pushover analysis of the bare frame and infilled frame. The results obtained from this analysis are meant to be compared with the ones obtained in Chapter 3, and ultimately give a reasonable estimate of the failure load, maximum displacement, and expected failure mode of the infilled frame during testing. Finally, SAP2000 was used in order to perform a simple elastic analysis of the frame, and compare these results to the ones obtained with the more refined pushover analysis.

6.1 STARTING ASSUMPTIONS

In order to obtain accurate results, the model must represent the real frame in a precise way. Dimensions of the frame were precisely measured in the lab. Material mechanical properties, as discussed previously, were not precisely measured by tests.

Concrete behaviour is built-in to the software, with all the mechanical properties that correspond to the selected concrete class (C20/25). Reinforcement (longitudinal and transversal) was adequately input to the model as well, in order to carry out the non-linear analysis. Polystyrene, however, is not built-in to the software, and needed to be adequately defined. Due to lack of refined experimental data describing the stress-strain relationship of the material, an initial elastic behaviour was assumed, followed by a perfectly plastic relationship.

The supports at the bottom of the columns were modelled as perfectly fixed (zero displacement and rotation at the base). Restraints during the test are such that will ensure this condition not to deviate much from reality.

6.2 RC FRAME

6.2.1 Modelling

First, the reinforced concrete frame was modelled, without any infill, in order to quantify the effect of adding the infill in a latter model. The frame characteristics are depicted in Figure 6-1 and Figure 6-2. The concrete material mechanical properties were assigned in the program, as shown in Figure 6-3 (a). Once the mechanical properties for the materials have been suitably defined, and the proper dimensions and reinforcement layout are assigned for beam and columns (Figure 6-3 (b) and (c)), the frame is then modelled (Figure 6-4).
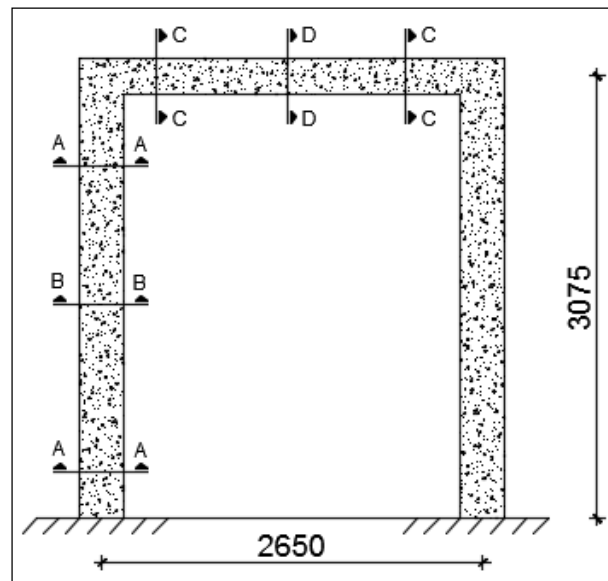
Figure 6-1. Bare frame geometry and layout
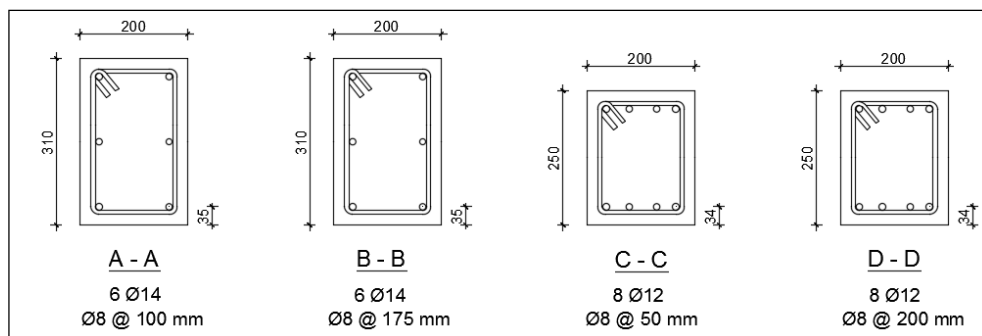
Figure 6-2. Beam and column cross sections and reinforcement layout

72
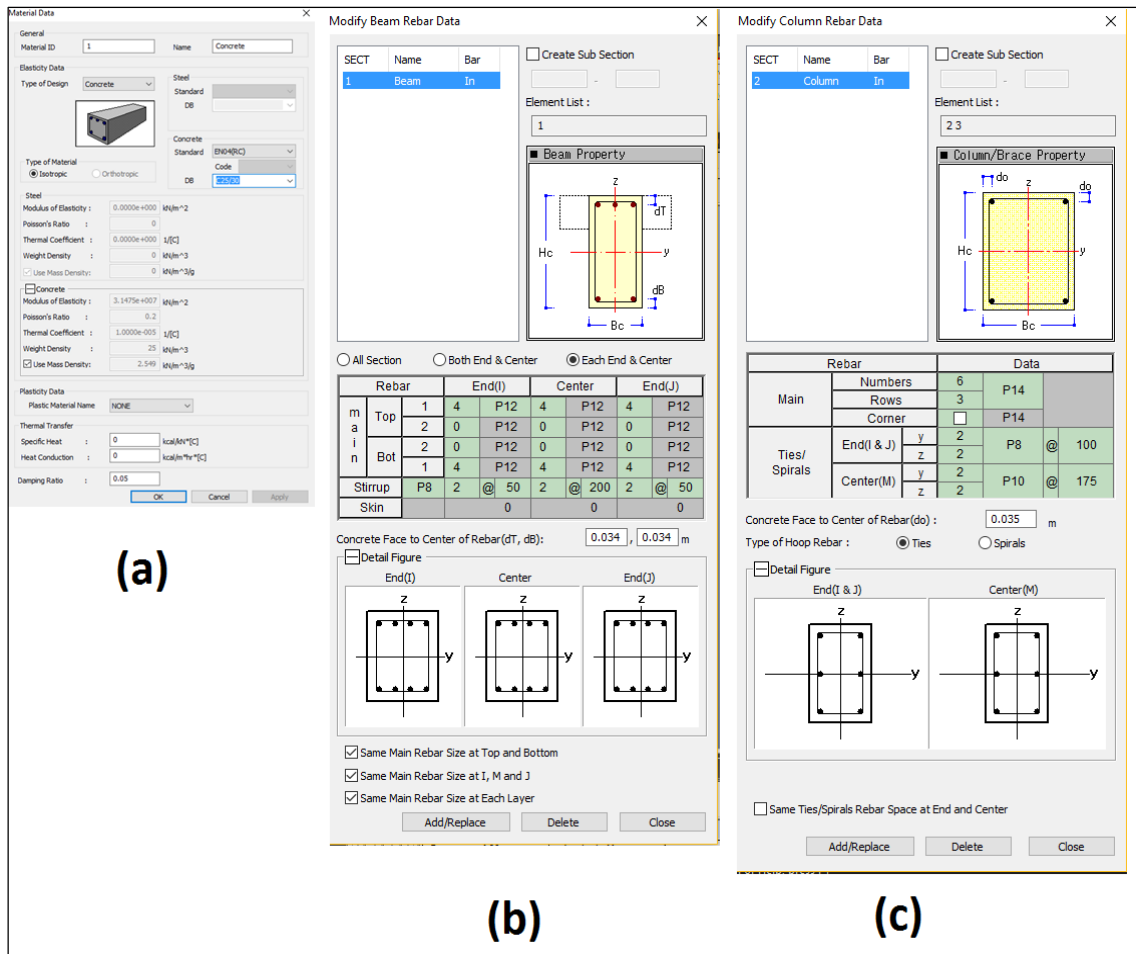
Figure 6-3. Assignment of concrete mechanical properties (a) and steel reinforcement (b) and (c) in MIDAS GEN
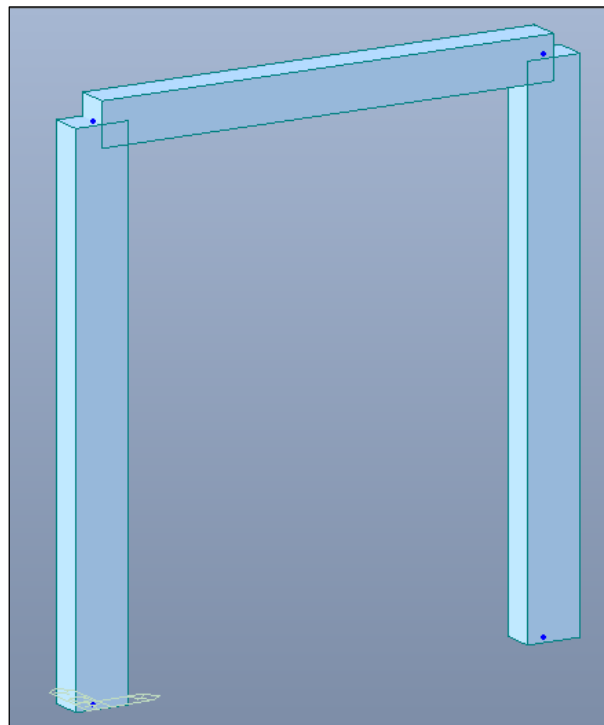
Figure 6-4. Reinforced Concrete Frame model in MIDAS GEN

73

6.2.2 Pushover analysis

Once the frame is modelled, a non-linear static analysis (pushover analysis) is performed on the frame structure. A pushover analysis consists basically in subjecting the structure to a monotonically increasing invariant lateral displacement pattern, (displacement of the top left corner of the frame in this case) until an incipient collapse situation is reached. The main output from this analysis is the so called "pushover curve", which describes the load-displacement behaviour of the structure under lateral loads, accounting for geometrical and material nonlinearities. Midas GEN includes a built-in option which performs this type of analysis, and was used for this research in order to obtain the pushover curve.

Nonlinear behaviour is considered in Midas by the lumped plasticity method, which considers two plastic hinges at each end of member (beam or column), where the nonlinear behaviour is lumped (1 flexural hinge, and 1 shear hinge, at each end of the member). Due to the nature of the lumped plasticity approach, possible plastic hinge locations must be defined before the pushover analysis is carried out (for this case, possible plastic hinges are defined at both ends of beam and columns), as depicted in Figure 6-5.
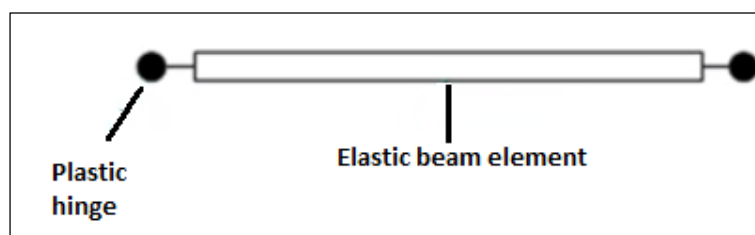
Figure 6-5. Lumped plasticity in beam elements

As mentioned before, each member end has 2 different types of plastic hinges (one for flexure and one for shear). The flexural plastic hinge is described by a moment-rotation behaviour, which is elastic up to yielding (A-B branch in Figure 6-6), then presents a perfectly plastic behaviour (B-C branch in Figure 6-6) where it can continue to rotate without taking additional load, until the ultimate rotation, where failure is achieved (point C in Figure 6-6). The shear plastic hinge, on the other hand, has a completely different behaviour to the flexural hinge, as shear phenomena is brittle by nature, and can't account for any post-elastic resources. Shear hinges are defined by a force-displacement behaviour, which is elastic up to failure (Figure 6-8). Plastic hinges in columns must account for the interaction between axial force and yield moment (Figure 6-7), while axial force interaction is neglected in beam plastic hinges.
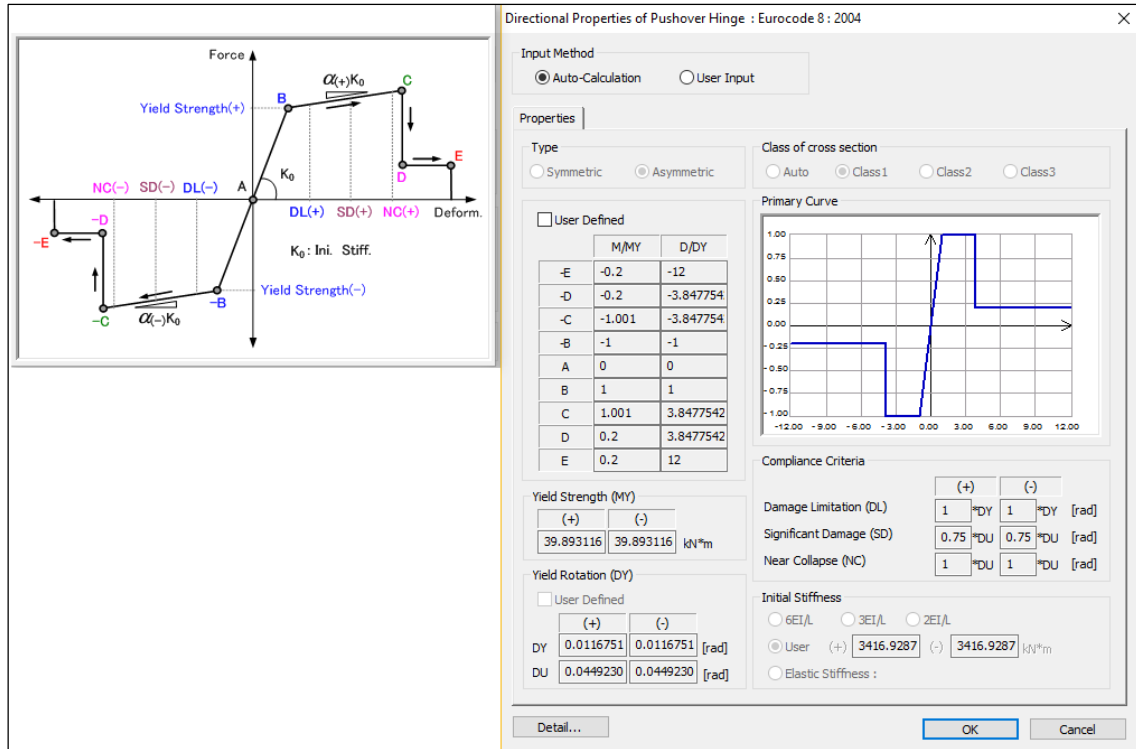
Figure 6-6. Flexural plastic hinge definition for beam in Midas Gen
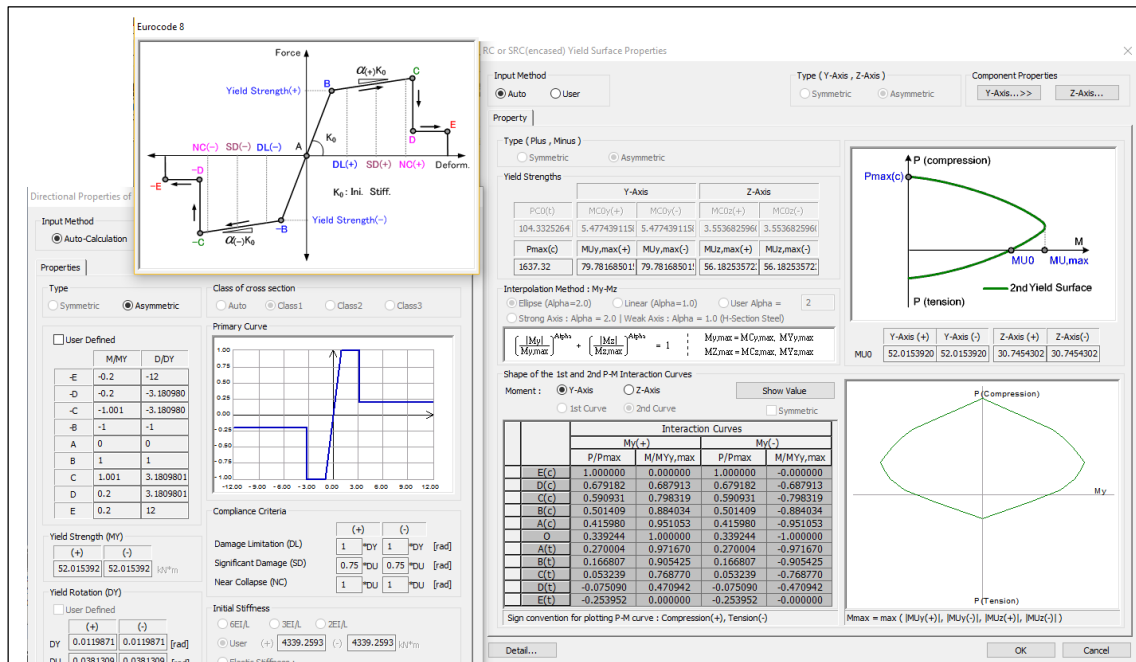
Figure 6-7. Flexural plastic hinge definition for column in Midas Gen
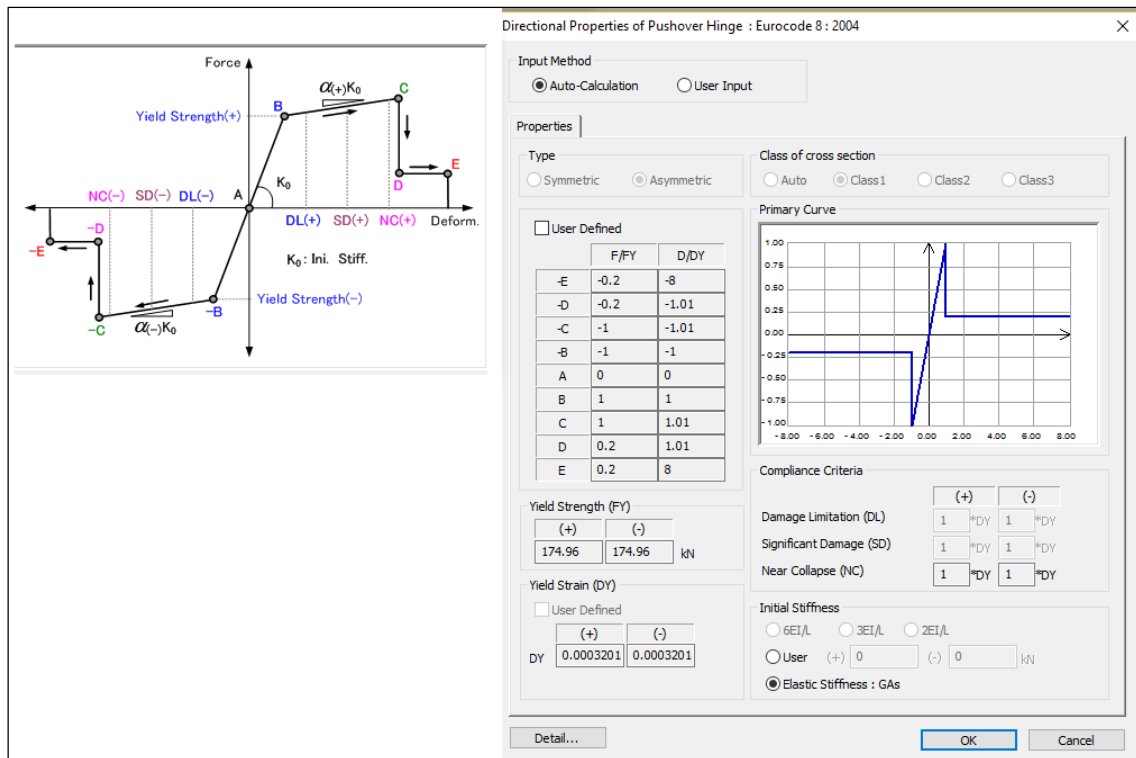
Figure 6-8. Shear plastic hinge definition for beam or column in Midas Gen

Once all the plastic hinge properties have been assigned, the master node is defined (top left corner of the frame). Displacements will be referred to this node, and the load is applied at this location also. Finally, the pushover load case is properly defined, with a maximum displacement of 15 cm, and sufficient increment steps in order to ensure convergence (2000 steps were considered for this case). The pushover curve for the bare frame can be seen in Figure 6-10. From the curve, a peak load of 59.43 kN is reached at a displacement of 10.80 mm. The maximum displacement, where failure of the structure is achieved, is equal to 119.10 mm.

For a quick check of the cross section capacity, a simple hand calculation was performed on the column and the beam cross sections, neglecting effects of the axial force and compression steel, since they can be considered negligible for this purpose. The calculations are presented below.

1. Column Resisting moment

- Calculation of the neutral axis:

$$A_s \cdot f_y = 0.8 \cdot f_{cd} \cdot b \cdot x$$

$$2 \cdot 308 mm^2 \cdot 500 MPa = 0.8 \cdot 20 MPa \cdot 200 mm \cdot x \rightarrow x = 96.25 \ mm$$

- Strain at mid layer

Due to the fact that the second layer of the steel is in the middle of the cross section, verification of yielding in steel is performed in this layer.

$$\frac{0.0035}{96.25mm} = \frac{0.0035 + y}{155mm} \rightarrow y = 0.00276$$

Where 155mm is the distance from the compressed edge to the mid layer of steel, and "y" is the corresponding strain at that layer.

Since "y" is greater than $\varepsilon_{sy} = 0.002$, the steel at mid layer has yielded.

- Resisting moment:

The resisting moment was calculated about the compressed edge of the cross section as follows:

$$M_{Rd} = 308mm^2 \cdot 500MPa \cdot (275mm + 155mm) - 0.8 \cdot 20MPa \cdot 200mm$$
$$\cdot 96.25 \cdot \left(\frac{0.8 \cdot 96.25}{2}\right) = 60 \, kN \cdot m$$

2. Beam Resisting Moment

- Calculation of the neutral axis:

$$A_s \cdot f_y = 0.8 \cdot f_{cd} \cdot b \cdot x$$
$$4 \cdot 113.1mm^2 \cdot 500MPa = 0.8 \cdot 20MPa \cdot 200mm \cdot x \rightarrow x = 70.63 \, mm$$

- Resisting moment:

The resisting moment was calculated about the compressed edge of the cross section as follows:

$$M_{Rd} = 452.39mm^2 \cdot 500MPa \cdot 216mm - 0.8 \cdot 20MPa \cdot 200mm$$
$$\cdot 70.63mm \cdot \frac{0.8 \cdot 70.63}{2} = 42.47 \, kNm$$

Actual steel used for this frame has yield strength of 500 MPa which is a characteristic value. Knowing that we can say that value of a limit later load for a bare frame can be increased between 20% to 30% with the respect to the one obtained in FEA.

The flexural capacities obtained by the means of simple hand calculations are in very good agreement with flexural plastic hinge resistance for beams and columns used during

pushover analysis, which can be seen in Figure 6-9. The column resistance is also in good agreement with the interaction diagram from Figure 3-4, considering no axial load.
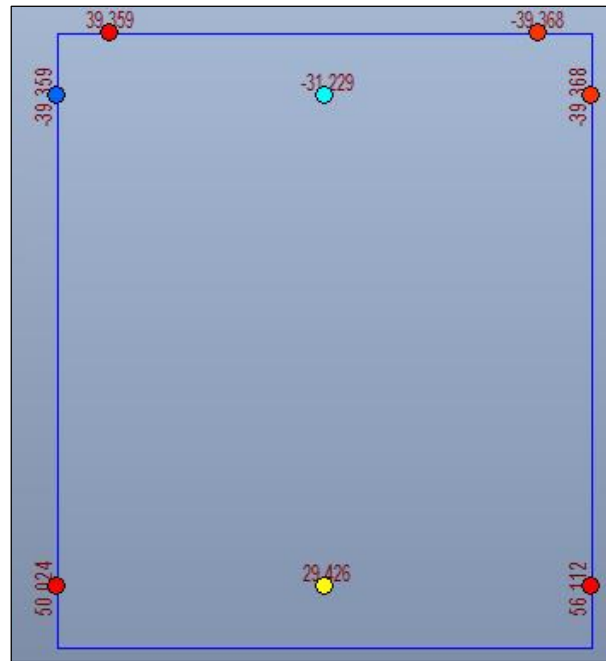
Figure 6-9. Yielding moments at plastic hinges

The pushover curve observed in Figure 6-10 presents a discontinuous nature. This can be explained by analysing the failure mode sequence of the frame, which consists of a series of plastic hinge activations, and plastic hinge failures, and are reflected in the curve by the discontinuities in the load-displacement curve, due to the sudden loss of stiffness.
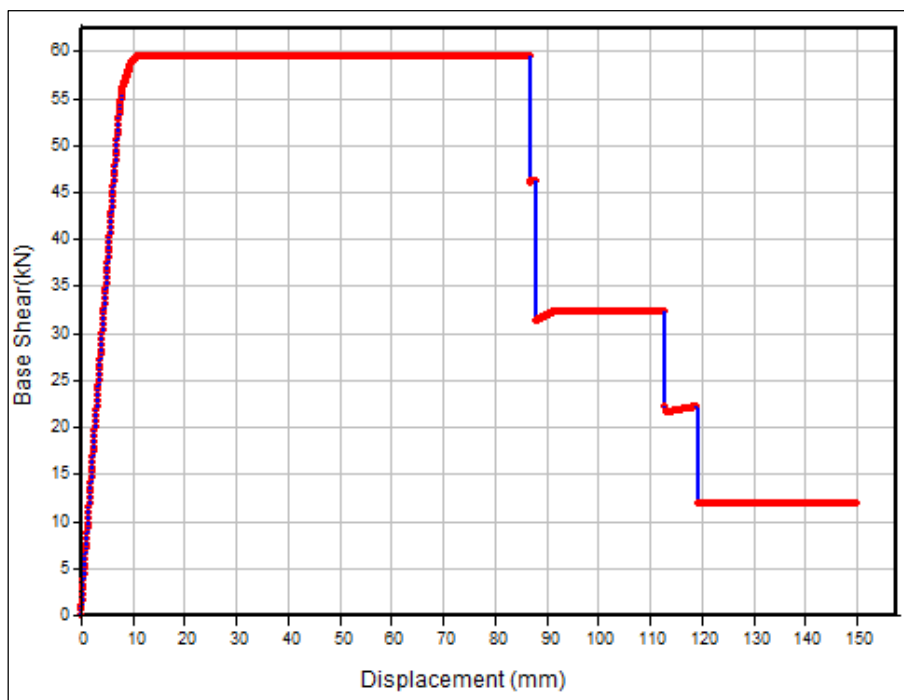
Figure 6-10. Pushover curve for RC Frame Structure

78

The aforementioned behaviour can be understood in a simple way by observing Figure 6-11 and Figure 6-12. In Figure 6-11 (a) the frame is still within the elastic range (the 6 plastic hinges defined at the ends of beams and columns are blue, which means they are still behaving elastically). The dot in the load-displacement curve below the frame shows the structure's current position, where it can be seen how the frame is still in the elastic range. Then, in Figure 6-11 (b) the plastic hinge at the base of the windward column has been activated. Similarly, Figure 6-11 (c) shows the moment when the plastic hinge is activated at the base of the leeward column. Figure 6-12 (a) and (b) show the moment of activation of plastic hinges on the beam ends. At this point, the frame has yielded and cannot take any more load, but it can still continue to deform, because of the ductile nature of the flexural plastic hinge.

After the long horizontal branch in the load-displacement curve, Figure 6-12 (c) shows the moment when the first plastic hinge reaches failure (at the base of the windward column). Finally, Figure 6-13 show the moment when the other three plastic hinges reach failure, represented as discontinuities in the load-displacement curve.
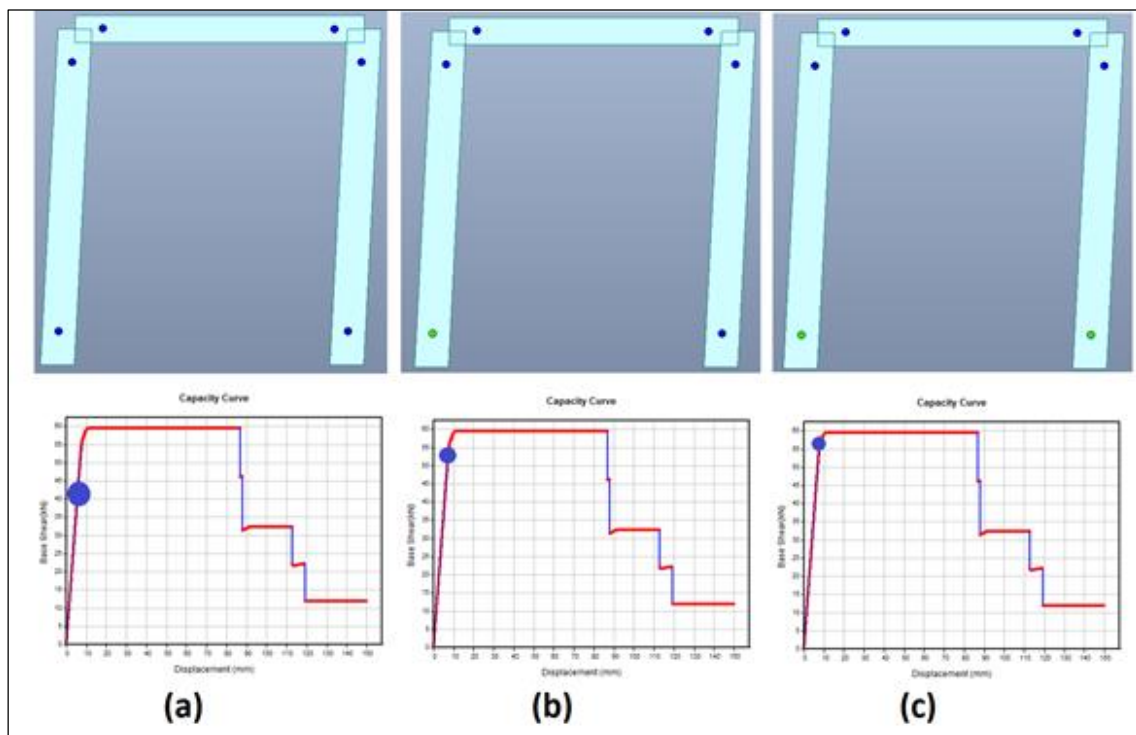
Figure 6-11. Pushover analysis plastic hinge sequence for bare frame in elastic regime

79
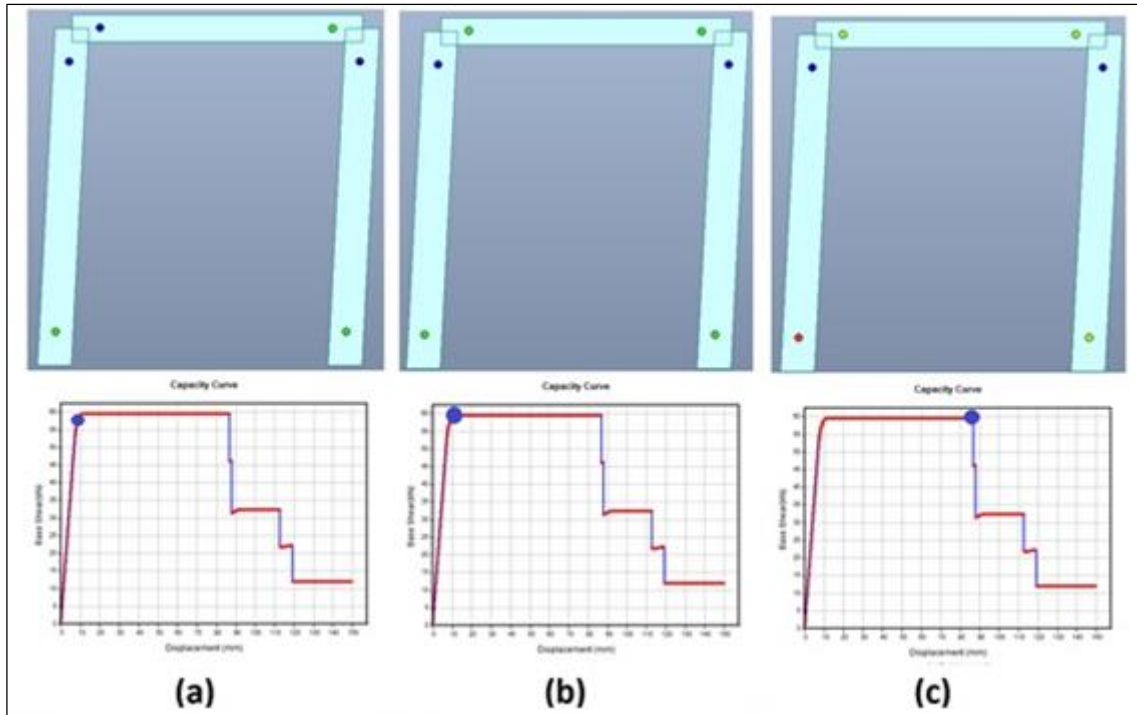
Figure 6-12. Pushover analysis plastic hinge sequence for bare frame after first yielding
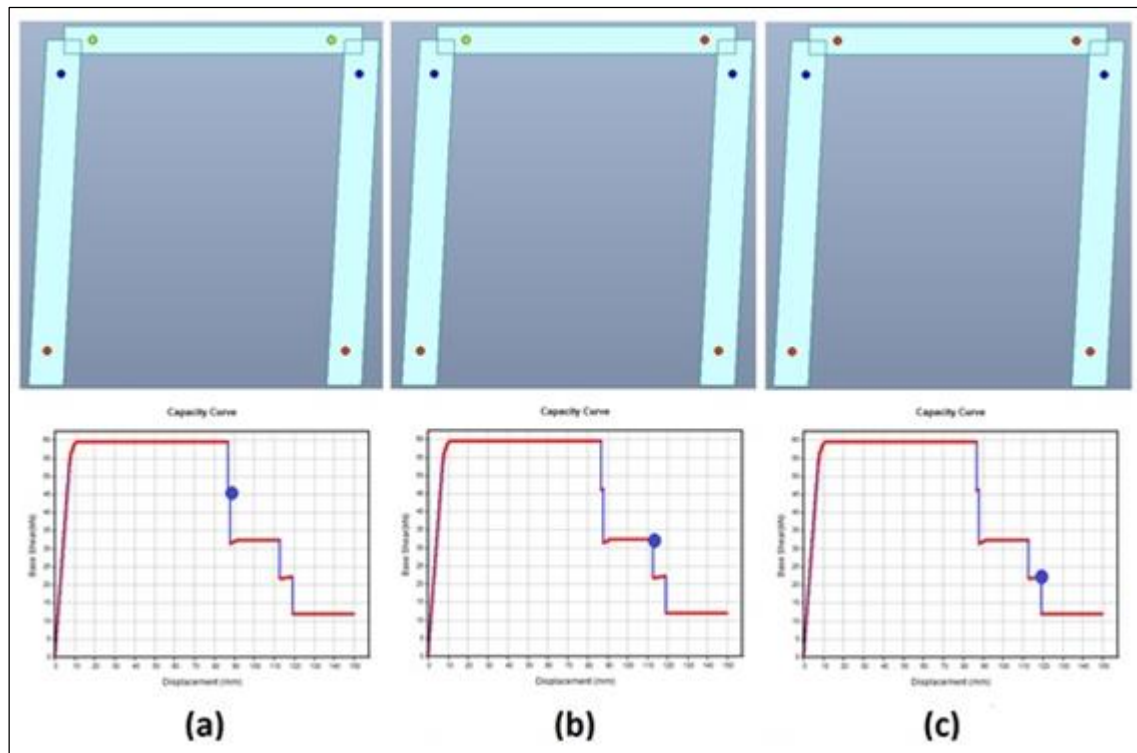
Figure 6-13 Pushover analysis plastic hinge sequence for bare frame after collapse of the columns

Failure of the structure is achieved when 4 plastic hinges are activated, as depicted in   Figure 6-13 (b). It's worth mentioning that the top sections of the columns are still

behaving elastically at the point of failure, and never achieve yielding. The most relevant results from the capacity curve in Figure 6-10 are presented in Table 6.1.

Table 6.1. Bare frame capacity curve most relevant results

	1st yield load [kN]	52.69
	Displacement at 1st yield [mm]	7.28
	2nd yield load [kN]	55.95
	Displacement at 2nd yield [mm]	8.03
	3rd yield load [kN]	58.73
	Displacement at 3rd yield [mm]	9.68
	4th yield load [kN]	59.43
	Displacement at 4th yield [mm]	10.80
	1st hinge failure load [kN]	59.43
	Displacement at 1st hinge failure [mm]	86.70
Bare frame	2nd hinge failure load [kN]	46.27
	Displacement at 2nd hinge failure [mm]	87.9
	3rd hinge failure load [kN]	32.37
	Displacement at 3rd hinge failure [mm]	112.88
	4th hinge failure load [kN]	22.13
	Displacement at 4th hinge failure [mm]	119.1
	Maximum Load [kN]	59.43
	Maximum Displacement [mm]	119.10
	Ductility $\left(\frac{\delta_y}{\delta_u}\right)$	16.36

6.3 POLYSTYRENE INFILL

6.3.1 Modelling

Polystyrene material was defined at this stage, in order to include the infill to the previous model, with the properties reported in Table 6.2 which are the same values used in Chapter 3. Figure 6-14 shows the assignment of polystyrene mechanical properties in MIDAS GEN.

Table 6.2. Polystyrene mechanical properties

Uniaxial yield strength	0.1 MPa
Initial elastic modulus	4.35 MPa
Poisson's ratio	0.01
Weight density	10.4 MPa
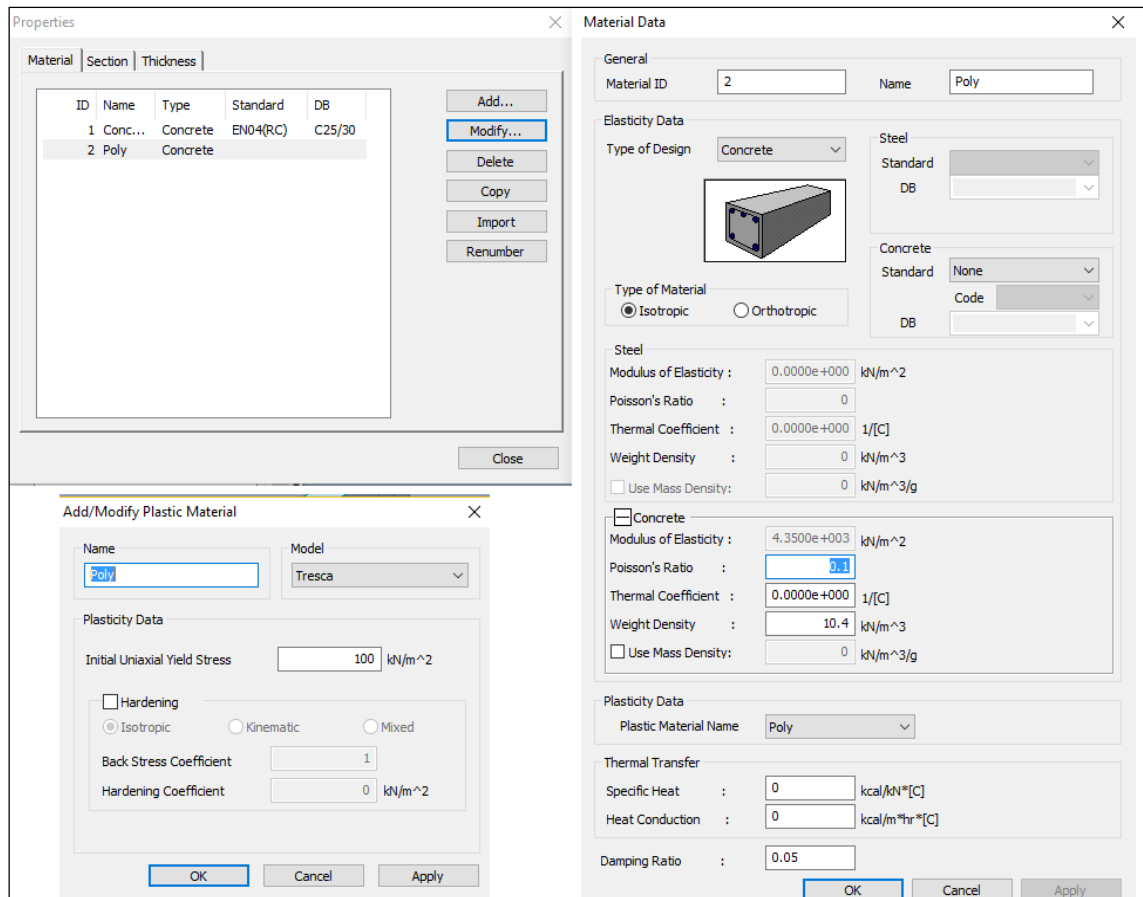
Figure 6-14. Definition of polystyrene material in MIDAS GEN
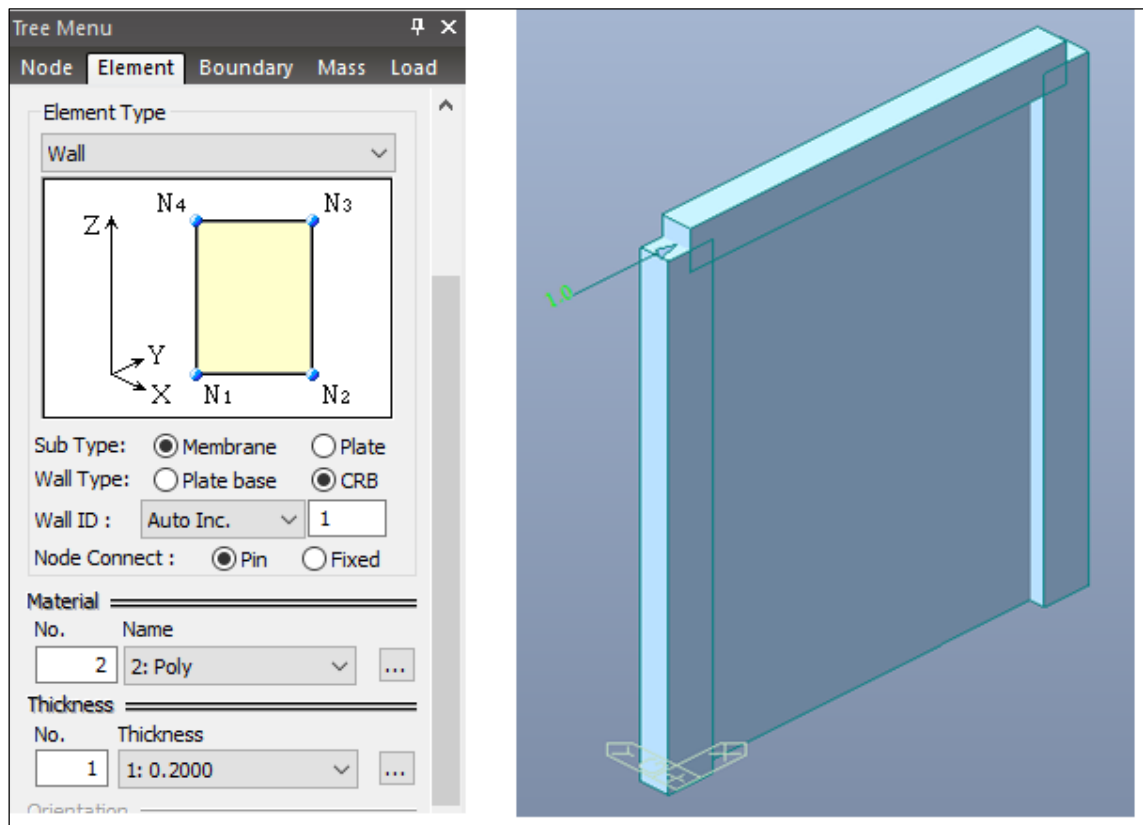
Figure 6-15. Infilled frame model in MIDAS GEN

82

Once the material has been defined, 200 mm thick Concrete Retaining Block (CRB) wall elements are defined, using membrane sub type elements, which are placed within the frame used in Figure 6-4. The new model is shown in Figure 6-15. In order to carry out the pushover analysis, reinforcement needs to be assigned to the wall (even though it has none). For this reason, a fictitious reinforcement layout of $2\phi4$ @ 1000 mm is chosen is both directions, just in order to be able to carry out the analysis, which corresponds to a reinforcement ratio of 0.0126%, which is extremely low.
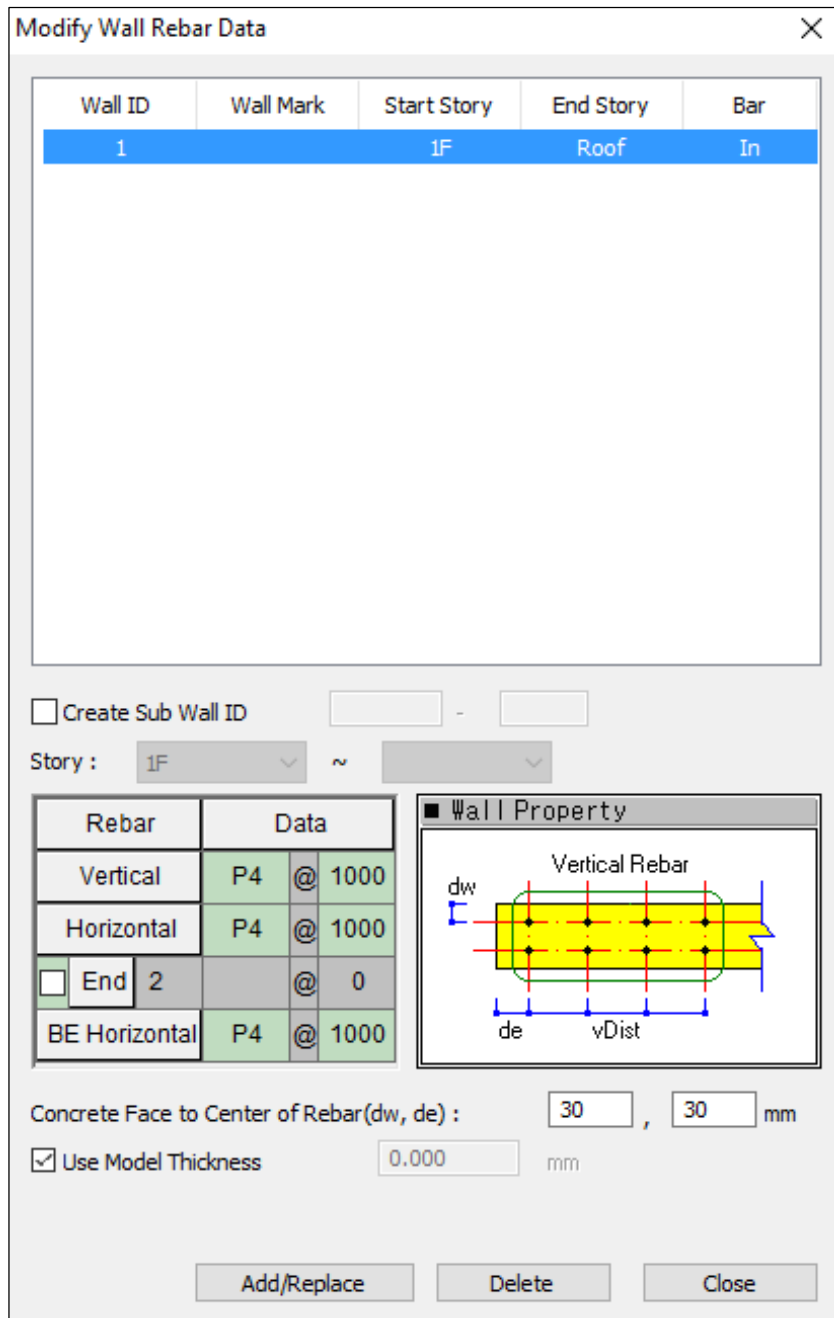
Figure 6-16. Fictitious wall reinforcement layout

6.3.2 Pushover Analysis

A similar analysis to the one performed in section 6.2.2 was carried out for this model, with the only difference that, in this case, the infill is present in the model, instead of performing the pushover analysis on the bare frame. One additional plastic hinge needed to be defined and then assigned to the top and bottom of the infill, as depicted in Figure 6-17 and Figure 6-18. The pushover curve for the infilled frame is shown in Figure 6-19.
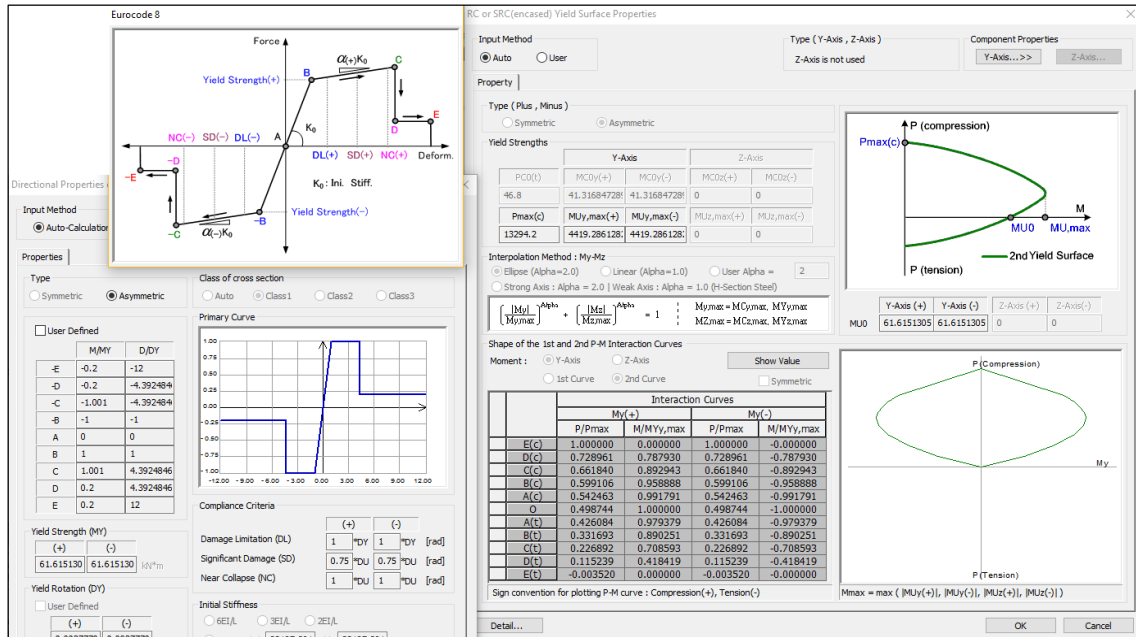
Figure 6-17. Wall flexural plastic hinge definition in Midas Gen
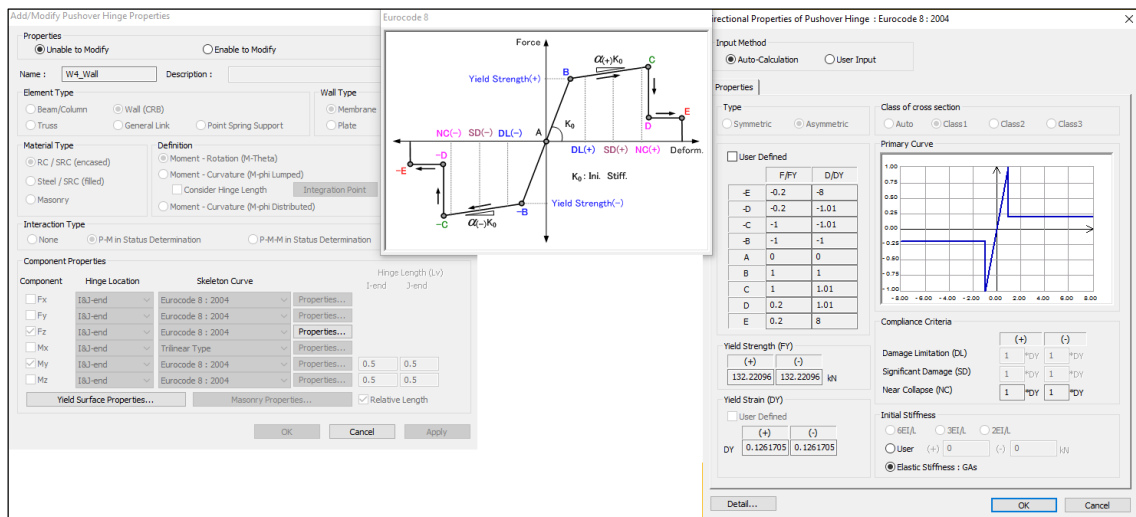
Figure 6-18. Wall shear plastic hinge definition in Midas Gen

84
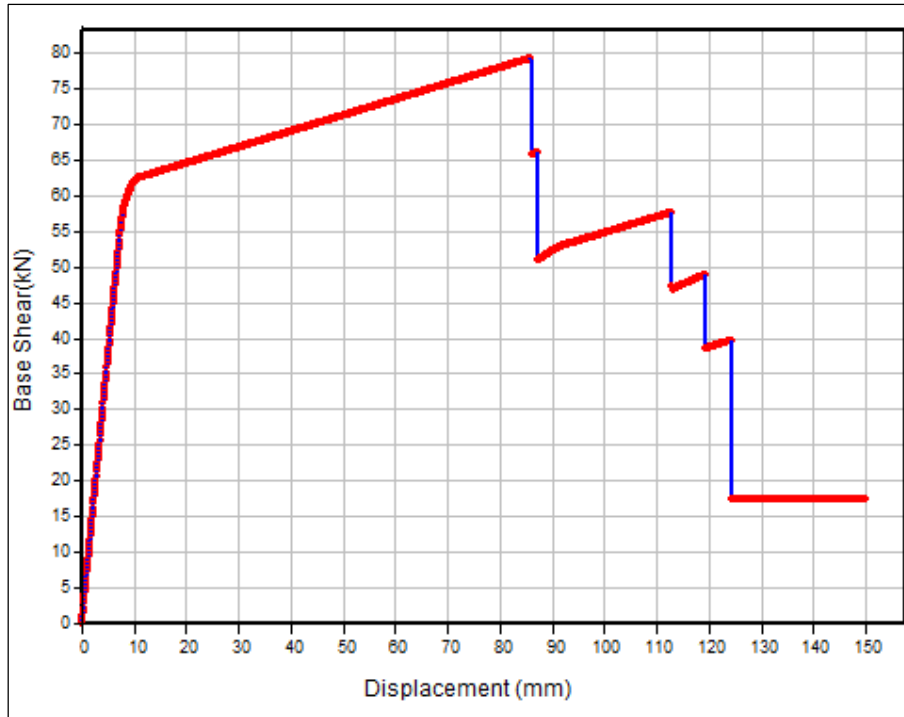
Figure 6-19. Pushover curve for infilled frame structure

From Figure 6-19 it is worth noticing how the initial behaviour of the infilled frame is quite similar to the one in Figure 6-10, of the bare frame, with a very similar yield strength, displacement and stiffness. The structure has an initial elastic behaviour (Figure 6-20 (a)). After the first plastic hinge yielding (Figure 6-20 (b)), the structure continues to take load, with a reduced stiffness. Figure 6-20 (c), (d) and (e) show the activation of the next 3 plastic hinges. At this point, the frame structure has achieved yielding and cannot continue to take additional load. Therefore, the only component which is still able to take more load is the infill, which is still behaving elastically up to this point.

After activation of the 4 plastic hinges on the frame, the structure continues to take additional load, with a significantly reduced stiffness, up until the first plastic hinge failure on the windward column (Figure 6-20 (f)), where the maximum load is achieved (79.24 kN). After the sudden drop, the structure continues to take additional load, with a constant stiffness, up until the failure of the second plastic hinge (Figure 6-21 (a)), where there is a second sudden drop in the load-displacement curve. Similarly, the structure continues to take additional load, with constant stiffness, and sudden drops where plastic hinges achieve failure (Figure 6-21 (b) and (c)). After the fourth plastic hinge has failed, the infill still behaves elastically. The structure is able to reload until reaching failure of the top plastic hinge of the infill, in shear, as depicted in Figure 6-21 (d). Due to the fact that the failure of the last plastic hinge is in shear, there is no ductile behaviour at the end, and the failure

85

occurs in a brittle way. At this point, the structure has achieved failure, at a maximum displacement of 119.18 mm. The most relevant results of the capacity curve from Figure 6-19 are presented in Table 6.3. A comparison of both capacity curves is proposed in Figure 6-22.
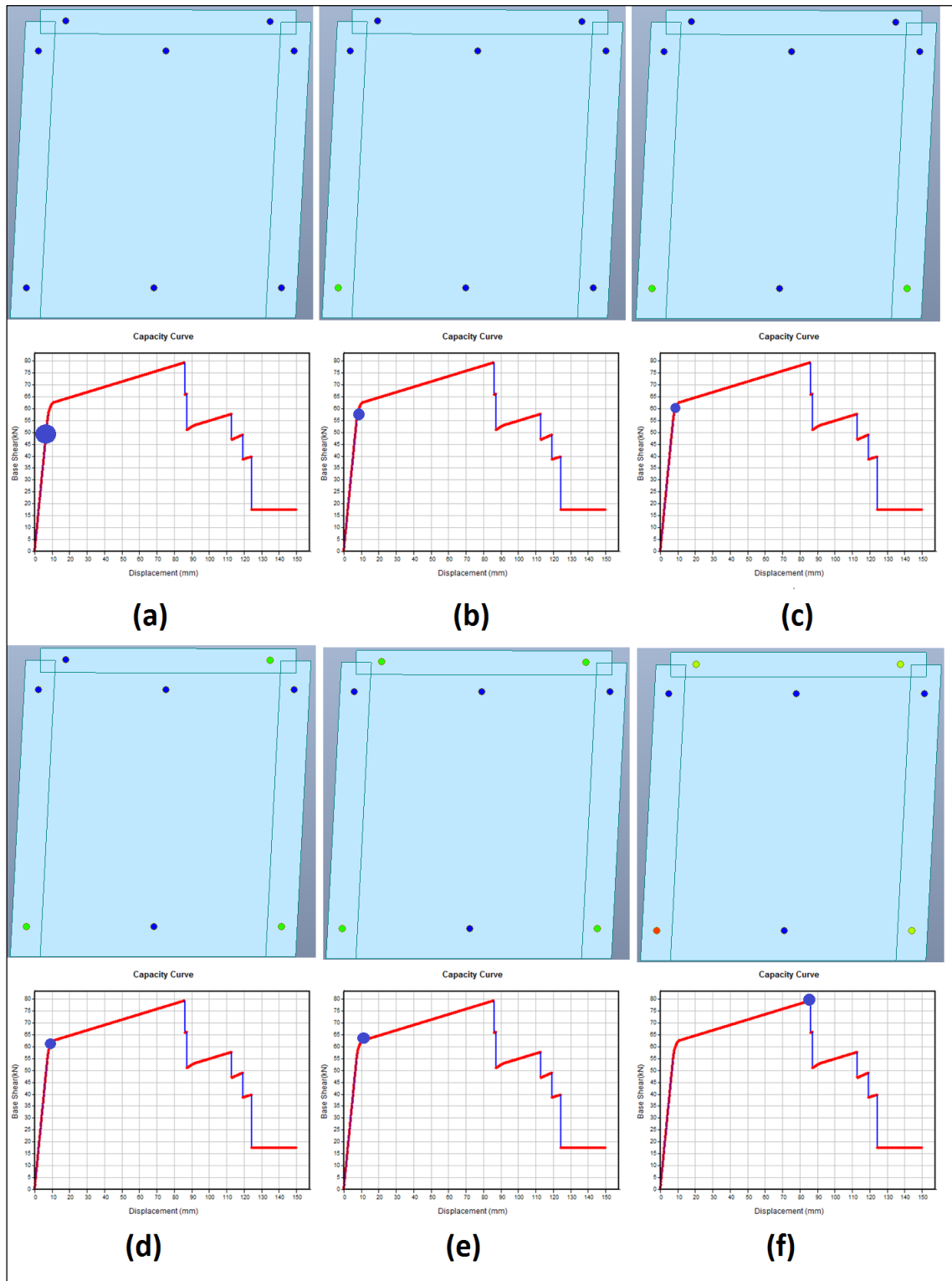
Figure 6-20. Pushover analysis plastic hinge sequence for infilled frame
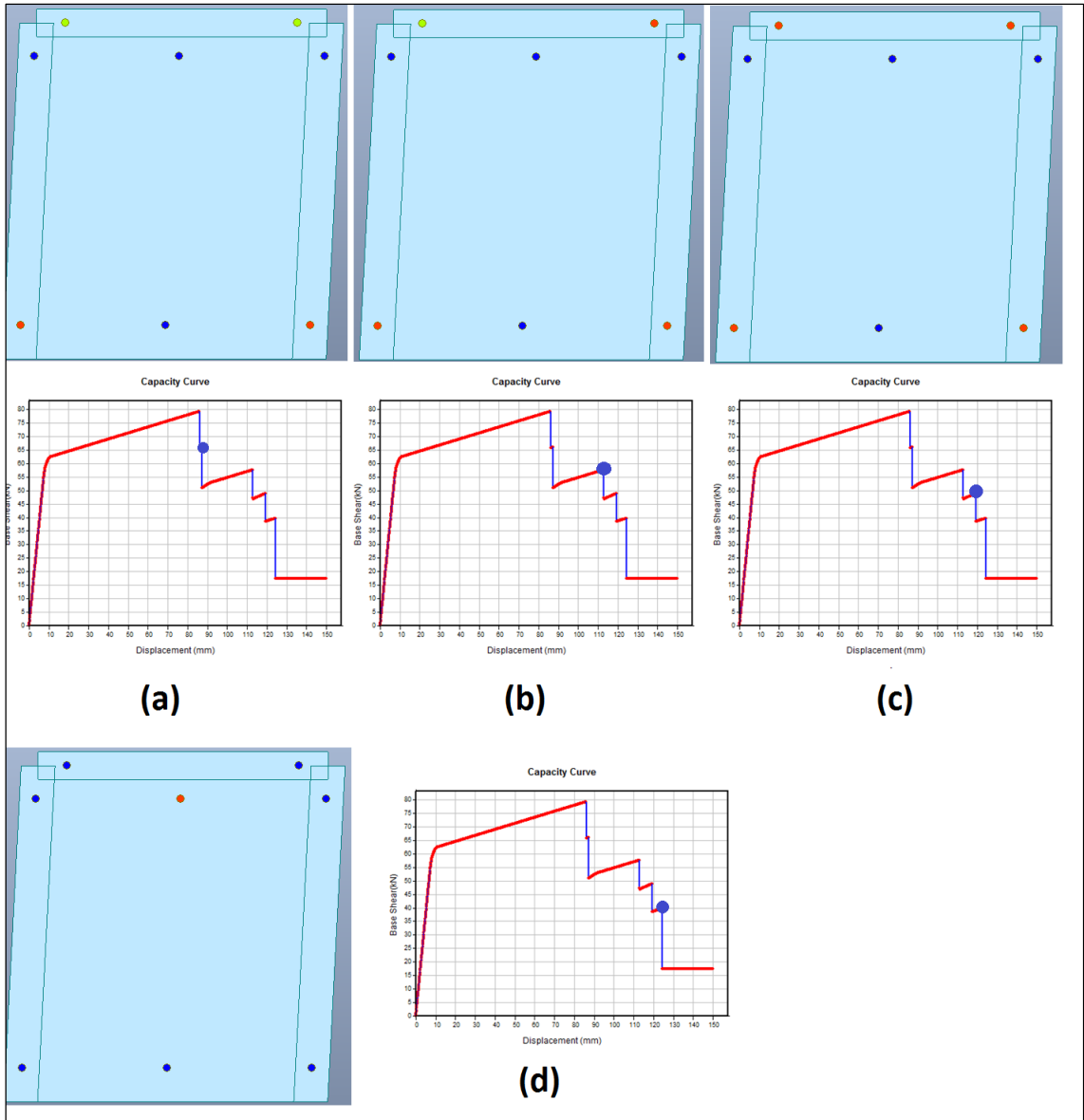
Figure 6-21. Pushover analysis plastic hinge sequence for infilled frame

Table 6.3. Infilled frame capacity curve most relevant results

	1st yield load [kN]	54.85
	Displacement at 1st yield [mm]	7.35
	2nd yield load [kN]	58.75
	Displacement at 2nd yield [mm]	8.18
	3rd yield load [kN]	61.53
	Displacement at 3rd yield [mm]	9.6
	4th yield load [kN]	62.4
	Displacement at 4th yield [mm]	10.65
	1st hinge failure load [kN]	79.24
	Displacement at 1st hinge failure [mm]	85.95
	Load increase [kN]	16.84
	2nd hinge failure load [kN]	66.10
	Displacement at 2nd hinge failure [mm]	87.23
Infilled frame	Load increase [kN]	0.46
	3rd hinge failure load [kN]	57.62
	Displacement at 3rd hinge failure [mm]	112.88
	Load increase [kN]	6.71
	4th hinge failure load [kN]	48.78
	Displacement at 4th hinge failure [mm]	119.18
	Load increase [kN]	1.18
	5th hinge failure load [kN]	39.60
	Displacement at 5th hinge failure [mm]	124.28
	Load increase [kN]	1.04
	Total load absorbed by infill [kN]	26.23
	Maximum Load [kN]	79.24
	Maximum Displacement [mm]	119.18
	Ductility $\left(\frac{\delta_y}{\delta_u}\right)$	16.21
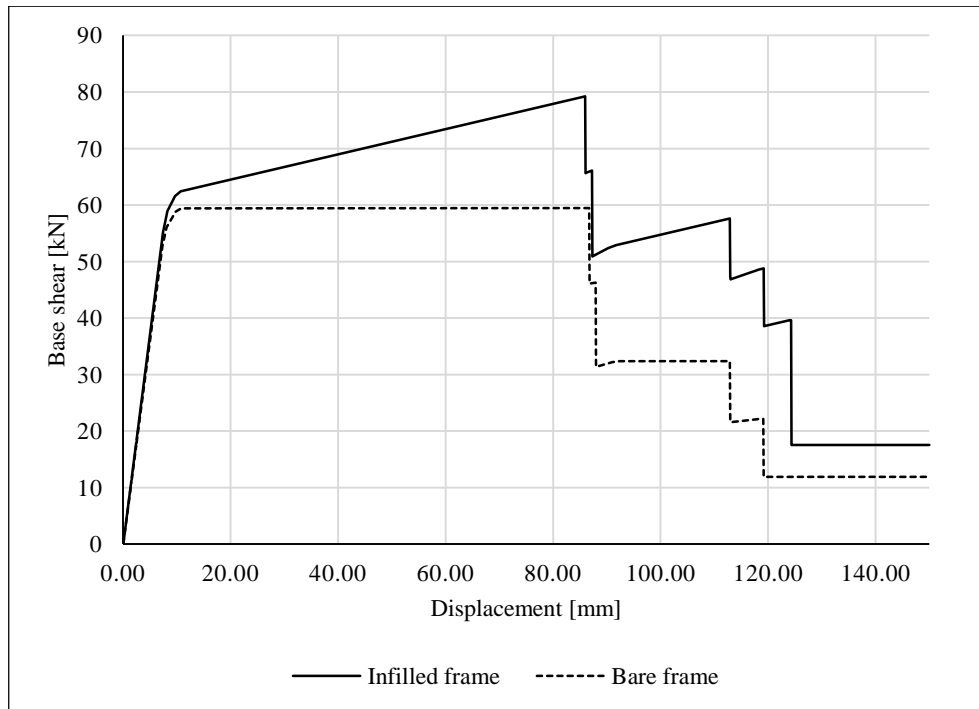
Figure 6-22. Comparison between infilled frame and bare frame capacity curves

6.4 ELASTIC MODEL WITH COMPRESSION STRUT

Another topic of interest for this investigation is the applicability of simplified methods for analysis (macro-models), instead of refined and more advanced approaches such as finite element analysis (micro-models). The use of an equivalent compression strut model for the analysis of masonry infilled RC frames under lateral load has been widely investigated and used in past years. The width of the equivalent strut, however, has been a topic of discussion and has several different approaches, as seen before in Figure 2-4. This section is dedicated to the development of a similar approach for polystyrene infilled RC frames under lateral load, using similar width-to-length ratios for the compressive strut, and comparing these results to the ones obtained by finite element analysis.

6.4.1 Modelling

Due to the fact that the purpose of this investigation is focused on simplified tools for analysis, a simple elastic approach is proposed, using 3 frame (Bernoulli beam) elements for the beam and columns, and a truss element for the equivalent compression strut, considering the elastic properties for each material accordingly (Table 6.2 for polystyrene properties, and the built in properties for C20/25 concrete in the software). Two elastic

89

models were carried out, in parallel, using the SAP2000 software: one for the frame with equivalent compression strut, and another one for the bare frame, as shown in Figure 6-23 (a) and Figure 6-23 (b) respectively. The reason for the latter model, is to use it as reference, in order to quantify the effect of adding the compression strut. It is also useful to compare it to the results obtained in section 6.2 for the bare frame.
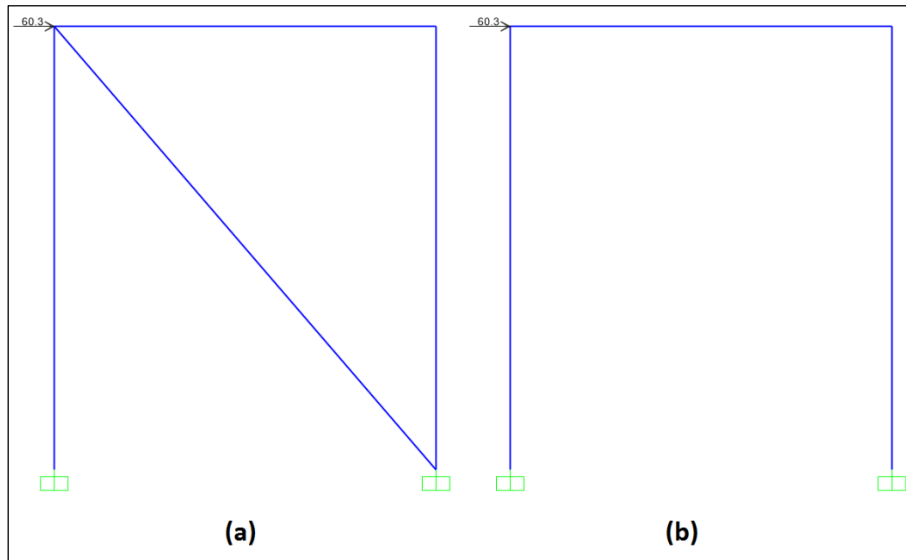
Figure 6-23. Elastic models of infilled frame with equivalent compression strut (a) and bare frame (b) in SAP2000

6.4.1.1 Bare Frame

From Table 6.1, it can be observed that the first yielding, corresponding to the base of the columns, occurs at a load equal to 52.69 kN. The internal actions on the frame, under a horizontal load of 52.69 kN, are depicted in Figure 6-24.
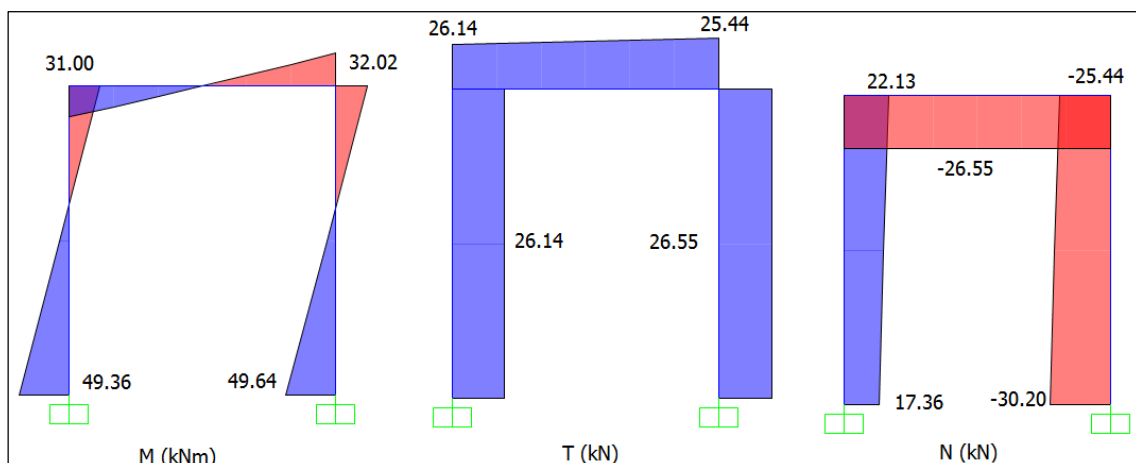
Figure 6-24. Internal actions diagrams for frame under 52.69 kN lateral load

After this first plastic hinge activation, the internal actions are "frozen", and an auxiliary structure is analysed. This auxiliary structure can be idealized as the same frame

having a hinge at the bottom section of the windward column, where the plastic hinge has been activated, and it can keep taking an additional 3.26 kN lateral load under the new structural scheme. Now, a third auxiliary structure is analysed, with 2 plastic hinges, one at the base of each column, and with a horizontal load equal to 2.78 kN. Finally, a third auxiliary structure is analysed, with one additional plastic hinge on the right hand side of the beam, and a horizontal load equal to 0.7 kN. At this point, the structure's internal actions are computed for the first model, and the three auxiliary models, and the actions are summed in order to obtain the final internal action diagrams.
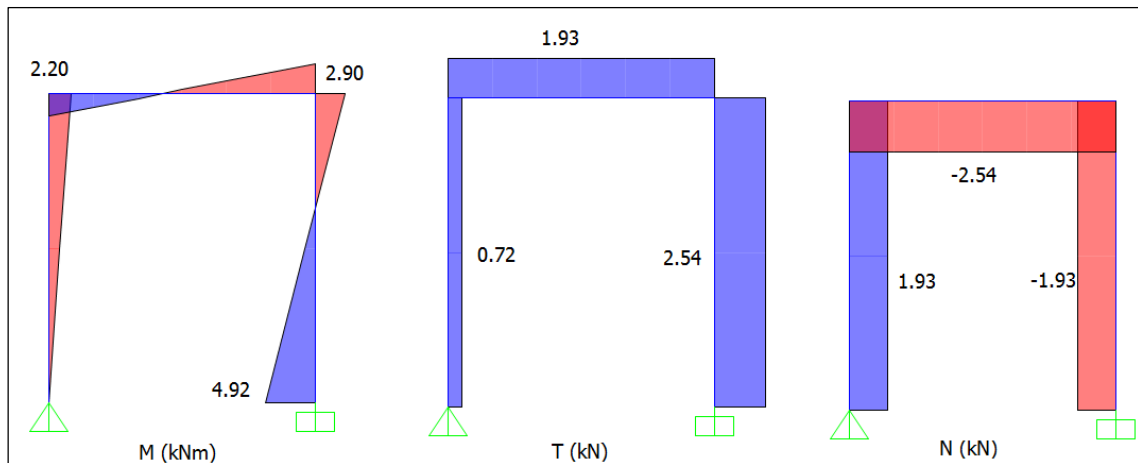
Figure 6-25. Internal actions diagrams for auxiliary structure 1
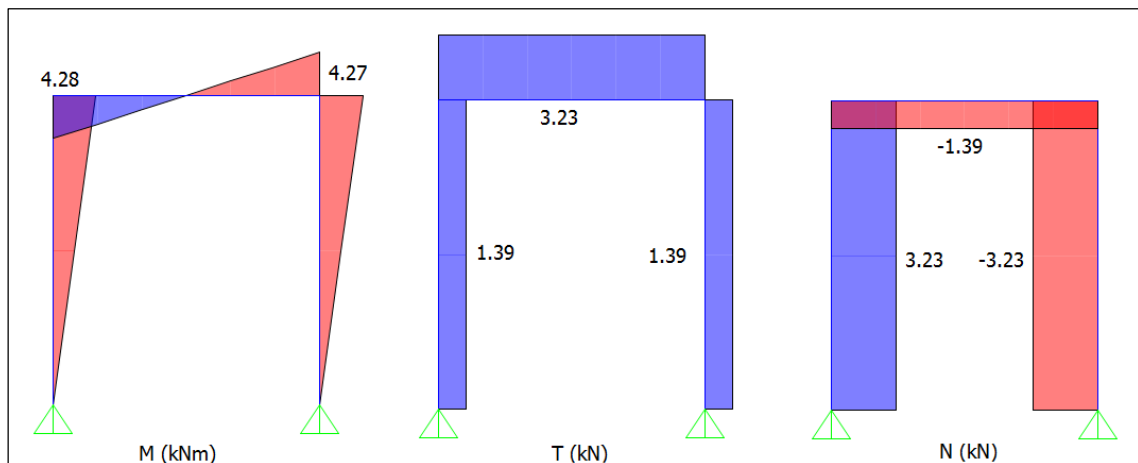
Figure 6-26. Internal actions diagrams for auxiliary structure 2
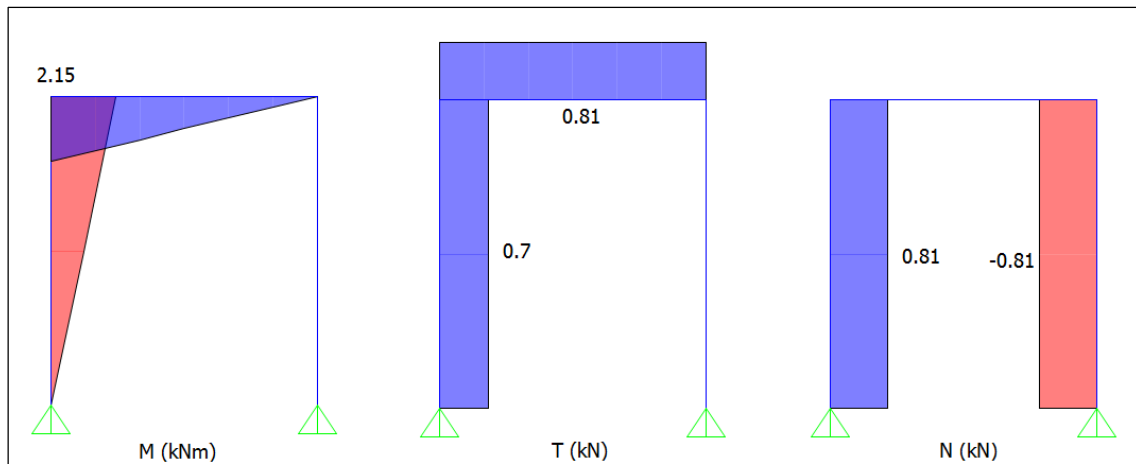
Figure 6-27. Internal actions diagrams for auxiliary structure 3

Finally, by means of the superposition principle, the internal action diagrams from Figure 6-24, Figure 6-25, Figure 6-26 and Figure 6-27 can be simply added to obtain the final diagram on the frame, under a total load of 59.43 kN, as depicted in Figure 6-28

Figure 6-28. Internal actions diagrams for frame at maximum load (59.43 kN) applying super-position principle

Finally, the corresponding horizontal displacements of the structure were computed, immediately before the formation of plastic hinges on columns and beams. The values are depicted in Table 6.4.

Table 6.4. Load-displacement points of frame structure just before activation of plastic hinges

Load [kN]	Displacement [mm]
52.69	7.29
55.95	8.04
58.73	9.73
59.43	10.94

92

6.4.1.2 Infilled frame

Similarly, an elastic analysis was carried out on the same frame structure, with the addition of a compression strut, as depicted in Figure 6-23 (a). Initially, a compression strut width/length ratio of $w/D = 0.25$ was considered, as a first approximation, which was later checked and adjusted. This results in using a strut with dimensions 200 x 1127 mm. From Table 6.3, the relevant points of interest to be analysed can be determined. Similar to the previous analysis, an incremental elastic analysis was performed. First, a 54.85 kN load was applied on the frame structure with compression strut, fixed at the bottom. Then, incremental loads were applied on the auxiliary models accordingly, in order to follow the plastic hinge activation sequence observed in Figure 6-20, similar to the analysis performed in section 6.4.1.1. Results can be seen in Figure 6-29 - Figure 6-34.
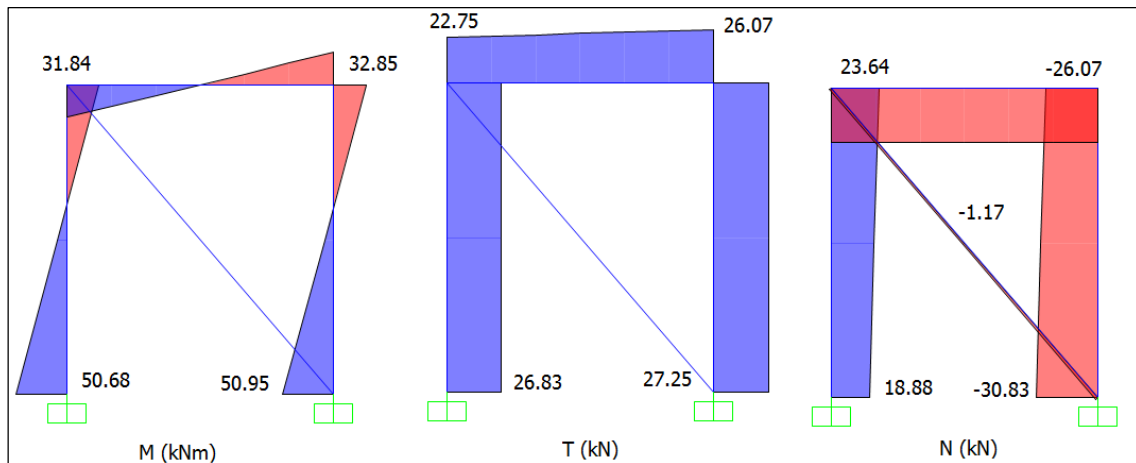
Figure 6-29. Internal actions diagrams for frame with strut under 54.85 kN lateral load
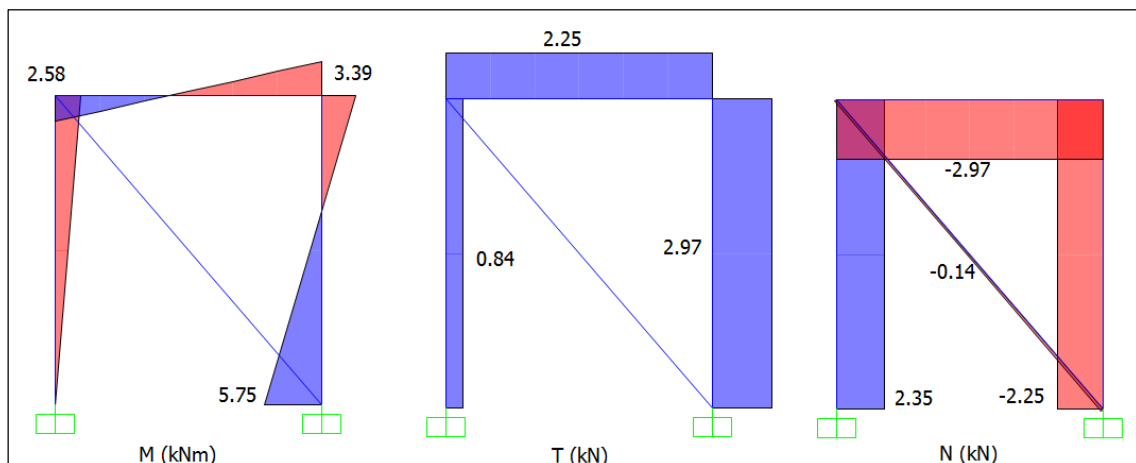
Figure 6-30. Internal actions diagrams for auxiliary structure 1
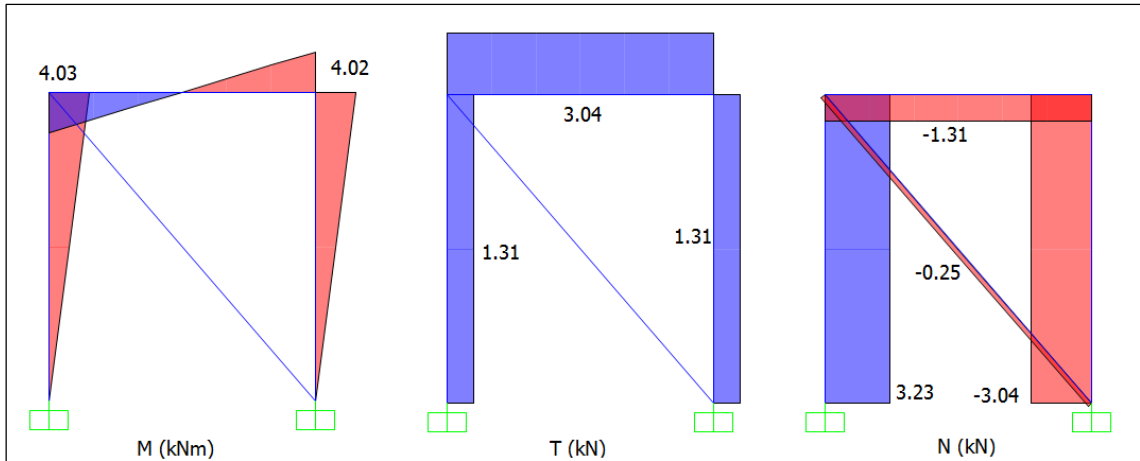
Figure 6-31. Internal actions diagrams for auxiliary structure 2
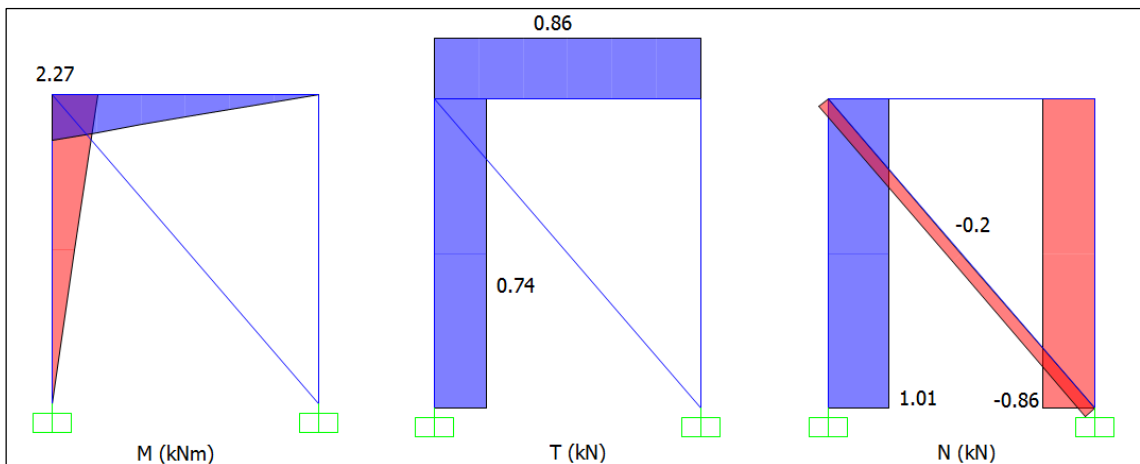
Figure 6-32. Internal actions diagrams for auxiliary structure 3
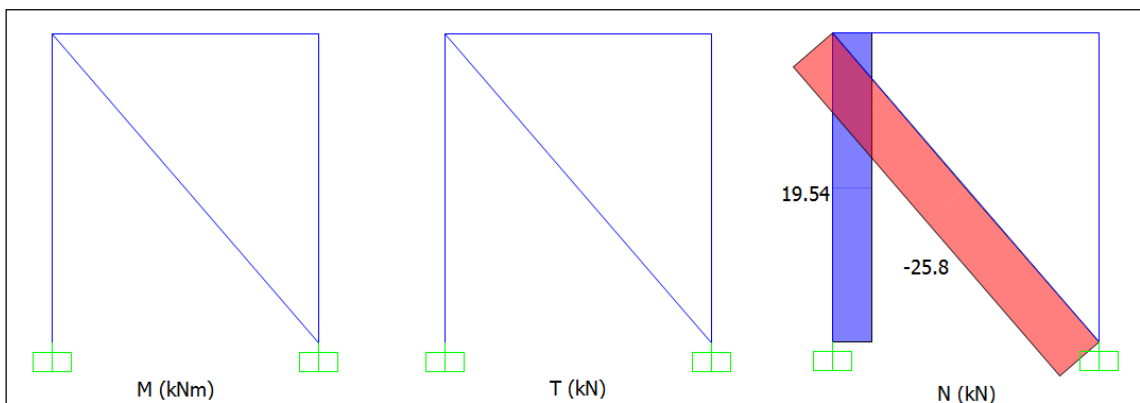
Figure 6-33. Internal actions diagrams for auxiliary structure 4

At this point, plastic hinges are activated at both, the base of the columns, and at the ends of the beams. From this point forward, the only component which is still able to carry additional load is the compression strut, through axial force. The strut carries an additional 16.84 kN before the failure of the first plastic hinge, reaching the maximum load of the capacity curve in Figure 6-19. After the sudden drop due to the failure of plastic hinges at

the base of the columns, the strut continues to take even more load. As shown in Table 6.3, the infill is able to carry an additional 26.23 kN in total, after the frame structure has completely yielded. The resulting internal actions at this point are depicted in Figure 6-34.
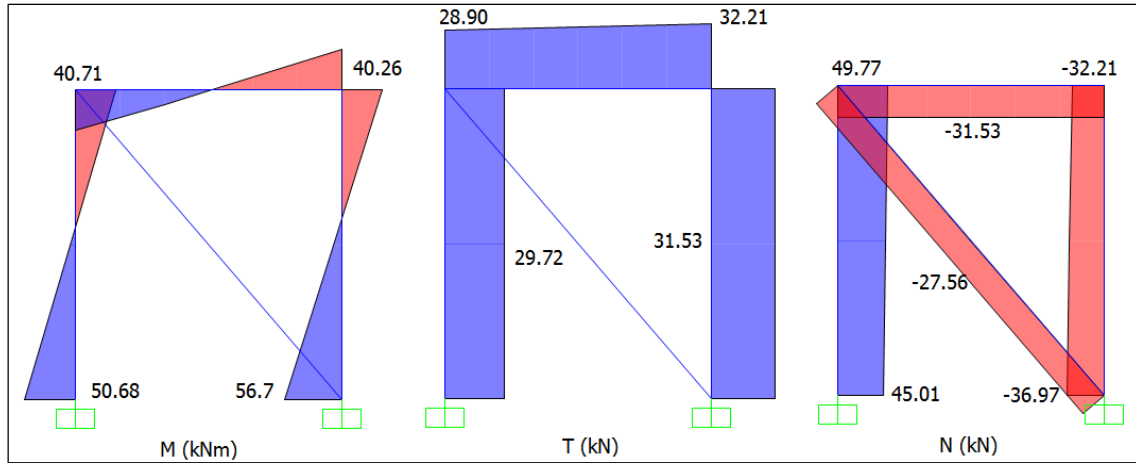
Figure 6-34. Internal actions diagrams for frame with strut at maximum load (79.24 kN) applying super-position principle [kN, m]

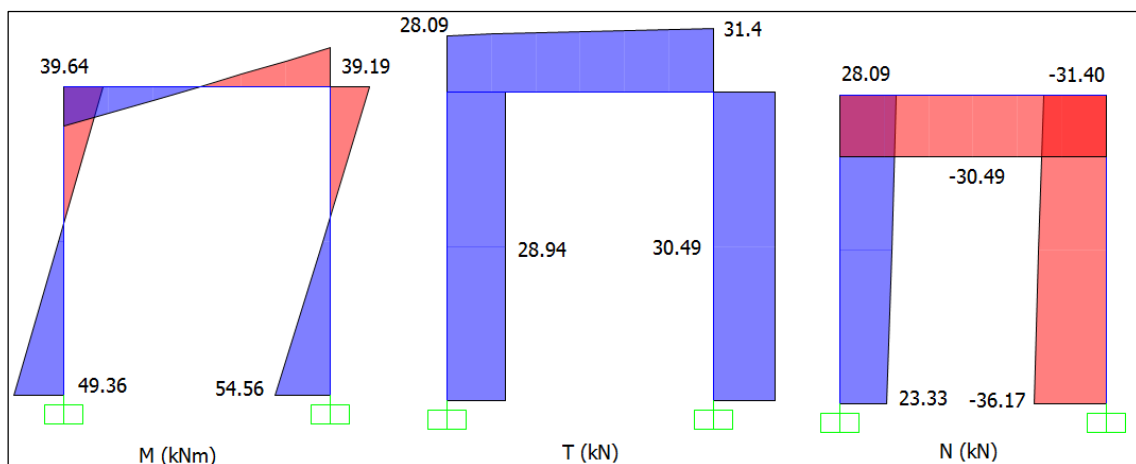Finally, the corresponding horizontal displacements of the structure were computed, immediately before the formation of plastic hinges on columns and beams, and at the moment the structure reaches its maximum load capacity. The values are depicted in Table 6.5.

Table 6.5. Load-displacement points of infilled frame structure just before activation of plastic hinges and at maximum load capacity

Load [kN]	Displacement [mm]
54.85	7.48
58.75	8.36
61.53	9.95
62.4	11.23
79.24	174.86

6.4.2 Elastic analysis and results

Two elastic models were carried out, in parallel, in order to quantify the influence of adding the compression strut, and to compare the results of a simple elastic approach to the pushover analysis from section 6.3. In order to model the post-elastic behaviour of the frame (after activation of the first plastic hinge and before collapse), auxiliary models were used with idealized hinges at the sections where plastic hinges have been activated. The internal actions from these auxiliary models were then super imposed to the ones where the structure is still behaving elastically, to obtain the final internal actions (Figure 6-28 and Figure 6-34).

95

It's worth mentioning that, for the purpose of this analysis, the strut was considered weightless, in order to compare the results with the ones of the bare frame adequately.

From Figure 6-29 - Figure 6-33, it is clear that the compressive strut, due to its very low elastic modulus (and hence low axial rigidity), has a negligible contribution on the structure's resisting mechanism against lateral force before activation of all four plastic hinges. It is not until the frame structure has completely yielded that the strut is really activated (Figure 6-33), and starts to take load. An additional analysis was performed, in which both, the bare frame and the frame with strut, were subjected to a 100 kN lateral load, during elastic phase, and at each activation of plastic hinge, in order to isolate and quantify the sole effect of adding the compression strut, at each stage. Internal actions at the sections of interest (see Figure 6-35) are reported in Table 6.6.
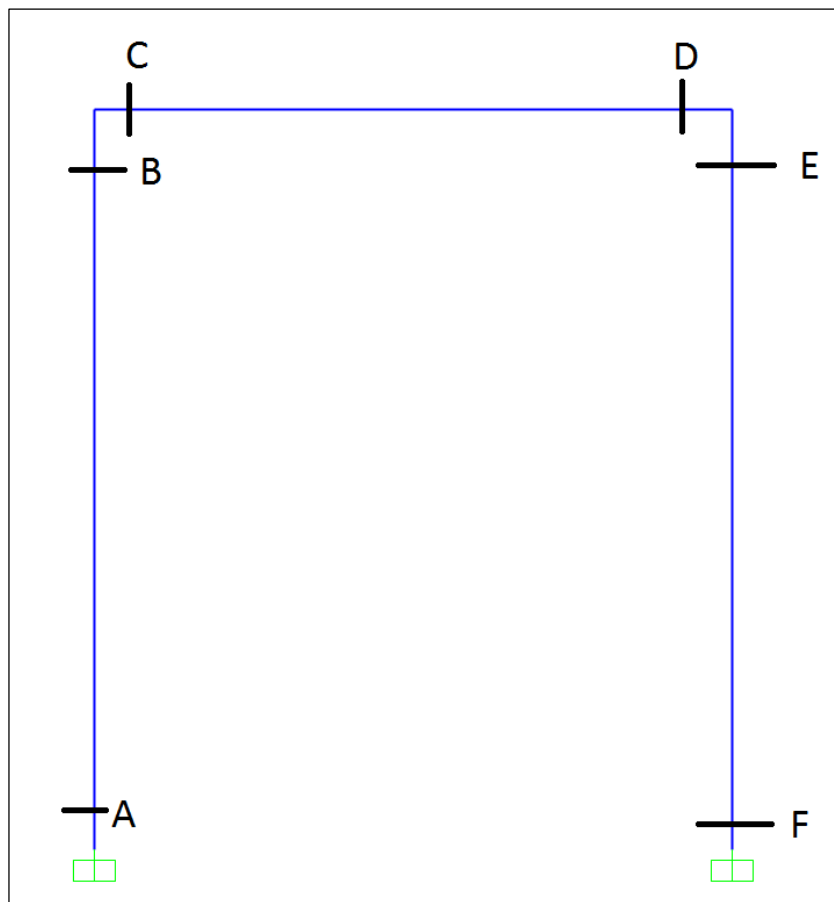
Figure 6-35. Sections of RC frame studied in order to quantify contribution of compression strut

Table 6.6. Internal actions on the bare frame and frame with strut, under 100 kN horizontal loading

Section	Stage	Bare frame				Frame with strut			
		M(x) [kN-m]	V(x) [kN]	N(x) [kN]	Top disp. [mm]	M(x) [kN-m]	V(x) [kN]	N(x) [kN]	Top disp. [mm]
A	No plastic hinges	94.2	50.11	45.14		92.89	49.41	46.12	
B		59.9	50.11	45.14		59.06	49.41	46.12	
C		59.9	45.14	-49.89		59.06	44.5	-49.19	
D		59.71	45.14	-49.89	13.83	58.87	44.5	-49.19	13.64
E		59.71	49.89	-45.14		58.87	49.19	-44.5	
F		93.69	49.89	-45.14		92.39	49.19	-44.5	
strut		-	-	-		-	-	-2.14	
A	With first plastic hinge	-	21.99	59.06		-	21.49	60.37	
B		67.63	21.99	59.06		66.07	21.49	60.37	
C		67.63	59.06	-78.01		66.07	57.69	-76.21	
D		88.87	59.06	-78.01	23.06	86.82	57.69	-76.21	22.53
E		88.87	78.01	-59.06		86.82	76.21	-57.69	
F		150.99	78.01	-59.06		147.52	76.21	-57.69	
strut		-	-	-		-	-	-3.53	
A	With first two plastic hinges	-	50.02	116.04		-	47.09	116.04	
B		153.81	50.02	116.04		144.8	47.09	116.04	
C		153.81	116.04	-49.98		144.8	109.24	-47.05	
D		153.69	116.04	-49.98	60.67	144.69	109.24	-47.05	57.13
E		153.69	49.98	-116.04		144.69	47.05	-109.24	
F		-	49.98	-116.04		-	47.05	-109.24	
strut		-	-	-		-	-	-8.97	
A	With three plastic hinges	-	100	116.04		-	84.86	116.04	
B		307.5	100	116.04		260.93	84.86	116.04	
C		307.5	116.04	-		260.93	98.47	-	
D		-	116.04	-	173.58	-	98.47	-	147.33
E		-	-	-116.04		-	-	-98.47	
F		-	-	-116.04		-	-	-98.47	
strut		-	-	-		-	-	-23.2	

Table 6.7 shows the error made by computing the internal actions and displacements on the bare frame, instead of the frame with the strut, assuming the values of the frame with the strut are the correct ones. As it can be observed, the error is quite negligible at the first three stages (6% difference). Finally, after the formation of the third plastic hinge, results are significantly different (more than 17%). In general, the internal actions on the bare frame are always slightly higher than the ones on the frame with strut. The results confirm once

again that, due to the great difference in rigidities to lateral loading between the frame and the strut, the contribution of the strut is negligible before the RC frame has reached at least 3 plastic hinge activations. Due to the fact that the third and fourth plastic hinge yield at practically the same load, for practical purposes, the latter stage has no significant contribution on the response either.

Table 6.7. Difference between internal actions on bare frame and frame with strut

Section	Load	M(x)	V(x)	N(x)	Top displacement
A	No plastic hinges	1.41%	1.42%	-2.12%	
B		1.42%	1.42%	-2.12%	
C		1.42%	1.44%	1.42%	
D		1.43%	1.44%	1.42%	1.39%
E		1.43%	1.42%	1.44%	
F		1.41%	1.42%	1.44%	
strut		-	-	-	
A	With first plastic hinge	-	2.33%	-2.17%	
B		2.36%	2.33%	-2.17%	
C		2.36%	2.37%	2.36%	
D		2.36%	2.37%	2.36%	2.35%
E		2.36%	2.36%	2.37%	
F		2.35%	2.36%	2.37%	
strut		-	-	-	
A	With first two plastic hinges	-	6.22%	0.00%	
B		6.22%	6.22%	0.00%	
C		6.22%	6.22%	6.23%	
D		6.22%	6.22%	6.23%	6.20%
E		6.22%	6.23%	6.22%	
F		-	6.23%	6.22%	
strut		-	-	-	
A	With three plastic hinges	-	17.84%	0.00%	
B		17.85%	17.84%	0.00%	
C		17.85%	17.84%	-	
D		-	17.84%	-	17.82%
E		-	-	17.84%	
F		-	-	17.84%	
strut		-	-	-	

6.5 SUMMARY AND ANALYSIS OF RESULTS

Two pushover analysis were carried out, one for the bare frame, and the other for the infilled frame, in sections 6.2 and 6.3 respectively. Section 6.4 focuses on an elastic analysis for two models separately, one of a bare frame, and one of a frame with a compression strut, which represents the infill contribution to the lateral load response. The purpose of the elastic analysis was to compare the results to the pushover analysis, in order to predict if simplified tools are appropriate for the task of modelling polystyrene infilled frames.

By comparing the two pushover curves in Figure 6-22 it can be observed how the initial stiffness is practically identical in both cases. This behaviour suggests that the infill is not contributing to the lateral response of the structure in the initial (elastic) branch, since the infilled frame presents the same response as the one of the bare frame, except for a very slight gain of strength (4.76%). After the frame yielding (at about 10.6mm in the load-displacement curve), the bare frame pushover curve presents a horizontal branch, since the frame cannot take any more load, while the infilled frame curve continues to take additional load. This means that the moment when the frame yields completely (4 plastic hinges have been activated), the infill begins to get loaded.

The fact that the infill presents a negligible contribution to the lateral load resistance before the frame achieves yielding is also confirmed by the elastic analysis performed in section 6.4.1.2, where the strut is practically unloaded before this point. Additionally, the influence of adding the strut was quantified for each stage of plastic hinge formation, and reported in Table 6.7. It can be noted that, similar to what was observed during the pushover analysis, before the activation of the four plastic hinges, the strut has a negligible contribution on the response to lateral loading.

Next, the load-displacement relationship was investigated and compared between the elastic approach and the pushover analysis. At every activation point of plastic hinges, displacements were computed for each respective load. An additional point was included before failure of the first plastic hinge in the case of the infilled frame. For this purpose, the displacement on the elastic model was constructed by the super position of several auxiliary models, in order to account for the plastic hinge formation at the base of columns and beam ends, as seen in section 6.4. The difference between both approaches was computed assuming the pushover analysis to be the correct one.

Table 6.8. Comparison of the load-displacement relation between elastic and pushover analysis

Structure	Load [kN]	Displacement [mm]		Difference [%]
		Elastic analysis	Pushover analysis	
Bare frame	52.69	7.29	7.28	0.14
	55.95	8.04	8.03	0.12
	58.73	9.73	9.68	0.52
	59.43	10.94	10.8	1.30
Infilled frame	54.85	7.48	7.35	1.77
	58.75	8.36	8.18	2.20
	61.53	9.95	9.6	3.65
	62.4	11.23	10.65	5.45
	79.24	174.86	85.95	103.44

Table 6.8 shows, in general, good agreement between the results of the pushover analysis and elastic approach of the bare frame, even after the activation of three plastic hinges. In the case on the infilled frame, there is also good agreement up until the formation of the third plastic hinge. After this point, and before reaching failure of the first plastic hinge, the results diverge greatly (more than 100%), which makes the elastic approach clearly unreliable after this point. Results can also be seen graphically in Figure 6-36 and Figure 6-37. In general, the elastic analysis leads to greater displacements. The great difference between either analyses at the last stage is partly due to assumptions made during the pushover analysis, such as the plastic hinge length (due to the lumped plasticity approach). Also, the strut width plays an important role at this point, as the axial stiffness of the strut depends on it.
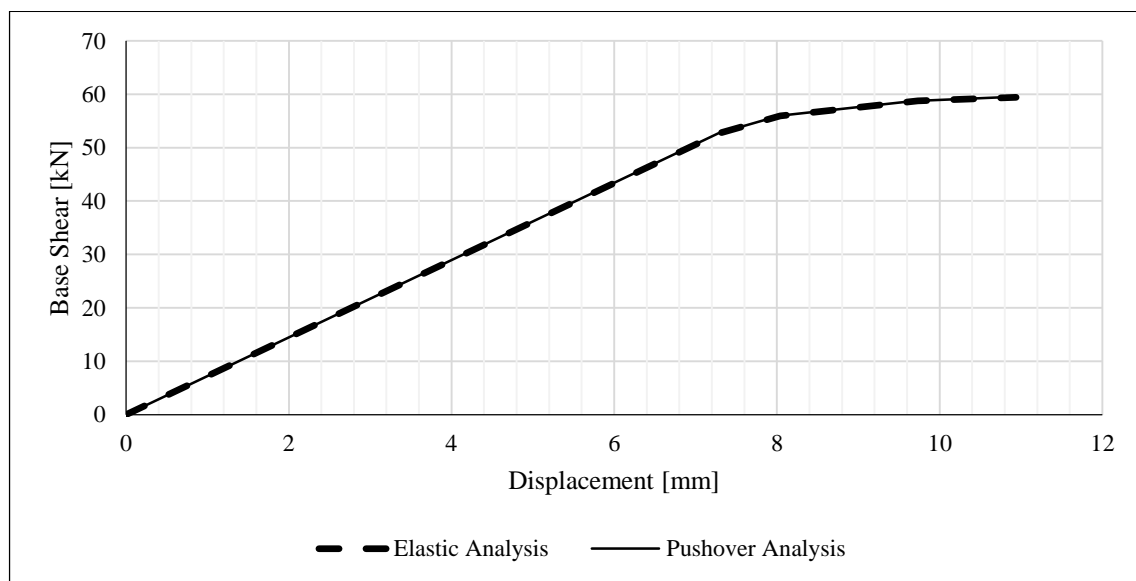

Figure 6-36. Load-displacement relationship of bare frame: Elastic analysis vs. Pushover analysis
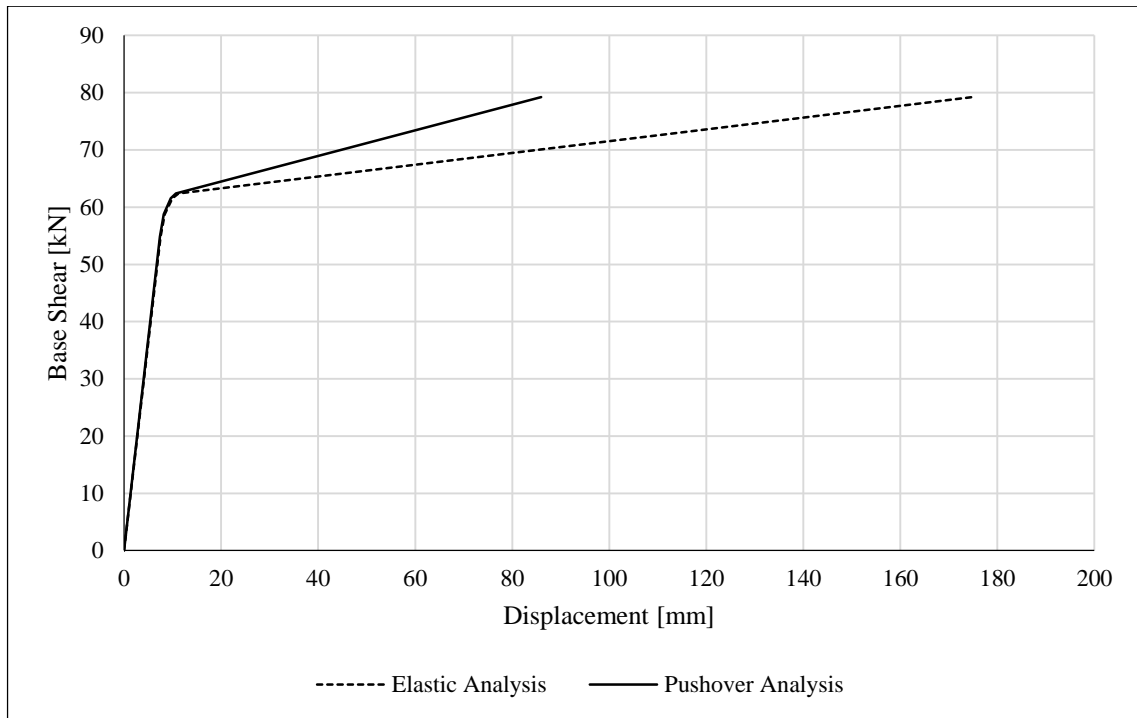
Figure 6-37. Load-displacement relationship of infilled frame: Elastic analysis vs. Pushover analysis

By analysing the capacity curve in Figure 6-19, it can be observed that the plot follows a constant linear stiffness after the frame structure has yielded (after approximately a 10.65 mm displacement). If the hinge failures on the concrete frame were disregarded (plastic hinges with infinite deformation capacity for the RC frame) the curve would follow a straight line from the point where the concrete frame has yielded, up until failure of the plastic hinge of the infill. This is, actually, in line with the fact that the infill is the only component which is still able to carry load after this point, and is behaving elastically, as discussed previously.

By computing the slope of the load-displacement curve in Figure 6-19, the elastic stiffness was obtained, as shown in (6-1), which is constant throughout all the "growing" or "loading" segments of the plot after frame has yielded.

$$K = \frac{\Delta V}{\Delta x} = 224 \ N/mm \qquad (\textbf{6-1})$$

Let us now consider the structure in Figure 6-23 (a). As mentioned before, after the frame structure has yielded, the only element still able to carry load is the compression strut. As it is behaving elastically, the strut, whose load carrying mechanism consists of axial loading only, has the well know elastic stiffness for an element under axial loading:

$$K = \frac{EA}{L} \qquad (\textbf{6-2})$$

Where:

- E = Elastic Modulus of Polystyrene: 4.35 MPa
- A = Cross section area of the strut [mm^2]
- L = Length of the strut: 4059 mm

The only unknown quantity is the cross section area of the strut. By fixing the out of plane thickness equal to 200 mm (equal to the thickness of the infill), the only unknown remains the strut width (w). The problem has one equation and one unknown. By equating expressions (6-2) and (6-1), the value for the strut width is determined.

$$K = \frac{EA}{L} = \frac{(4.35\ MPa) \cdot (200\ mm) \cdot w}{4059\ mm} = 224\ \frac{N}{mm} \qquad\qquad (\textbf{6-3})$$

$$w = 1045\ mm \qquad\qquad (\textbf{6-4})$$

$$^{w}/_{D} = {^{1045}}/_{4059} = 0.257 \qquad\qquad (\textbf{6-5})$$

According to the previous expressions, in order to analyse the structure with an equivalent compression strut, a 200 x 1045 mm strut should be used. The strut width ratio, in this case, corresponds to w/D = 0.26 (practically identical to the w/D = 0.25 used during the elastic analysis in section 6.4), which is inside the common value range used for masonry infilled frames, as discussed in Chapter 2.

Chapter 7

Conclusions

After an experimental test and a few numerical analyses were performed, we can sum up some highlights which will be presented in this chapter. Giving emphases to the experimental part of this thesis, we can conclude:

- Experimental results
    - The mortar layer gave an initial strong contribution to the lateral resistance of the frame after which an almost constant contribution of the infill was present;
    - Values of the curvature obtained for column cross sections were very reasonable and similar to the ones for bare frame. Critical sections were able to dissipate energy which is not the case when masonry infill is used;
    - Polystyrene infill does not prevent cracks from occurring;
    - Formed cracks were concentrated in areas which are in tension, while compressed parts stayed almost intact;
    - Sliding failure mode was noticed (in Chapter 3 named as failure mode 5);
    - In the final stages of the experiment, infill got detached from the bottom of the testing frame along its whole length, crack was around 6 mm wide;
    - Cracks in windward column occurred but without crushing of the concrete;
    - Overall behaviour of the mock-up can be regarded as ductile.

- Modelling results
    - When FEA and analytical solutions are being used, with characteristic values for material strength, values of about 30% lower compared to the experimental ones are obtained, which is good from the designing point of view;

- When modelling a frame infilled with polystyrene panels, an increase of 25% in resistance is occurring compared with models of a bare frame;
- Elastic analysis with compressed strut can be used during elastic phase.

- Comparison of the experimental results with numerical solutions
    - Both experimental and numerical solutions show us that when using polystyrene infill an increase of 25% in strength is occurring;
    - Even when characteristic values are used during modelling, failure occurs at similar displacement (for this case was at 120 mm);
    - Pushover curve obtained from the experiment has the same stiffness (during elastic phase) as the one for the bare frame obtained by means of numerical analysis (Figure 5-15).

Finally, numerical modelling can be successfully used to predict the limit strength of a frame infilled with the polystyrene panels (laboratory tests are recommended to be carried out, in order to determine the mechanical properties of the materials used for future investigations (concrete, polystyrene, reinforcing steel, etc.); if characteristic values are used, obtained results should be increased by 25-30%).

Appendix A

Testing frame verification - bolts

Verification will be done for 80 kN force since that is the highest expected force to occur. This value was obtained in Chapter 6. Layout of the frame is depicted in Figure A-1. Resulting forces are shown in Figure A-2.
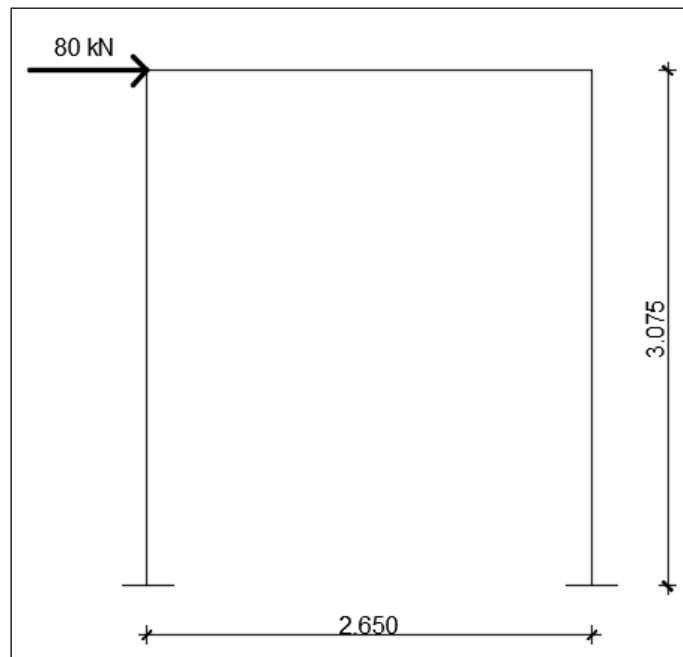

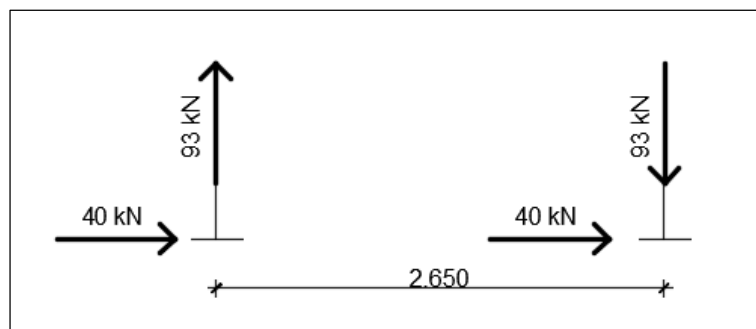**Figure A-1.** Layout of the frame

Figure A-2. Resulting forces

Both columns have 6 x M24 8.8 bolts.

Forces acting on one bolt:

$$V = \frac{40kN}{6} = 6.67kN \quad F = \frac{93kN}{6} = 15.5kN$$

In the worst case only two bolts are taking shear force so it is 40 kN per bolt in shear.

Properties of M24 8.8 bolt:

$$f_{yb} = 640MPa \qquad f_{ub} = 800MPa \qquad A_s = 353mm^2$$

Tension verification:

$$F_{t,Rd} = k_2 f_{ub} \frac{A_s}{\gamma_{M2}} = 0.9 \cdot 800MPa \cdot \frac{353mm^2}{1.25} = 203kN > 15.5kN$$

Shear verification:

$$F_{v,Rd} = \alpha_v f_{ub} \frac{A_s}{\gamma_{M2}} = 0.6 \cdot 800MPa \cdot \frac{353mm^2}{1.25} = 135kN > 40kN$$

Combination:

$$\frac{15.5}{203} + \frac{40}{135} = 0.37$$

Everything is satisfied.

Appendix B

Linear analysis of the bare frame

Results of a linear elastic analysis of the bare frame subjected to a lateral force of 1 kN, are presented here. Their purpose is to easily obtain values of moments for moment-curvature diagrams presented in section 5.4.

The analysis was performed in SAP2000 and the resulting diagram is shown in Figure B-1.
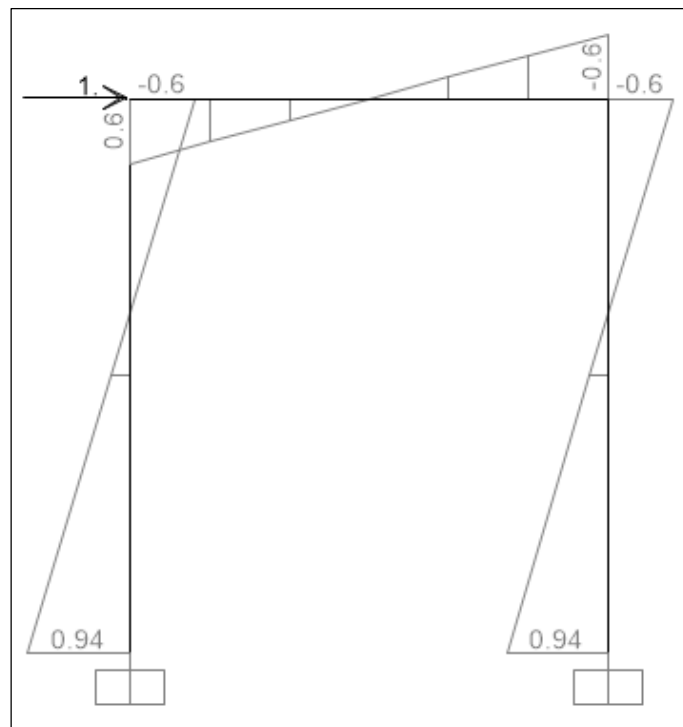

Figure B-1. Bending moment under 1 kN lateral load

REFERENCE

Calvi, M., Bolognini, D., & Penna, A. (2004). *Seismic Performance of Masonry-Infilled RC Frames - Benefits of slight reinforcements.* Guimarães: SÍSMICA 2004 - 6º Congresso Nacional de Sismologia e Engenharia Sísmica.

Crisafulli. (1997). *Seismic Behaviour of Reinforced Concrete Structures with Masonry Infills.* Christchurch: University of Cantebury.

Decanni, L., Mollaioli, F., Mura, A., & Saragoni, R. (2004). *SEISMIC PERFORMANCE OF MASONRY INFILLED R/C FRAMES.* Vancouver: 13th World Conference on Earthquake Engineering.

Fiorato, A. E., Sozen, M. A., & Gamble, W. L. (1970). *An Investigation of the Interaction of Reinforced Concrete Frames with Masonry Filler Walls.* Champaign: University of Illinois.

Holmes, M. (1961). Steel frames with brickwork and concrete infilling. In *Proceedings of the Institution of Civil Engineers* (pp. 473-478). UK: Thomas Telford.

Kakaletsis, & Karayannis. (2008). Influence of Masonry Strength and Openings on Infilled RC Frames Under Cycling Loading. *Journal of Earthquake Engineering, 12*(2), 197-218.

Liuaw, T. C., & Kwan, K. H. (1985). Unified Plastic Analysis for Infilled Frames. *Journal of Structural Engineering, 111*(7), 1427-1448.

Mehrabi, A. B., & Shing, P. B. (2003). Seismic Analysis of Masonry-Infilled Reinforced Concrete Frames. *TMS Journal, 21*, 81-94.

Mehrabi, A. B., Shing, B. P., Schuller, M. P., & Noland, J. L. (1994). *Performance of Masonry-Infilled R/C Frames Under In-Plane Lateral Loads.* Dept. of Civil, Environmental, and Architectural Engineering. Boulder: University Colorado.

Moretti, M. L., Papatheocharis, T., & Perdikaris, P. C. (2014, September). Design of Reinforced Concrete Infilled Frames. *Journal of Structural Engineering, 140*(9), 10.

Radovanović, Ž., Siđić Grebović, R., Dimovska, S., & Serdar, N. (2015). The Mechanical Properties of Masonry Walls - Analysis of the Test Results. *International Scientific Conference Urban Civil Engineering and Municipal Facilities.* Elsevier Ltd.

Stafford, S. B. (1962). Lateral Stiffness of Infilled Frames. *Journal of Structural Division, 88*(ST6), 183-199.

Valiasis, T., & Stylianidis, K. (1989). Masonry Infilled R/C Frames under Horizontal Loading - Experimental Results. *European Earthquake Engineering, 3*(3), 10-20.